Indian J Chem
DECEMBER 1992
CODEN: IJOCAP 31A(12) 903-986 (1992)
ISSN : 0376-4710

INDIAN JOURNAL OF CHEMISTRY

SECTION A

(Inorganic, Bio-inorganic, Physical, Theoretical & Analytical Chemistry)

Published by
PUBLICATIONS & INFORMATION DIRECTORATE, CSIR, NEW DELHI
in association with
THE INDIAN NATIONAL SCIENCE ACADEMY, NEW DELHI

The Treatise on Indian Medicinal Plants

Editors: Asima Chatterjee and Satyesh Chandra Pakrashi

Pages: 172
Price: Rs. 250/-

Ayurveda, the indigenous system of medicine, advocates the application of various Indian herbs in curing many maladies. Several drugs of plant origin are used in Ayurveda.

The Treatise on Indian Medicinal Plants, Vol. I, the first in a series of six volumes, covers 111 plants. The write-up on each plant includes its vernacular name, occurance and distribution, botanical description, and therapeutic uses along with important chemical constituents of the plant extract. A distinctive feature of the book is inclusion of authentic Sanskrit *slokas*, both in Devnagri and Roman scripts. The *slokas* explain the therapeutic uses of individual plants. A glossary gives the meanings of Sanskrit/Ayurvedic and medical terms. Also, a list of books referred to has been given for ready reference.

The book is profusely illustrated with both coloured and black and white pictures to enable proper identification of plant species.

The editors of the book are eminent scientists in the field. Professor Chatterjee, a Padma Bhushan and a winner of the S.S. Bhatnagar Award, is a chemist of world repute. She is currently the coordinator of the Centre of Advanced Studies on Natural Products, Department of Pure Chemistry, Calcutta University. Dr Pakrashi, the former Director of Indian Institute of Chemical Biology, Calcutta and a Fellow of the Indian National Science Academy is at present a Distinguished CSIR Fellow.

This volume would prove immensely useful to teachers, researchers and specialists in the field of Ayurveda and medicinal plants.

Insight into Scientific Research in Indian Universities & the Institutes of Technology

Rais Ahmed and Madhulika Rakesh

Pages : v + 155
Price : Rs 140/-

The roie of scientific research in industry, trade, defence and in the day-to-day life of an individual cannot be over-emphasized. It, therefore, becomes pertinent to take a holistic view not only of the various parameters of research but also to assess its organizational patterns, and human relations, values and attitudes associated with it, which are the main factors responsible for the germination and growth of research *per se*.

Insight into Scientific Research encompasses an exhaustive yet interesting study of the quality, character and efficiency of scientific research in Indian universities and other research institutions.

Several recommendations ranging from adequate financial support, reform of education leading to research, and utilization of research results would enlighten the reader. The book also throws light on what should be the research policy for Indian universities and research institutions.

One of the authors, Professor Ahmed, a Padma Bhushan is a renouned physicist. At present he is Executive Director of the Tertiary Education Commission in Mauritius. The coauthor Ms. Rakesh is an experienced researcher in the field of investigating conditions, process and value systems of scientific research.

Order for the books should be accompnied by M.O./D.D. made payable to **"Publications & Information Directorate"** and sent to:
Sales and Distribution Officer.
PUBLICATIONS & INFORMATION DIRECTORATE
Dr. K.S. Krishnan Marg,
New Delhi-110012.

Well illustrated with graphs and tables, which aid the text, the book should be a valuable possession for all involved in the scientific and technological development of the country.

RENEWAL NOTICE

Your subscription which expires with the despatch of December 1992 issue of the journal, stands for renewal. We request you to be so good as to return the enclosed order form duly filled, early, so as to ensure continuity in despatch.

Sales & Distribution Officer

Order No..... DATED :

The Sales & Distribution Officer
Publications & Information Directorate, C.S.I.R.
Dr. K.S. Krishnan Marg, New Delhi-110012 (INDIA)

Dear Sir,

Please renew my subscription/enrol me as a subscriber to :

			Rs	$	£
1.	Journal of Scientific & Industrial Research	(Monthly)	250.00	100.00	80.00
2.	Indian Journal of Chemistry, Section A	(Monthly)	400.00	150.00	100.00
3.	Indian Journal of Chemistry, Section B	(Monthly)	400.00	150.00	100.00
4.	Indian Journal of Experimental Biology	(Monthly)	350.00	150.00	80.00
5.	Indian Journal of Technology	(Monthly)	300.00	150.00	80.00
6.	Indian Journal of Pure & Applied Physics	(Monthly)	300.00	150.00	80.00
7.	Indian Journal of Biochemistry & Biophysics	(Bimonthly)	150.00	75.00	40.00
8.	Indian Journal of Marine Sciences	(Quarterly)	160.00	65.00	40.00
9.	Indian Journal of Radio & Space Physics	(Bimonthly)	150.00	75.00	40.00
10.	Indian Journal of Fibre & Textile Research	(Quarterly)	160.00	65.00	40.00
11.	Research & Industry	(Quarterly)	160.00	65.00	40.00
12.	Medicinal & Aromatic Plants Abstracts	(Bimonthly)	300.00	125.00	75.00
13.	Current Literature on Science of Science	(Monthly)	150.00	90.00	48.00
14.	C.S.I.R. News	(Semi-Monthly)	50.00	20.00	12.00

(Please tick the periodicals you would like to subscribe).

for one year from January 1993 for which I am/we are enclosing a cheque/Demand Draft No . . . . . .dated . . . . . for a sum of Rs . . . . . £ . . . . . .$ . . . . . in favour of

PUBLICATIONS & INFORMATION DIRECTORATE, NEW DELHI

COMPLETE MAILING ADDRESS

Name . . . . . .

Address . . . . . .

Country/State . . . . . .

(Signature)

Notes :

1. Subscription at annual rates for all the periodicals are enlisted for the full volumes, i.e. for the period from January to December only.
2. The Cheque/Demand Draft may please be drawn in favour of "PUBLICATIONS & INFORMATION DIRECTORATE, NEW DELHI". Banking charges shall be borne by the subscriber. For inland/outstation cheques please add Rs.10.00 for Foreign Cheques please add $ 2.00 or £ 1.00.
3. The supply will commence on receipt of subscription in advance.
4. Foreign subscription rates are for delivery by surface mail. Air mail rates will be supplied on request.

INDIAN JOURNAL OF CHEMISTRY

Section A: Inorganic, Bio-inorganic, Physical, Theoretical & Analytical Chemistry

Published by the Publications & Information Directorate, CSIR, Dr K.S. Krishnan Marg, New Delhi 110012

Director: Dr G P Phondke

The Indian Journal of Chemistry is issued monthly in two sections: A and B. Communications regarding contributions for publication in the journal should be addressed to the Editor, Indian Journal of Chemistry, Publications & Information Directorate, Dr K.S. Krishnan Marg, New Delhi 110 012.

Correspondence regarding subscriptions and advertisements should be addressed to the Sales & Distribution Officer, Publications & Information Directorate, Dr K.S. Krishnan Marg, New Delhi 110 012.
Phone 586301 Gram: PUBLIFORM Telex: 031-77271

The Publications & Information Directorate (CSIR) assumes no responsibility for the statements and opinions advanced by contributors. The Editorial Board in its work of examining papers received for publication is assisted, in an honorary capacity by a large number of distinguished scientists, working in various parts of India.

Annual Subscription: Rs. 400.00 £ 100.00 $ 150.00; 50% discount admissible to research workers and students and 25% discount to non-research individuals on annual subscription.

Single Copy: Rs. 40.00 £ 10.00 $ 15.00

Payments in respect of subscriptions and advertisements may be sent by cheque, bank draft, money order or postal order marked payable to Publications & Information Directorate, Dr K.S. Krishnan Marg, New Delhi 110 012.

Claims for missing numbers of the journal will be allowed only if received within 3 months of the date of issue of the journal plus the time normally required for postal delivery of the journals and the claim.

AUTHOR INDEX

Indian Journal of Chemistry

Sect. A: Inorganic, Bio-inorganic, Physical, Theoretical & Analytical

VOL 31A NUMBER 12 DECEMBER 1992

CONTENTS

Contd

Authors for correspondence are indicated by (*)

Indian Journal of Chemistry
Vol. 31A, December 1992, pp. 903-908

Microstructure and glass transition temperature determination of styrene-methyl acrylate copolymers by ^{13}C-NMR spectroscopy

A S Brar* & Sunita

Department of Chemistry, Indian Institute of Technology, Hauz Khas, New Delhi 110016, India

Received 10 February 1992; revised and accepted 27 April 1992

Styrene-methyl acrylate (S/M) copolymers of different monomer compositions have been prepared by bulk polymerization using benzoyl peroxide as an initiator. Copolymer composition is determined from NMR spectrum and comonomer reactivity ratios have been determined by the method of Kelen-Tudos. The copolymerization parameters such as terminal, penultimate reactivity ratios, diad concentrations, conditional probabilities, number-average sequence lengths and run number in the copolymers have been calculated from the observed triad sequence distribution determined from ^{13}C[^{1}H]-NMR spectra. The observed triad sequence concentrations as determined from ^{13}C[^{1}H]-NMR spectroscopy are in good agreement with those calculated from reactivity ratios. Glass transition temperature (T_g) values of various copolymers calculated from NMR spectra (using Barton's equation) give good agreement with the values obtained from DSC.

In our earlier papers we have reported the microstructure of acrylonitrile-methyl methacrylate[1], styrene-methyl methacrylate[2], acrylonitrile-ethyl methacrylate[3] and acrylic acid-vinyl acetate[4] copolymers using ^{13}C-NMR spectroscopy. This study is a continuation of earlier work in which microstructure parameters, e.g., terminal and penultimate reactivity ratios, number-average sequence lengths, run number, block character and T_g of styrene-methyl acrylate copolymers have been calculated from triad and diad concentrations obtained from ^{13}C[^{1}H]-NMR spectra. The effects of copolymer composition and monomer sequence distribution on T_g has been investigated for some copolymers[5-8]. Koinuma *et al.*[9] have theoretically calculated the tacticity and sequence dependence of ^{13}C-NMR spectra of styrene-methyl acrylate copolymer. De Vries *et al.*[10] have reported the intramolecular structure (triad distribution and tacticity parameters) of S/M copolymers obtained by low conversion solution polymerization and high conversion by mean of both solution and emulsion polymerization. They have also used ^{1}H-NMR to determine the fractions of various S- and M-centered triads but we have used only ^{13}C-NMR spectra to calculate the fractions of various triads because of the poor resolution of ^{1}H-NMR spectra.

Materials and Methods

Polymerization

Monomers were distilled under reduced pressure and stored below 5°C. Benzoyl peroxide (0.5% by weight) was added to a mixture of monomers and polymerization was carried out at 70°C. The conversion was kept low (5-10%) and copolymers were precipitated in excess of methanol after 40 min. Several copolymers having various compositions were prepared similarly.

NMR Analyses

^{1}H-NMR and ^{13}C[^{1}H]-NMR spectra were recorded on the Bruker W H 270 NMR spectrometer operating at 270 MHz and 67.5 MHz respectively. The detailed conditions of the operations are as follows: temperature of the probe, 25°C; reference, centre peak of $CDCl_3$ assigned as 77.0 ppm; spectral width, 13500 Hz; pulse repetition time, 5 sec; 16 K data points for fourier transform. The details of recording the spectra and Lorentzian shape curve fitting have been described elsewhere[2,3].

Molecular weight determination

The molecular weight distribution of styrene-methyl acrylate copolymers was determined on Water's GPC instrument at 25°C using a 5 μ-PL-gel mixed column. Chloroform was used as the mobile phase and a refractive index detector was used. Calibration was done with narrow molecular weight distributed poly(methyl methacrylate) (PMMA) as reference standard.

Results and Discussion

Reactivity ratios determination

The composition of styrene-methyl acrylate (S/M) copolymers prepared by bulk polymeriza-

tion was found from ^{1}H-NMR spectra of the copolymers by comparing the intensities of the $-OCH_3$ (M unit) and $-C_6H_5$ (S unit) proton resonances. The styrene mole fraction (F_S) in the copolymers can readily be determined by using the relationship:

$$F_S = \frac{3I(-C_6H_5)}{3I(-C_6H_5)+5I(-OCH_3)} \quad \ldots (1)$$

where $I(-OCH_3)$ and $I(-C_6H_5)$ represent the intensities of $-OCH_3$ and $-C_6H_5$ proton resonances respectively. To ascertain normal copolymer kinetic behaviour, a plot of theoretical composition of the copolymer obtained from copolymer equation by using terminal model reactivity ratios ($r_S = 1.20$, $r_M = 0.18$) along with experimental data was drawn (Fig. 1). Both these values are in good agreement with each other and the concave shape of the curve indicates that the monomer distribution is statistical in nature and in no case homopolymer formation is expected at low conversion. The copolymer composition data were used to calculate the terminal model reactivity ratios by the method of Kelen-Tudos[11]. The values of reactivity ratios obtained from Kelen-Tudos plot are $r_S = 1.20$ and $r_M = 0.18$. The value of the product of r_S. r_M is about 0.22, which indicates that S/M comonomer pair polymerizes neither in random nor in alternate manner. The reported values[10] of the reactivity ratios are $r_S = 0.73$ and $r_M = 0.19$. In the reported study the copolymers were prepared by the solution and emulsion polymerization through free radical initiation, while in the present case copolymers were prepared by bulk polymerization as explained earlier. This indicates that the values of reactivity ratios depend on the method of polymerization.

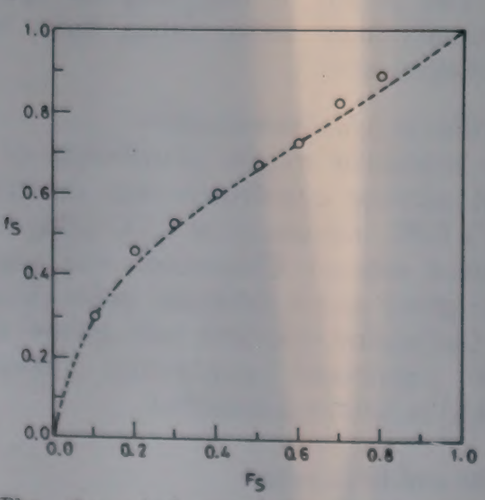

Fig. 1 – The theoretical copolymer composition curve (– – –) obtained from copolymer composition equation by using terminal model reactivity ratios ($r_S = 1.20$, $r_M = 0.18$) along with the experimental points (0).

Molecular weight distribution

The PMMA equivalent number average ($\bar{M}_n$), weight average ($\bar{M}_W$), Z average ($\bar{M}_Z$) and Z+1 average ($\bar{M}_{Z+1}$) molecular weights and the polydispersity of the S/M copolymers determined from GPC measurements are given in Table 1. The $\bar{M}_n$ varies from 0.40 to 0.76×10^5, $\bar{M}_W$ varies from 0.69 to 1.26×10^5, $\bar{M}_Z$ varies from 1.19 to 2.04×10^5, $\bar{M}_{Z+1}$ varies from 1.86 to 3.06×10^5 and $\bar{M}_V$ varies from 0.69 to 1.26×10^5. The polydispersity value of all the copolymers is almost of the same order (≈ 1.7), so the heterogeneity of the copolymers and the molecular weight distribution is of the same order.

^{1}H-NMR studies

In the case of S/M copolymer, the $-(OCH_3)$ protons appeared around 3.6 ppm. The broad signal from 2.3 to 2.0 ppm can be attributed to $(-CH)$ proton of both styrene and methyl acrylate monomers. The other broad signal from 1.7 to 1.3 ppm can be assigned to $(-CH_2)$ protons of both monomers. The aromatic protons in all the copolymers appeared as a doublet, one due to *ortho* (6.6-6.8 ppm) and another due to *meta* and *para* (7.1-7.8 ppm) protons.

^{13}C-NMR studies

Various resonance signals in the $^{13}C[^1H]$-NMR spectrum of S/M copolymer have been assigned by comparing the spectrum of the copolymer with those of homopolymers. In the case of polystyrene (PS), a sharp singlet centered around 40.8 ppm can be assigned to $(-CH)_S$. The methylene $(-CH_2)_S$ carbon shows a multiplet in the range 43.0-46.0 ppm, which shows sensitivity toward tacticity. In the multiplet, the peak around 43.4 ppm can be assigned to isotactic polystyrene, that at 44.8 to heterotactic and that at 45.7 ppm can be assigned to syndiotactic polystyrene. The aromatic carbons in polystyrene show splitting ac-

Table 1 – Study of molecular weight distribution of styrene-methyl acrylate (S/M) copolymers

S.No.	S. mol. fraction (in feed)	$\bar{M}_n$ [10^{-5}]	$\bar{M}_W$ [10^{-5}]	$\bar{M}_Z$ [10^{-5}]	$\bar{M}_V$ [10^{-5}]	$\bar{M}_{Z+1}$ [10^{-5}]	Polydispersity ($\bar{M}_W/\bar{M}_n$)
1.	0.7	0.74	1.24	2.04	1.24	3.06	1.67
2.	0.6	0.60	0.97	1.54	0.97	2.24	1.63
3.	0.5	0.76	1.26	1.98	1.26	2.79	1.65
4.	0.4	0.59	1.04	1.78	1.04	2.67	1.76
5.	0.3	0.40	0.69	1.19	0.69	1.86	1.75
6.	0.2	0.60	1.03	1.71	1.03	2.71	1.71

cording to their environments. A highly complex aromatic ring carbon resonance pattern is exhibited by the quaternary carbon ($-\dot{C}-$) around 145.0-146.1 ppm, while no splitting was observed for either the *ortho*, *meta* or *para* carbon, which appeared around 128.6, 127.2 and 126.0 ppm respectively. The multiplicity of quaternary carbon indicates its sensitivity towards configurational sequence and a peak around 146.0 ppm can be assigned to isotactic polystyrene, one around 145.5 ppm can be assigned to heterotactic and the peak around 145.2 ppm can be assigned to syndiotactic polystyrene[12].

In the case of PMA, resonance signals around 174.7, 51.2, 42.1 and 34.5 ppm can be assigned to $(>C=0)_M$, $(OCH_3)_M$, $(-CH)_M$ and $(-CH_2)_M$ carbons respectively. $^{13}C[^1H]$-NMR spectrum of S/M copolymer (S = 53.0 mole per cent in copolymer) recorded in $CDCl_3$ at room temperature along with assignments and the positions of various functional groups is shown in Fig. 2. The quaternary carbon of S unit appeared as a well resolved multiplet at 143.0-145.8 ppm, showing its sensitivity towards different monomer placements. The carbonyl carbon resonance signal in the S/M copolymer appeared as a multiplet around 176.5-174.5 ppm, which indicates that the splitting of carbonyl signal is due to its sensitivity toward different compositional sequences. In the case of S/M copolymer, the positions of various functional groups of S and M units shift as compared to the positions in the homopolymers, which may be due to the change in the nature of adjacent monomeric units in copolymer which changes the chemical shift of S and M centered triad.

The carbonyl ($>C=O$) carbon expansion of S/M copolymer (S = 53.0 mole per cent in copolymer) is shown in Fig. 2. Free radical PMA shows a singlet around 174.7 ppm. As the per cent of styrene in the copolymer increases, signals characteristic of homopolymer decrease, whereas set of signals centered around 175.4 ppm start appearing. These signals, with a further increase in the S content, increase to a maximum value and then decrease, whereas a third new set of resonance signal appears around 176.2 ppm. Three sets of signals whose intensities change with the copolymer composition can be assigned to carbonyl carbon centered in SMS, SMM (MMS), MMM triad sequences from low to high field. In the case of M-centered triad, introduction of S unit in MMM triad causes the downfield shift in the position of SMM (by ≈0.8 ppm) and SMS (by ≈0.70 ppm). Concentrations of various M-centered triads can be calculated from the relative areas of respective signals. Table 2 contains the compositional information concerning various M-centered triads along with calculated values obtained from Alfrey-Mayo model[13] (first order

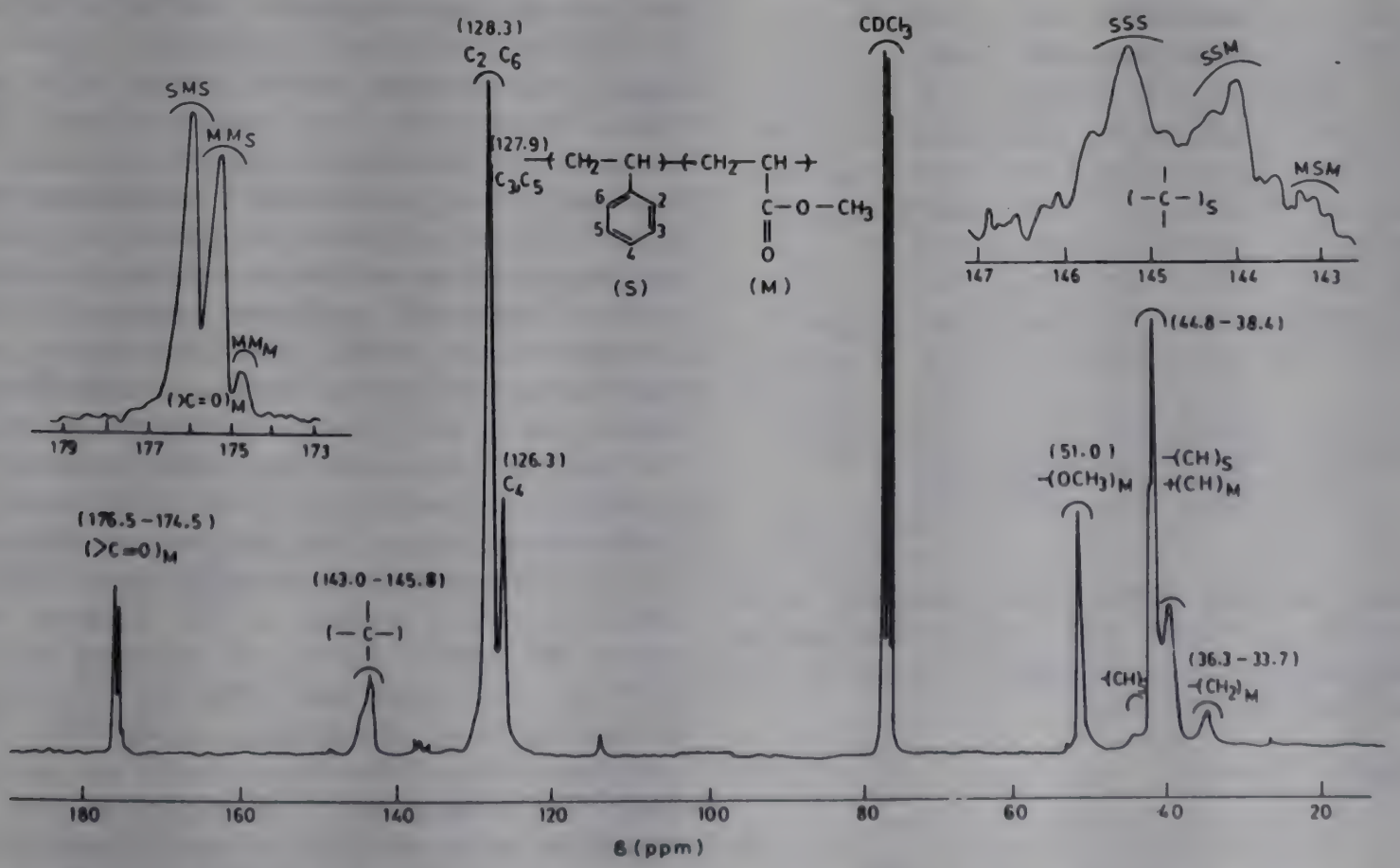

Fig. 2 – $^{13}C[^1H]$-NMR spectrum of styrene-methyl acrylate copolymer (S = 53.0 mole per cent in copolymer) in $CDCl_3$ at room temperature along with the expanded carbonyl $(>C=O)_M$ and quaternary $(-\dot{C}-)_S$ carbon resonance signals.

Table 2 – Calculated and observed fractions of S- and M-centered triad in styrene-methyl acrylate (S/M) copolymers

S.No.	S. mol. fraction (in feed)	Triad	Triad Obs.	Concentrations Calc. from		Penultimate reactivity ratios
				Alfrey-Mayo model	Harwood Pen. model	
1.	0.7	SSS	0.54	0.52	0.53	$r_{SS} = 1.01$
		SSM	0.39	0.44	0.40	$r_{MS} = 2.35$
		MSM	0.07	0.04	0.07	$r_{MM} = 0.00$
		MMM	0.00	0.00	0.00	$r_{SM} = 0.17$
		MMS	0.14	0.13	0.13	
		SMS	0.86	0.87	0.87	
2.	0.6	SSS	0.41	0.38	0.40	$r_{SS} = 1.15$
		SSM	0.46	0.44	0.47	$r_{MS} = 0.82$
		MSM	0.13	0.18	0.13	$r_{MM} = 0.15$
		MMM	0.01	0.01	0.01	$r_{SM} = 0.20$
		MMS	0.19	0.21	0.19	
		SMS	0.80	0.78	0.80	
3.	0.5	SSS	0.30	0.30	0.29	$r_{SS} = 1.33$
		SSM	0.49	0.45	0.50	$r_{MS} = 0.90$
		MSM	0.21	0.25	0.21	$r_{MM} = 0.20$
		MMM	0.02	0.03	0.02	$r_{SM} = 0.22$
		MMS	0.26	0.30	0.26	
		SMS	0.72	0.67	0.72	
4.	0.4	SSS	0.20	0.22	0.19	$r_{SS} = 1.43$
		SSM	0.49	0.46	0.50	$r_{MS} = 1.08$
		MSM	0.31	0.32	0.31	$r_{MM} = 0.20$
		MMM	0.05	0.05	0.04	$r_{SM} = 0.18$
		MMS	0.33	0.33	0.34	
		SMS	0.62	0.62	0.62	
5.	0.3	SSS	0.11	0.08	0.11	$r_{SS} = 0.85$
		SSM	0.45	0.44	0.45	$r_{MS} = 1.07$
		MSM	0.44	0.48	0.44	$r_{MM} = 0.13$
		MMM	0.08	0.06	0.07	$r_{SM} = 0.17$
		MMS	0.42	0.41	0.42	
		SMS	0.50	0.53	0.51	
6.	0.2	SSS	0.05	0.05	0.05	$r_{SS} = 1.18$
		SSM	0.36	0.34	0.36	$r_{MS} = 1.11$
		MSM	0.59	0.61	0.59	$r_{MM} = 0.17$
		MMM	0.17	0.16	0.15	$r_{SM} = 0.17$
		MMS	0.49	0.48	0.50	
		SMS	0.34	0.36	0.35	

Markov terminal model) using reactivity ratios ($r_S = 1.20$, $r_M = 0.18$). The relation between intramolecular structure (fractions of S and M centered triad) are given below:

$$F_{MMM} = [1 - P_{(S/M)}]^2 \quad \ldots (2a)$$

$$F_{MMS} = F_{SMM} = 2[P_{(S/M)}].[1 - P_{(S/M)}] \quad \ldots (2b)$$

$$F_{SMS} = [P_{(S/M)}]^2 \quad \ldots (2c)$$

$$F_{SSS} = [1 - P_{(M/S)}]^2 \quad \ldots (2d)$$

$$F_{SSM} = F_{MSS} = 2[P_{(M/S)}].[1 - P_{(M/S)}] \quad \ldots (2e)$$

$$F_{MSM} = [P_{(M/S)}]^2 \quad \ldots (2f)$$

where $P_{(S/M)} = \left(\frac{1}{1 + r_M/q}\right)$ and $P_{(M/S)} = \left(\frac{1}{1 + r_S \cdot q}\right)$

$q = [S]/[M]$ is the instantaneous feed ratio. F represents the fractions of triad normalized to unity. Penultimate reactivity ratios were evaluated (Table 2) from experimentally obtained triad distributions from carbonyl carbon resonance of $^{13}C[^1H]$-NMR spectra by using the following equations:

$$r_{MM} = \frac{2\,[MMM]}{[MMS + SMM]} \cdot [S_f]/[M_f] \quad \ldots (3a)$$

$$r_{SM} = \frac{[SMM + MMS]}{2[SMS]} \cdot [S_f]/[M_f] \quad \ldots (3b)$$

The values of r_{MM} and r_{SM} are listed in Table 2. The values of penultimate reactivity ratios vary with copolymer composition.

Similar compositional information regarding S-centered triads can be made using the $(-\underset{'}{C}-)$ carbon resonance region. The quaternary carbon $(-\underset{'}{C}-)$ resonance expansion of S/M copolymer (S = 53.0 mole per cent in copolymer) is shown in Fig. 2. A multiplet around 143.0-145.8 ppm shows the splitting into three envelopes. The chemical shift difference within the resonance signals and splitting pattern shows its sensitivity towards monomer sequence and cotacticity in the quaternary carbon resonance. As the concentration of S unit in the copolymer increases the most downfield signal of the quaternary carbon centered around 145.2 ppm increases, while the upfield signal centered around 143.2 ppm decreases. On the basis of compositional variation in the intensities of S-centered triad, the most downfield resonance signal may be assigned to SSS triad and the most upfield due to MSM triad. The addition of methyl acrylate to SSS centered triad causes the upfield shift in the chemical shift of SSM (by ≈ 0.9 ppm) and MSM (by ≈ 1.1 ppm). S-Centered triad distributions along with those calculated using Alfrey-Mayo model are given in Table 2. On the basis of the triad resonance assignments made as described earlier, penultimate reactivity ratios were evaluated for S/M copolymer from the triad fractions determined from qua-

ternary carbon resonance of $^{13}C[^1H]$-NMR spectra by using the following equations:

$$r_{SS} = \frac{2\,[SSS]}{[SSM + MSS]} \cdot [M_f]/[S_f] \quad \ldots (3c)$$

$$r_{MS} = \frac{[SSM + MSS]}{2[MSM]} \cdot [M_f]/[S_f] \quad \ldots (3d)$$

The values of r_{SS} and r_{MS} are listed for individual copolymers in Table 2. Using the average values of penultimate reactivity ratios, the triad sequence distribution as obtained by using Harwood program[14] is given in the Table 2.

From the results of composition of various S- and M-centered triads, the conditional probabilities P_{SM} and P_{MS} have been calculated using the equations:

$$P_{SM} = \frac{[MSM] + [MSS]/2}{[MSM] + [MSS] + [SSS]} \quad \ldots (4a)$$

$$P_{MS} = \frac{[SMS] + [MMS]/2}{[MMM] + [MMS] + [SMS]} \quad \ldots (4b)$$

where P_{SM} is the probability that S-M unit comes about as a result of S growing chain end adding M and P_{MS} is the probability that M-S unit comes about as a result of M growing chain end adding S. The value of P_{SM} increases from 0.22 to 0.78 with the increase in the content of methyl acrylate in the copolymers while the value of P_{MS} decreases from 0.93 to 0.60 with the decrease in the concentration of styrene in the copolymers. The number average sequence lengths ($\bar{N}_s$ and $\bar{N}_M$), being the reciprocal of the conditional probabilities, were also calculated. The value of $\bar{N}_S$ decreases from 4.46 to 1.28 with the decrease in the concentration of S in the copolymer, while the values of $\bar{N}_M$ increases from 1.07 to 1.67 with the decrease in the content of S in the copolymers.

The block character (η) is an adequate way to characterize the sequence distribution in the copolymers. It is given by the expression[15]:

$$\eta = \frac{[SM]}{2[S][M]} \quad \ldots (5)$$

where [SM] is the mole fractions of SM dyad and [S], [M] are the mole fractions of S and M monomers in the copolymers. The value $0 < \eta < 1$ reflects more block character and $1 < \eta < 2$ means more alternating tendency of the copolymer than that expected from the random distribution. The value of η for S/M copolymerization lies in the range 0.67 - 0.88 ($0 < \eta < 1$), which shows that S/M copolymer has more tendency toward block copolymerization.

The run number (R) of this copolymer is defined as the average number of the segments of either type per 100 monomer units. This may be written as[16]:

$$R = \frac{200}{\bar{N}_S + \bar{N}_M} \quad \ldots (7)$$

where $\bar{N}_S$ and $\bar{N}_M$ are the number average sequence lengths of S and M monomer units in the copolymers. In the case of S/M copolymer, the value of R lies in the range 36.17-71.68. All the copolymerization parameters are given in Table 3.

Barton[17] and Johnston[18] described the effect of sequence distribution of monomeric unit in the linear copolymers on its glass transition temperature (T_g) and considered the contribution of the diad. Barton equation showed the dependence on sequence as follows:

$$T_{g,P} = N_{SS}T_{g,SS} + N_{MM}T_{g,MM} + (N_{SM} + N_{MS})T_{g,SM}. \quad \ldots (8)$$

$T_{g,P}$ is the T_g of a copolymer containing mole fractions (N) of various diads (SS, MM, SM, MS). $T_{g,SS}$ and $T_{g,MM}$ are the glass transition temperatures of polystyrene and polymethyl acrylate respectively, whereas $T_{g,SM}$ is the T_g of the alternating copolymer. Barton[17] has reported the value of T_{SM} for styrene-methyl acrylate copolymer as 58.3°C. This value seems to be logical looking from the view point of T_g of homopolymers. The values of T_g for polystyrene was taken as 100°C

Table 3 – Copolymerization parameters of S/M copolymer determined by ^{13}C-NMR spectroscopy

S.No.	S. mol. fraction (in feed)	P_{SM}	P_{MS}	$\bar{N}_S$	$\bar{N}_M$	$[\eta]$	R
1.	0.7	0.22	0.93	4.46	1.07	0.67	36.17
2.	0.6	0.40	0.88	2.50	1.13	0.73	55.10
3.	0.5	0.47	0.82	2.11	1.22	0.67	60.06
4.	0.4	0.50	0.78	2.00	1.27	0.69	61.16
5.	0.3	0.70	0.73	1.43	1.36	0.88	71.68
6.	0.2	0.78	0.60	1.28	1.67	0.78	67.80

Table 4 – Glass transition temperature (T_g) and diad compositions data for S/M copolymers

S.No.	S. mole. fraction (in feed)	Diad fractions	T_g (K)	
			Calc. from Barton eqn.	Obtained from DSC
1.	0.7	[SS] = 0.74 [MM] = 0.07 [MS] = 0.19	359	360
2.	0.6	[SS] = 0.60 [MM] = 0.12 [MS] = 0.28	350	349
3.	0.5	[SS] = 0.53 [MM] = 0.18 [MS] = 0.29	344	343
4.	0.4	[SS] = 0.45 [MM] = 0.22 [MS] = 0.33	339	–
5.	0.3	[SS] = 0.30 [MM] = 0.26 [MS] = 0.44	330	–
6.	0.2	[SS] = 0.22 [MM] = 0.40 [MS] = 0.38	320	–

and of polymethyl acrylate as 6°C. By using the Barton's equation (Eq. 8), the values of T_g were calculated for these copolymers. The values thus calculated were found to be in agreement with the values obtained from DSC. Table 4 contains the diad concentrations calculated from $^{13}C[^1H]$-NMR spectra along with the T_g data. The T_g's of the copolymers having less than 60% of styrene (in copolymer) are not reported here because these are very low.

Acknowledgement

The authors are thankful to Prof. C.L. Khetrapal, I.I.Sc. Bangalore, for recording ^{13}C-NMR spectra.

References

1 Kapur G S & Brar A S, *Polymer*, 32 (1991) 1112.
2 Brar A S & Kapur G S, *Polym J*, 20 (1988) 371.
3 Kapur G S & Brar A S, *J polym Sci polym Chem*, 29 (1991) 479.
4 Brar A S & Sunita, *Eur Polym J*, 27 (1991) 17.
5 Sanchez-Chaves M, Arranz F & Montes M, *Polymer*, 29 (1988) 2244.
6 Arranz F, Sanchez-Chaves M & Molinero A, *Macromol Chem*, 185 (1984) 2153.
7 Harris S H & Gilbert R D, *J polym Sci polym Chem Ed*, 20 (1982) 1653.
8 Schneider H A & Neto H N, *Polym Bull*, 9 (1983) 457.
9 Sato K, Koinuma H & Hirai H, *Macromol Chem*, 4 (1983) 821.
10 van Doremaele G H J, German A L, De Vries N K & van der veldon G P M, *Macromolecules*, 23 (1990) 4206.
11 Kelen T & Tudos F, *J Macromol Sci Chem*, A9 (1975) 1.
12 Randall J C, *Polymer sequence determination: Carbon-13 NMR method*, Chap. 6 (Academic Press, New York), 1977, 116.
13 Koenig J L, *Chemical microstructure of polymer chain*, Chap. 3 (Wiley Interscience, New York), 1980, 39.
14 Harwood H J, *J polym Sci Part C*, 25 (1968) 37.
15 Ito K & Yamashita Y, *J polym Sci*, A3 (1965) 2165.
16 Allcock H R & Lampe F W, *Contemporary polymer chemistry* Chap. 12/II Ed. (Englewood Cliffs, New Jersey), 1990, 116.
17 Barton J M, *J polym Sci Part C*, 30 (1970) 573.
18 Johnston N W, *J Macromol Sci rev Macromol Chem*, 14 (1976) 215.

Indian Journal of Chemistry
Vol. 31A, December 1992, pp. 909-914

Investigation of Cr^{3+} substituted γ-Fe_2O_3 catalyst in its active form

A C Sengupta, M L Kundu*, G C Maiti, B Sen & S K Ghosh
R&D Division, Projects & Development India Ltd., Sindri 828 122, Dhanbad
and
P Banerjee, S Ganguli & M Bhattacharya
Saha Institute of Nuclear Physics, Sector-1, Block-AF, Bidhan Nagar, Calcutta 700 064

Received 13 January 1992; revised 20 April 1992; accepted 17 August 1992

The Cr^{3+} ion substituted γ-Fe_2O_3 catalysts after reduction in their active states for water gas shift reaction, prepared by three different routes have been investigated using TG, XRD, IR and Mössbauer techniques. The TG and XRD results indicate that Cr^{3+} could be substituted in the magnetite lattice and the IR and Mössbauer investigations reveal that Cr^{3+} gets included in the octahedral sites of Fe_3O_4. The inclusion of Cr^{3+} produces ultrafine particles indicative of lattice instability which depends on the method of preparation. Ultrafine particles have been registered through the average crystallite size measurement by XRD and the superparamagnetic doublet in Mössbauer spectra. On the basis of correlation between relative abundance of ultrafine particles and the concentration of Cr^{3+} ions, the criteria for the best catalytic function have been suggested invoking ordering of Cr^{3+} ions/vacancies and the electron hopping between Fe^{2+} and Fe^{3+} in the magnetite lattice.

Chromia promoted iron oxide is widely used as an industrial catalyst for water gas shift reaction[1]. The catalyst Fe_2O_3 has two structural forms, viz., α-Fe_2O_3 and γ-Fe_2O_3, which get reduced to its active component Fe_3O_4 before putting into actual operation. The catalyst based on α-Fe_2O_3 forms solid solutions with isostructural Cr_2O_3 in all proportions[1-3]. The incorporation of Cr_2O_3 into the Fe_2O_3 lattice promotes structural stability of the catalysts[4-8]. Study of the catalyst based on γ-Fe_2O_3 is of importance, since Fe_3O_4 and γ-Fe_2O_3 have the same structure, the only difference being the presence of ~ 11% vacancies at iron site in the latter case. As such the reduction of γ-Fe_2O_3 into Fe_3O_4 is a topotactic transformation which significantly inhibits the sintering of the active phase. The incorporation of Cr^{3+} in γ-Fe_2O_3 further facilitates this process. Moreover, the sulphur contamination can be minimised in the case of γ-Fe_2O_3. For these reasons, presently the γ-Fe_2O_3 route is preferred over the α-Fe_2O_3 route for the commercial production of the HT CO conversion catalyst. In a previous communication[9] the structural characteristics of chromia promoted γ-Fe_2O_3 catalysts and their correlation with the catalytic activity have been reported.

The present work concentrates on the investigation of Cr^{3+} substituted γ-Fe_2O_3 catalyst in its reduced form. Fe_3O_4 is an inverse spinel in which Fe^{3+} ions are distributed equally in the tetrahedral (A) and octahedral (B) sites, whereas Fe^{2+} ions occupy only octahedral (B) sites. The samples have been investigated by TGA, XRD, IR and Mössbauer techniques in order to identify the role of chromia on the structural characteristics of Fe_3O_4, which are related to the efficacy of the catalyst.

Materials and Methods

Three series of samples designated as A1, A3, B1, B2, B3 and C1, C2 and C3 were prepared by wet mixing, direct coprecipitation and reverse coprecipitation methods respectively as described elsewhere[9]. The numbers 1, 2 and 3 denote chromia concentrations of the order of 10%, 15% and 20% respectively and P stands for the parent oxide Fe_3O_4. All the samples were reduced at 360°C by a reducing gas mixture of approximate composition 22% CO, 6% CO_2, 60% H_2 and 2% CH_4 in presence of steam. Steam was used to prevent reduction of Fe_2O_3 beyond Fe_3O_4[10,11].

Thermogravimetric analysis under the same gas mixture was carried out using an instrument fabricated in PDIL workshop. For XRD, IR and Mössbauer measurements the reduced samples were coated with colloidion[12] to prevent oxidation of the samples. XRD measurements of the samples were performed with a Philips X-ray diffractometer using FeK_α radiation. For lattice parameter (a_0) measurement, three strongest diffraction lines from 220, 311 and 440 planes were considered and the *d*-values were corrected by comparison with NBS Si diffrac-

Table 1—Crystal phase compositions, lattice parameters and crystallite sizes of Fe_3O_4 in different Fe_3O_4/Cr_2O_3 catalysts

Sample	%Cr as Cr_2O_3*	Crystalline phase	Lattice parameter (a_0) in Å	Crystallite sizes in Å
P	0	Fe_3O_4	8.391 (5)	720
A1	8.4	Fe_3O_4	8.343 (8)	600
A3	18.71	Fe_3O_4, Cr_2O_3 (trace)	8.353 (7)	410
B1	9.86	Fe_3O_4	8.343 (6)	410
B2	15.01	Fe_3O_4	8.353 (2)	390
B3	19.74	Fe_3O_4	8.352 (2)	360
C1	9.62	Fe_3O_4	8.350 (3)	480
C2	14.76	Fe_3O_4	8.353 (5)	310
C3	19.48	Fe_3O_4	8.346 (20)	100

*determined by chemical method

tion lines. The crystallite sizes were measured using the Scherrer formula. The IR spectra were recorded in a Perkin-Elmer 1728 Fourier Transform IR spectrometer using samples in KBr matrix. The Mössbauer spectra were recorded at room temperature in a spectrometer (Wissel-1000) operating in a constant acceleration mode, coupled with a CMCA 1000A multichannel analyser and an Apple IIe computer. A one mCi ^{57}Co source in Rh matrix from Amersham was used. An Fe absorber was employed for calibration.

Results and Discussion

Thermogravimetric analysis

The thermograms of all the samples were recorded. The shifting of the starting reduction temperature by 25°C in the case of chromia containing samples from that of the parent oxide indicates that Cr_2O_3 increases the stabilization of the Fe_2O_3 lattice to some extent[13]. In the A series the total weight loss up to 400°C decreases with the increase of chromia concentration because of the fact that chromia remains in the +3 oxidation state after reduction, only Fe_2O_3 being transformed into Fe_3O_4. Also the measured weight losses do not differ significantly from the theoretical value for the conversion from Fe_2O_3 to Fe_3O_4. In the B and C series, the weight loss up to 400°C is much higher than that in the A series. The higher weight loss may be attributed to the removal of a larger amount of absorbed moisture. The weight loss as a function of chromia concentration in the B and C series is opposite to that of the A series. Explanation in this regard will be provided in the subsequent discussion. Since the reduction of all the samples completes ~350°C, as revealed from TG studies and other complementary measurements, samples were reduced at 360°C for subsequent measurements.

X-ray diffraction

The results of X-ray investigation are presented in Table 1. Fe_3O_4 is the major phase in all the samples. In the sample A3, in addition to Fe_3O_4 diffraction lines, a very weak and broad line corresponding to the *d*-value 2.67 Å has been detected. This line seems to be due to the presence of a trace amount of Cr_2O_3. In the B and C series, no free Cr_2O_3 has been detected in the X-ray diffractograms. The lattice parameter (a_0) values of Fe_3O_4 in the A, B and C series are more or less same but differ significantly from that of the sample P. However, a_0 values are insensitive to chromia concentration in all the series. These observations indicate that a chromia substituted mixed lattice has been formed in all the series.

The crystallite sizes of Fe_3O_4 in the chromia containing samples are less than that of pure Fe_3O_4. Moreover, in the B series the crystallite size decreases monotonically, while in the C series it decreases abruptly with increase of chromia concentration. From these observations, it is predicted that at low concentration of chromia there may exist some ordering of cations in the mixed lattice and this cationic ordering decreases with an increase of chromia concentration. However, we could not detect any superlattice line as an evidence of cationic ordering contrary to the reports[14,15] on γ-Fe_2O_3. The absence of superlattice lines is possibly due to the fact that the cationic ordering which creates an ordered superstructure may not be perfect enough at the chromia concentration under investigation.

A careful observation of the gradual reduction of the particle size with chromia concentration furnishes an explanation for the observed opposing trends of weight loss mentioned in the earlier section. A higher loss in weights in B and C series has been earlier attributed to absorbed moisture. If the inclusion of water is due to adsorption, the amount of water absorbed will depend on the exposed surface area of the materials. Since XRD results show that particle size decreases with Cr^{3+} concentration, the surface area and hence the amount of water adsorbed increases with chromia concentration. This explains the observed fact.

Infrared spectra

The IR spectra of samples belonging to the A, B and C series along with the parent oxide (P) were recorded. The IR spectrum of γ-Fe_2O_3 shows strong spectral bands at 640 and 565 cm^{-1} which may be assigned for Fe – O bond in the tetrahedral configu-

Table 2—^{57}Fe Mössbauer parameters of chromia substituted Fe_3O_4 catalysts

Sample	Tetrahedral site				Octahedral site				Superparamagnetic component			
	I.S. mm/s	G.S. mm/s	H_{eff} K.Oe	Γ mm/s	I.S. mm/s	G.S. mm/s	H_{eff} K.Oe	Γ mm/s	I.S. mm/s	G.S. mm/s	H_{eff} K.Oe	Γ mm/s
P	0.30	0	501	0.35	0.68	0.13	474	0.45				
A1	0.30	0.09	498	0.35	0.65	0.17	474	0.60				
A3	0.28	0.04	498	0.60	0.69	0.17	471	0.69				
B1	0.28	0.04	495	0.35	0.65	0.17	468	0.78	0.26	0.78		0.78
B2	0.28	0.04	495	0.69	0.63	0.13	471	0.86	0.25	0.68		0.78
B3	0.30	0.08	493	0.50	0.65	0.17	468	0.95	0.30	0.60		0.78
C1	0.30	0	495	0.50	0.63	0.13	468	0.78	0.26	0.52		0.78
C2	0.30	0.04	490	0.86	0.65	0.10	465	0.95	0.26	0.69		0.78
C3	*	*	485†	*	*	*	485†	*	0.30	0.60		0.78

*Sites are not measurable; †sites are not resolved; error in I.S. & G.S. is ± 0.04 mm/s; error in Γ is ± 0.08 mm/s; error in H_{eff} is ± 3.0 K.Oe; shifts are measured with respect to α-Fe.

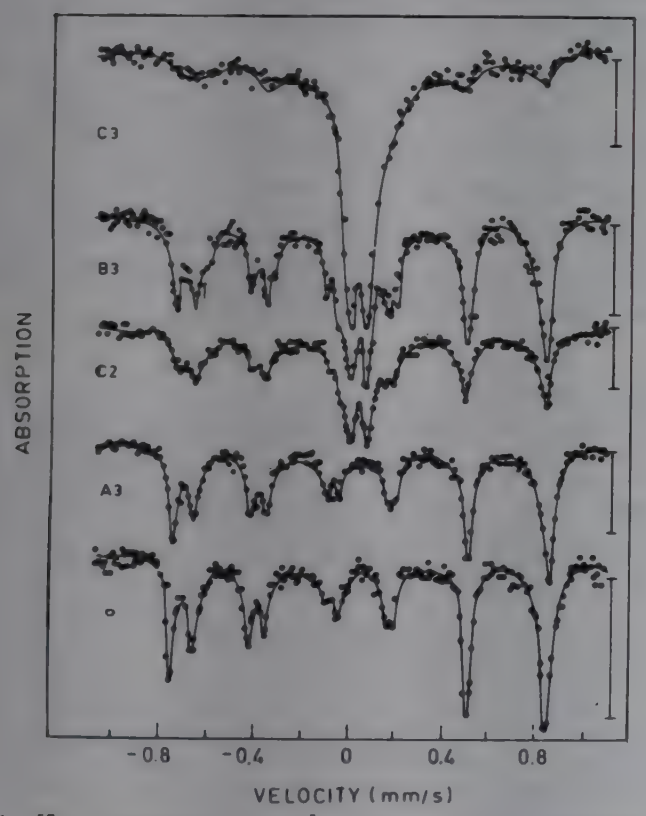

Fig. 1—^{57}Fe Mössbauer spectra of Fe_3O_4/Cr_2O_3 catalysts and Fe_3O_4. The vertical bar in the figure represents 5% absorption for each case.

ration and three bands at 440, 410 and 330 cm^{-1} may be assigned to Fe−O octahedral mode of vibration[16,17]. The IR spectrum of Fe_3O_4 shows a broad band at 578 cm^{-1} due to the tetrahedral mode of vibration and mainly two absorption bands at 448 and 409 cm^{-1} due to the octahedral mode. In the case of chromia containing samples the bands due to the octahedral mode are mainly perturbed whereas those due to the tetrahedral mode are slightly broadened. In the case of A series the perturbation of the octahedral bands is less compared to that in the B and C series. Moreover, a weak shoulder peak at 640 cm^{-1} appears in the IR spectrum of the sample A3, which may be assigned to the free Cr_2O_3 vibrations. In the B and C series, intensities of the octahedral bands diminish, shift as well as broaden with the increase of chromia concentration. The results indicate that in the chromia substituted magnetite lattice, Cr^{3+} ions occupy mainly the octahedral cationic positions of Fe_3O_4 supporting earlier work[18] and the increase of Cr^{3+} concentration causes a distortion in the mixed lattice (B and C series). This is more pronounced in the sample C3. The presence of foreign cations (Cr^{3+}) in the Fe_3O_4 lattice may introduce some disorder in the lattice as suggested by Gillot *et al.*[19].

Mössbauer spectra

The Mössbauer spectra of the sample P and four representative spectra of samples belonging to the A, B and C series (Fig. 1) show two sets of superimposed sextets which arise from two distinct magnetic fields at tetrahedral and octahedral sites. The outer sextet originates from the tetrahedral site and the inner one from the octahedral site of Fe_3O_4 spinel. In addition, a superparamagnetic doublet characteristic of ultrafine particles[20] appeared in the spectra of B and C series. Further, the intensity of the superparamagnetic doublet increased with the increase of chromia concentration.

The isomer shift (IS), quadrupole splitting (QS) line width (Γ) (full width at half maximum, FWHM) and the magnetic field (H_{eff}) at the Mössbauer nuclei for different sites are presented in Table 2. The

Table 3—Correlation of ^{57}Fe Mössbauer parameters and crystallite size (by XRD) of chromia substituted Fe_3O_4 catalysts

Sample	Conc. of Cr_2O_3(%)	Γ(Tetra) (mm/s)	Γ(Octa) (mm/s)	% of SP phase	Crystallite size (Å)
P	0.0	0.35	0.45	—	720
A1	8.4	0.35	0.60	—	600
B1	9.86	0.35	0.78	2	410
C1	9.62	0.50	0.78	10	480
B2	15.01	0.69	0.86	20	390
C2	14.76	0.86	0.95	30	310
A3	18.71	0.60	0.69	—	410
B3	19.74	0.50	0.95	25	360
C3	19.48	—	—	90	100

Table 4—Proposed molecular formulae of the chromia-promoted Fe_3O_4 having vacancies

Concentration of Cr^{3+} x (%)	Molecular formulae	No. of vacancies per unit cell
0 (0)	$(Fe^{3+}_1)_A\,(Fe^{3+}_1\ Fe^{2+}_1)_B\,O_4$	0
1/6 (5.5)	$(Fe^{3+}_1)_A\,(Fe^{3+}_{11/12}\ Cr^{3+}_{1/6}\ Fe^{2+}_{7/8}\ \square_{1/24})_B\,O_4$	1/3
1/5 (6.6)	$(Fe^{3+}_1)_A\,(Fe^{3+}_{9/10}\ Cr^{3+}_{1/5}\ Fe^{2+}_{17/20}\ \square_{1/20})_B\,O_4$	2/5
1/4 (8.3)	$(Fe^{3+}_1)_A\,(Fe^{3+}_{7/8}\ Cr^{3+}_{1/4}\ Fe^{2+}_{13/16}\ \square_{1/16})_B\,O_4$	1/2
1/3 (11.0)	$(Fe^{3+}_1)_A\,(Fe^{3+}_{5/6}\ Cr^{3+}_{1/3}\ Fe^{2+}_{3/4}\ \square_{1/12})_B\,O_4$	2/3
1/2 (16.5)	$(Fe^{3+}_1)_A\,(Fe^{3+}_{3/4}\ Cr^{3+}_{1/2}\ Fe^{2+}_{5/8}\ \square_{1/8})_B\,O_4$	1

Mössbauer parameters of sample P are close to the values reported elsewhere[5,6,8,21]. Table 3 offers an opportunity to correlate various Mössbauer parameters with particle size determined from XRD. The sextet arising from the tetrahedral site for A1, B1 and C1 does not show appreciable broadening in comparison to P. However, the same sextet exhibits broadening in B2, B3 and C2. The line width for the sextet arising from the octahedral site in the A, B and C series progressively increases with the increase in Cr^{3+} concentration and it is minimum in A series, medium in B series and maximum in C series. The fact that the line broadening is insignificant for the sextet arising from the tetrahedral site, whereas it is appreciable for that arising from the octahedral site even for A1, B1 and C1, indicates the inclusion of Cr^{3+} at the octahedral site of Fe_3O_4 lattice. In the spectrum of C3 an intense superparamagnetic doublet in the background of feeble unresolved sextet indicates an abrupt enhancement in the concentration of ultrafine particles. At this concentration of Cr^{3+} ions, strains produced by the Cr^{3+} in the lattice may induce disruption, whereby the crystallisation of the sample is highly inhibited. This has been corroborated by XRD.

Though there are two species of Fe ions viz., Fe^{2+} and Fe^{3+} at the octahedral site in Fe_3O_4, one observes[21] a single set of sextet with broad lines due to electron hopping between Fe^{2+} and Fe^{3+} ions. In the case of rapid hopping, only a time-averaged hyperfine field is experienced by all the nuclei located at the octahedral site. Thus the lines for the octahedral site are broader than those for the tetrahedral site even in pure Fe_3O_4. The width of the lines depends on the hopping rate. If the hopping rate slows down, the lines are broadened further. The enhanced broadening of octahedral lines with respect to P may be attributed to slowing down of hopping process and to a distribution of the hyperfine field depending on certain degree of disorder following the inclusion of Cr^{3+} ions. Both the processes are additive so far as the broadening is concerned.

The shoulders (indicated by arrows in Fig. 1) appearing in the spectra of B3 and C2 may be attributed to the limiting low value of hopping rate which causes Fe^{2+} and Fe^{3+} ions at octahedral site to begin to show their distinguishable features.

Role of long range order

The defect structure of solid which includes vacancies, has been reported[22] to be of paramount importance particularly in the case of oxide catalysts which very often participate in the reaction mechanism by simultaneous donation and reception of one of its constituents viz., oxygen. It may be pointed out that the Cr^{3+} substituted Fe_3O_4 lattice contains vacancies, the role of which is described below. The catalysts in the present case have been prepared from γ-Fe_2O_3 which can be represented by a molecular formula[23,24].

$$(Fe^{3+}_1)_A\,(Fe^{3+}_1\ Fe^{3+}_{2/3}\ \square_{1/3})_B\,O_4$$

where $\square$ indicates vacancy. Cr^{3+} ion substitutes Fe^{3+} ions at the octahedral B site in γ-Fe_2O_3. If Cr^{3+} replaces an equal amount of Fe^{3+} ions from octahedral sites producing a compound $Fe_{2-x}Cr_xO_3$, the molecular formula showing cationic distribution in A and B sites may be described as,

$$(Fe^{3+}_1)_A\,(Fe^{3+}_{1-x/2}\ Cr^{3+}_x\ Fe^{3+}_{2/3-x/2}\ \square_{1/3})_B\,O_4 \qquad \ldots (1)$$

where x is the concentration of Cr^{3+} ions. The sample under investigation is basically a catalyst in the

reduced state, which being the reduced form of (1), may be represented as,

$$(Fe^{3+}_1)_A (Fe^{3+}_{1-x/2}\ Cr^{3+}_x\ Fe^{2+}_{1-3x/4}\ \square_{x/4})_B\ O_4 \quad \ldots (2)$$

This implies that unlike the parent oxide Fe_3O_4, the chromia-promoted catalyst in its reduced form always contains vacancies whose number depends on the chromia concentration.

Haneda and Morrish[15] showed that with 8/3 cation vacancies per unit cell, γ-Fe_2O_3 exhibits superlattice lines in the X-ray diffraction pattern arising from the long range ordering of the vacancies, provided particle sizes are $\geqslant 300$ Å. The long range order is predominant at some critical stoichiometries. At non-stoichiometric situations around these critical compositions, the material is only partly ordered. The molecular formula (2) shows that at very low concentration of Cr^{3+} ions, vacancies are widely dispersed. Only for the concentration of Cr^{3+} ion represented by $x = 1/6, 1/5, 1/4, 1/3$ and $1/2$, critical stoichiometry having long range vacancy ordering is of significance. Table 4 presents the exact molecular formula of chromia-promoted active catalyst for various concentrations of Cr^{3+} ions.

The vacancy concentration increases with the concentration of Cr^{3+} ions, facilitating the long range order, whereas the particle size decreases (Table 3) with increase in the concentration of Cr^{3+} ions, imhibiting the order. It is observed that at $\sim 15\%$ Cr^{3+} concentration (samples B2, C2), the strain produced in the lattice is sufficient to disrupt it, as has been observed by the appearance of superparamagnetic particles (20%-30%) and by the decrease of particle size (Table 3). Since up to the concentration of the order of 10% the particle size is sufficiently large, the vacancies in the system and consequently the included Cr^{3+} ions are expected to exhibit high degree of order. In this situation the widths of the lines arising from tetrahedral sites are more or less close to that of the parent oxide, as expected. The broadening of the lines arising from octahedral sites in A1, B1 and C1 may be attributed to the reduction in the electron hopping rate. The additional broadening of the sextet due to ions at octahedral sites in B2, B3 and C2 is indicative of break down of long range order because of the pronounced reduction of particle size.

Of all the samples investigated, sample C1 acts as the best catalyst[9]. Even this sample contains 10% ultrafine particles indicative of the onset of lattice instability. Doppler *et al.*[8] have reported that chromia-promoted catalyst with Cr^{3+} concentration at $\sim 8\%$ is the best. These facts suggest that the optimum catalyst is one which contains 8.3% of Cr^{3+} ions so as to retain large particle size as well as enough vacancies to support long range order. At this concentration electron hopping between Fe^{2+} and Fe^{3+} at octahedral site is well maintained. Though the catalytic activity is usually related to exposed surface area, the catalyst C1 having a large particle size and hence less surface area acts as the best catalyst, contrary to the expectations. This perhaps upholds a new feature wherein the role of cationic ordering/vacancies and the charge hopping on the catalytic activity is being emphasized by the present investigation.

The results obtained in the present investigation help us to arrive at the following conclusions:

The incorporation of Cr^{3+} ions stabilises the γ-Fe_2O_3 lattice as revealed by TG and XRD studies. The IR and Mössbauer studies indicate that Cr^{3+} ions occupy the octahedral sites of Fe_3O_4 spinel. It is also revealed that up to Cr^{3+} concentration of the order 10%, the long range order is retained and the electron hopping between Fe^{3+} and Fe^{2+} at the octahedral sites is well maintained. The ordering of cations/vacancies and the charge hopping show an influence on the catalytic activity.

Accordingly, the catalytic activity of the water gas shift reaction can be improved by means of careful optimisation of Cr^{3+} ion concentration, particle size and the charge hopping by preparing the catalyst through a suitable route.

References

1 Newsome D S, *Catal Rev Sci Engng*, 21 (1980) 275.
2 Maiti G C & Ghosh S K, *Indian J Chem*, 24 (1985) 513.
3 Dicerbo R K & Seybolt A K, *J Am Ceram Box*, 42 (1959) 430.
4 Levenstein H J, Robbins M & Capio C, *Mat Res Bull*, 7 (1972) 27.
5 Topsoe H & Boudart M, *J Catal*, 31 (1973) 346.
6 Robbins M, Wertheim G K, Sherwood R C & Buchanan D N E, *J phys Chem Solids*, 32 (1971) 717.
7 Volenik K, Hanousek F & Strauch B, *Czech J Phys*, B31 (1981) 86.
8 Doppler G, Trautwein A X, Ziethen H M, Ambach E, Lehnert R, Sprague M J & Gonser U, *Applied Catalysts*, 40 (1988) 119.
9 Kundu M L, Sengupta A C, Maiti G C, Sen B, Ghosh S K, Kuznetsov V I, Kustova G N & Yurchenko E N, *J Catal*, 112 (1988) 375.
10 Borgers D G & Bridges G W, *Chemy Ind*, 19 (1968) 1426.
11 Borgers J & Campell J S, *Ammonia*, Vol. 3 (Marcel Dekker Inc N.Y.) 1977, p. 57.
12 Sengupta G, Gupta D K, Kundu M L & Sen S P, *J Catal*, 67 (1981) 223.
13 Sengupta A C, Ph.D. Thesis (1988) Indian School of Mines, Dhanbad, India.
14 Van Oosterhout G W & Rooijmans C J M, *Nature*, 181 (1958) 44.
15 Haneda K & Morrish A H, *Solid State Commun*, 22 (1977) 779.
16 Preudhomme J & Tarte P, *Spectrochim Acta*, A27 (1971) 1817.

17 Ishii M, Nakahira M & Yamanaka T, *Solid State Commun*, 11(1)(1972) 209.
18 Smit J & Wijn H P J, *Ferrites* (Wiley, New York) 1959.
19 Gillot B, Jemmali F & Rousset J, *Solid State Chem*, 50 (1983) 138.
20 Kundig W, Bommel H, Constabaris G & Lindquist R H, *Phys Rev*, 142 (1966) 327.
21 Kundig W & Hargrove R S, *Solid State Commun*, 7 (1969) 223.
22 Haber J, *Catalysis science and technology*, edited by J R Anderson & M Boudart (Springer-Verlag Berlin, Heidelberg N.Y.) Vol. 2, 1981, p. 13.
23 Verwey E J W, *Z Kristallogr*, 91 (1935) 65.
24 Kordes E, *Z Kristallogr*, 92 (1935) 139.

Indian Journal of Chemistry
Vol. 31A, December 1992, pp. 915-920

Effect of alkali halide additives on the gamma radiolysis of thorium nitrate

(Miss) N G Joshi & A N Garg*

Department of Chemistry, Nagpur University, Nagpur 440 010, India

Received 27 January 1992; revised 15 May 1992; accepted 2 September 1992

Gamma radiolytic decomposition of thorium nitrate and its binary mixtures with potassium halides has been studied over a wide absorbed dose range (upto 600 kGy) and at different compositions. $G(NO_2^-)$ values decrease on the addition of halides, except for several fold enhancement at 75% composition in low dose region. A part of the energy is taken up by the additive and later transferred to the nitrate thus affecting its decomposition. Reflectance spectra of irradiated binary mixtures show characteristic bands corresponding to the formation of X_2^- and colour centres (V and F). Thermoluminescence (TL) studies of pure halides and its binary mixtures with thorium nitrate suggest the formation of radical species affecting the decomposition. EPR measurements on γ-irradiated thorium nitrate indicate the presence of $^{\cdot}NO_2$, O_3^- and O_2^-. A plausible mechanism has been proposed.

Gamma ray induced decomposition of inorganic nitrates is affected by several factors such as size, charge and polarizability of the cation[1-4] free space volume in the crystal lattice[3], water of crystallization[5], linear energy transfer, absorbed dose[6,7] and the nature and concentration of additives[8-10]. Several workers[11-14] have observed that alkali halides and other additives act as sensitizer in the gamma radiolysis of nitrate systems. Jones[15] first showed that decomposition of KNO_3 is enhanced by the KBr addition. Earlier we have studied gamma radiolytic decomposition of zirconium nitrate with potassium halides[16] and pure thorium nitrate in hydrated and anhydrous forms[5]. In order to further investigate the effect of halide additives and the mechanism of decomposition we have carried out γ-radiolysis of binary mixtures of thorium nitrate with KCl, KBr and KI at different doses and compositions. EPR, reflectance spectra and thermoluminescence measurements have been carried out to support the formation of radical species participating in the γ-radiation induced decomposition. Results on decomposition of thorium nitrate by 100 MeV ^{12}C beam are also reported.

Materials and Methods

Thorium nitrate was of Analar grade (BDH). All the halides were of GR grade (S. Merck). Solutions were prepared in doubly distilled water. Binary mixtures of thorium nitrate with potassium halides were prepared by mechanical grinding of the weighed amounts in an agate mortar (50 mesh). All irradiations were carried out in a Cobalt-60 Gamma Chamber-900 at a dose rate of 0.90 kGy h^{-1} determined by Fricke dosimeter with $G(Fe^{3+}) = 15.6$. It was also checked using alanine dosimeter[17] at BARC. The radiation damage product $[NO_2^-]$ was estimated by following modified Shinn's method of diazotization[18,19]. The absorbances were recorded at $\lambda_{max} = 540$ nm using a Shimadzu Model-240 spectrophotometer. $G(NO_2^-)$ values of binary mixtures of halides on the basis of corrected dose were calculated by electron fraction[20]. Reflectance spectra of solid powders were recorded on a Shimadzu Model UV 240 spectrophotometer. EPR measurements of γ-irradiated thorium nitrate were carried out on a Brucker ESP 800 EPR X-band spectrometer using microwave frequency of 9.74 GHz and DPPH as the field marker. Thermoluminescence (TL) of the irradiated samples were recorded at a linear heating rate of 150 K min^{-1} using an Indotherm temperature control in conjunction with a RCA 931A photomultiplier and a millivolt recorder.

About 1 g thorium nitrate was pelletised in a circular disc (dia 10 mm; thickness 3 mm) and bombarded with 100 MeV ^{12}C beam for 5 min at 9.6×10^{12} particles cm^{-2} in a 15 UD Pelletron at the Nuclear Science Centre, New Delhi.

Results and Discussion

Radiolytic decomposition of thorium nitrate and its binary mixtures with KCl, KBr and KI was studied at 25, 50, 60, 75 and 85% compositions

and at various absorbed doses upto 600 kGy. $G(NO_2^-)$ values for pure thorium nitrate and its binary mixtures with halides vary with the absorbed dose. A typical plot for 75% KX composition is shown in Fig. 1. In Table 1 are listed $G(NO_2^-)$ values for pure thorium nitrate and 25% binary mixtures with KX at different doses.

All inorganic nitrates undergo decomposition under the influence of gamma radiation to yield NO_2^- and O_2 as final products[1,21]. Chen and Johnson[7] have proposed the following mechanism:

$$NO_3^- \rightsquigarrow NO_2^- + O \quad \ldots (i)$$

$$NO_3^- + O \rightarrow NO_2^- + O_2 \quad \ldots (ii)$$

$$NO_2^- + O \rightarrow NO_3^- \quad \ldots (iii)$$

$$O + O \rightarrow O_2 \quad \ldots (iv)$$

Various experimental evidences have shown that NO_2^- is not formed directly but via ionization and/or excitation of NO_3^- followed by the formation of species such as NO_3^{2-}, NO_2^{2-}, NO_2, $^*NO_3$, etc. Room temperature electron spin resonance spectra of thorium nitrate irradiated at 200 kGy (Fig. 2) shows a triplet and a singlet due to $^*NO_2$ ($g_{av} = 2.0112$ and $A = 60$ G) and O_3^- ($g_{av} = 2.0110$) radical species respectively[22]. g_{av} values of these radical species are comparable with those reported by Silver *et al.*[23] and Tagaya[24]. High resolution studies with decrease in modulation also showed the presence of O_2^- with $g_{av} = 2.0135$ ($g_{\parallel} = 2.036$ and $g_{\perp} = 2.001$). Bennett *et al.*[25] have proposed

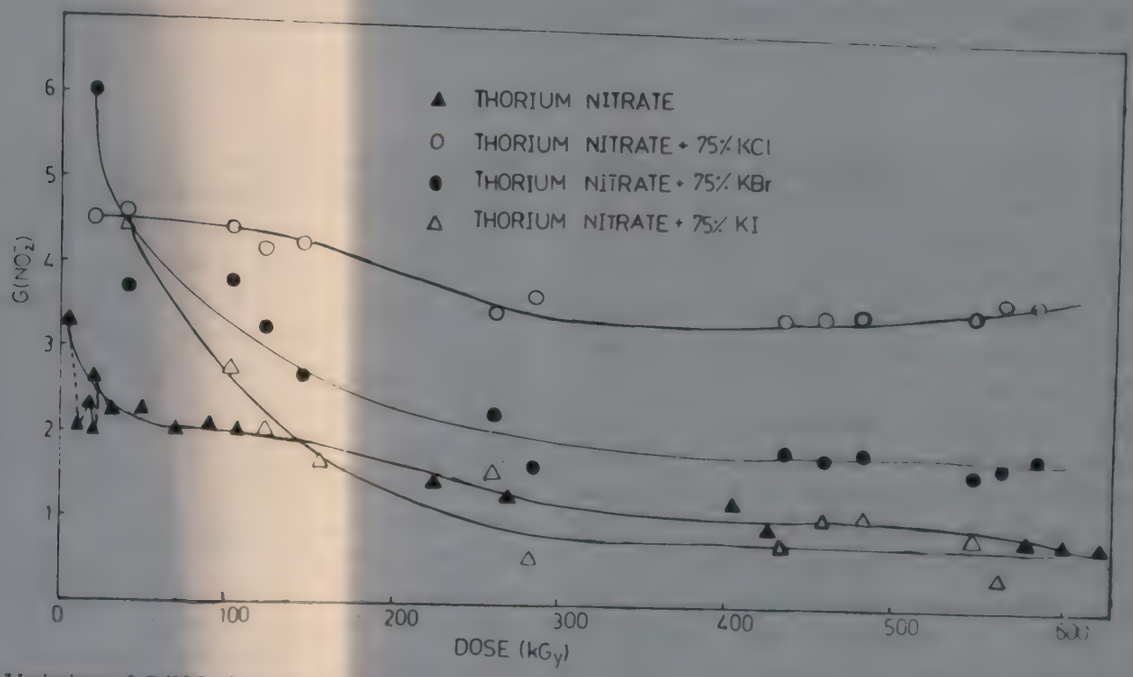

Fig. 1—Variation of $G(NO_2^-)$ with absorbed dose in thorium nitrate and its binary mixtures with potassium halides.

Table 1—$G(NO_2^-)$ values of thorium nitrate and its 25% binary mixtures with potassium halides at different doses

Dose (kGy)	$G(NO_2^-)$			
	$Th(NO_3)_4$	$Th(NO_3)_4 + KCl$	$Th(NO_3)_4 + KBr$	$TH(NO_3)_4 + KI$
63.4	2.1 ± 0.1	0.74 ± 0.06	0.50 ± 0.03	—
148	1.85 ± 0.07	0.91 ± 0.07	0.71 ± 0.06	0.85 ± 0.09
191	1.65 ± 0.08	0.81 ± 0.06	0.59 ± 0.07	0.48 ± 0.08
275	1.20 ± 0.10	0.70 ± 0.03	0.59 ± 0.06	0.27 ± 0.08
362	1.00 ± 0.03	0.55 ± 0.04	0.56 ± 0.03	0.27 ± 0.04
474	0.95 ± 0.03	0.41 ± 0.03	0.29 ± 0.06	0.013 ± 0.003
f*	—	0.743	0.755	0.764

*Electron fraction factor for binary mixtures with halides. Dose was corrected using these factors.

larger value of $g_{\parallel}$ due to a hole in the π^* level and a negative shift for $g_{\perp}$ arising from incomplete quenching of the orbital motion.

It has been observed that, in general, $[NO_2^-]$ increases linearly with the absorbed dose. At low doses the overall reaction follows a first order kinetics with the absorbed dose and is governed by the rate law[4]: $[NO_2^-] = kD$ where k is the rate constant and D is absorbed dose. In the higher dose range, however, and for some compositions, decomposition process seems to become complex due to predominance of the backward reaction[5], $(NO_2^- + O \rightarrow NO_3^-)$. It has been suggested that, rate determining reactions may be accelerated or retarded depending on the absorbed dose, nature of cation, nature and amount of impurities or additive[1,3,10,14].

Furukawa and Ohno[26] have reported decomposition of KNO_3 by 100 keV ions extracted from a discharge of He, N_2 and O_2. In our experiments using ^{12}C beam, $[NO_2^-] = 13 \pm 2$ ppm was observed. This is much less compared to other nitrates (of Na, K, Zr) presumably because a major fraction of energy is shared by Th having Z = 90.

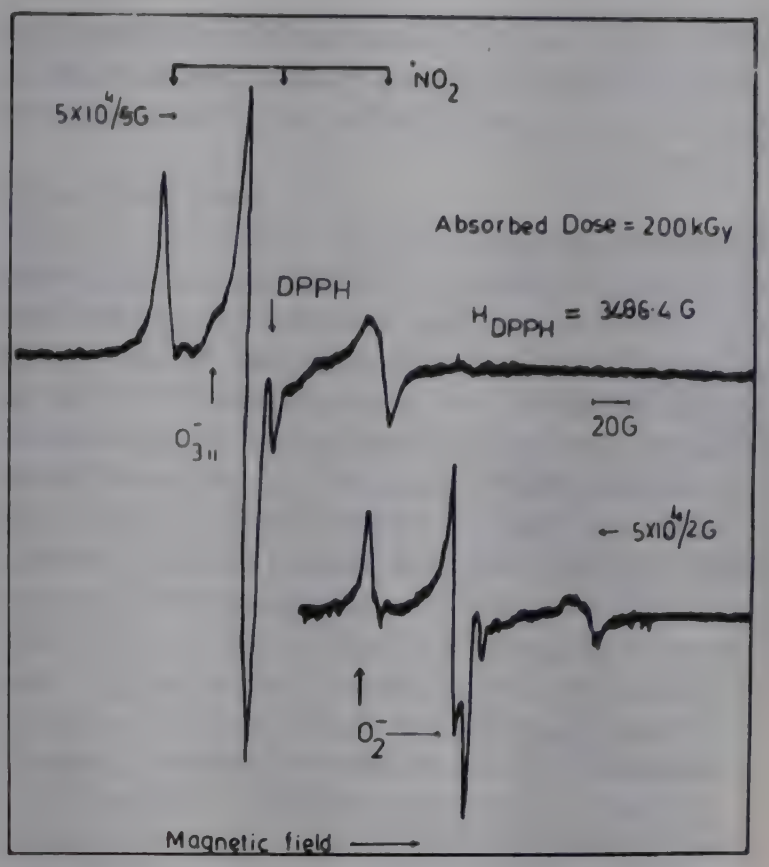

Fig. 2—Room temperature ESR spectrum of thorium nitrate irradiated by ^{60}Co γ-rays at an absorbed dose of 200 kGy (sweep scale, 3480/kG).

Variation of $G(NO_2^-)$

In general, $G(NO_2^-)$ values for thorium nitrate and its binary mixtures show exponential decreasing trend with the absorbed dose. Earlier, a similar trend was observed for anhydrous and hydrated thorium nitrates[5]. However, the extent of variation depends on the nature of additive and the composition of binary mixtures. In lower composition range of 25-60% halides, change is not so significant but at higher concentrations of the halides (beyond 60%), it becomes more prominent. It is observed from Fig. 1 that at 75% KX composition, $G(NO_2^-)$ of all the binary mixtures is enhanced in the entire dose range upto 600 kGy except for the binary mixture with KI in the dose range beyond 150 kGy.

In the lower dose region, variation of $G(NO_2^-)$ is not smooth but somewhat irregular. The enhancement is in the order: KBr > KCl > KI. It is further observed from Fig. 1 that for KCl binary mixture, $G(NO_2^-)$ does not decrease exponentially but instead it remains almost constant in the entire dose range. Maximum enhancement in $G(NO_2^-)$ for KBr binary mixtures in low dose range is in agreement with the observations of Franklin *et al.*[27] who suggested more efficient energy transfer by KBr in solids.

In Fig. 3 is plotted $G(NO_2^-)$ versus composition for thorium nitrate binary mixtures with KBr at three different doses of 20, 200 and 300 kGy. It

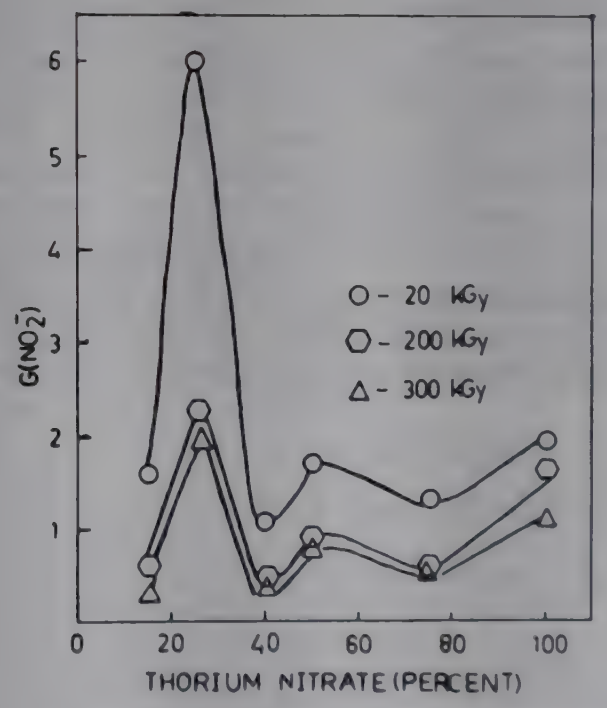

Fig. 3—Variation of $G(NO_2^-)$ with percent compoisiton of thorium nitrate in $KBr + Th(NO_3)_4$ system at various doses.

is observed that the enhancement is maximum (by three-fold) at 20 kGy but its extent decreases with increasing absorbed dose. With the addition of KBr, first $G(NO_2^-)$ values decrease and then at 75% of KBr G-values are maximum at all the doses. Interestingly, on further addition of KBr, G-values are lowered even compared to those for pure thorium nitrate. It suggests the formation of

some typical radical species in KBr systems which seem to be dependent on composition as well as dose and are responsible for the enhancement of G-values.

Reflectance spectra

The binary mixtures of thorium nitrate with KCl, KBr and KI show purple, blue-green and brown-yellow colours respectively upon γ-irradiation, similar to earlier observations[12,16]. This is primarily due to the formation of colour centres and radical (defect) species[12,28] as evidenced by a characteristic band at 400 nm (Fig. 4) in all cases. Binary mixture of KCl shows another intense band at 560 nm. For binary mixture with KBr additional bands are observed at 490 and 630 nm whereas in the case of binary mixture with KI only a shoulder at 700 nm is observed. These may be assigned to the formation of X_2^- and F centres on the basis of literature studies[28,29]. Hersh[27] reported a band at 560 nm for X-ray irradiated KCl and attributed it to the formation of F-centre. It seems that the position of F-centre band depends on the nature of the halide; it shifts from 560 nm (KCl) to 630 nm (KBr) and finally to 700 nm (KI). Dhoble *et al.*[30] have observed that in the case of pure KI, the intensity of F-band decreases with particle size, while the intensity of V-band at 360 nm increases. Therefore, in the case of binary mixtures with KI the shoulder at 700 nm is essentially due to F-centre. Hence, the colour centres formed in binary mixtures upon γ-irradiation seem to interact with the transient radical species (NO_3^{2-}, NO_3^*, $^*NO_2$ etc.) in a complex manner and thus affect $G(NO_2^-)$. For binary mixture with KBr, a medium intensity band observed at 490 nm is difficult to assign. Probably the species corresponding to it may be responsible for the anomalous enhancement of decomposition.

Thermoluminescence (TL) studies

TL glow plots were recorded for γ-irradiated KX and their binary mixtures with thorium nitrate. Typical TL plots of KCl and KCl + 75% $Th(NO_3)_4$ are shown in Fig. 5.

TL studies of pure KCl, KBr and KI exhibit characteristic glow peaks at 360, 420 and 390 K respectively due to the recombination of F-centres with interstitial halogen atoms which are thermally released from traps[31]. Interestingly, pure $Th(NO_3)_4$ irradiated at 50 kGy does not show any glow peak (Fig. 5) suggesting a positive role of defect centres formed by alkali halides. In the case of binary mixtures with 75% KX, however, a glow peak at 415 ± 5 K is observed whereas binary mixture of KCl and KBr show an additional peak at 480 K. Evidently intensity of glow peaks is reduced significantly suggesting the interaction of the species. Delgado and Alvarez Riwas[32] suggested that irradiated alkali halides store energy which is later released. It may be noted that intensity of glow peaks for KBr and its binary mixture is approximatley 30 times higher compared to that for KCl and KI systems. This may provide further evidence for the role of KBr in accelerating the decomposition process.

Energy transfer

It is now well known that additives like

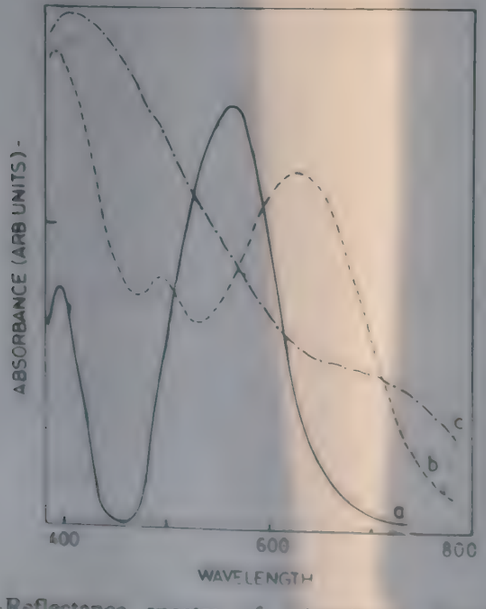

Fig. 4—Reflectance spectra of γ-irradiated thorium nitrate + 85% KCl (a), KBr (b) and KI (c)

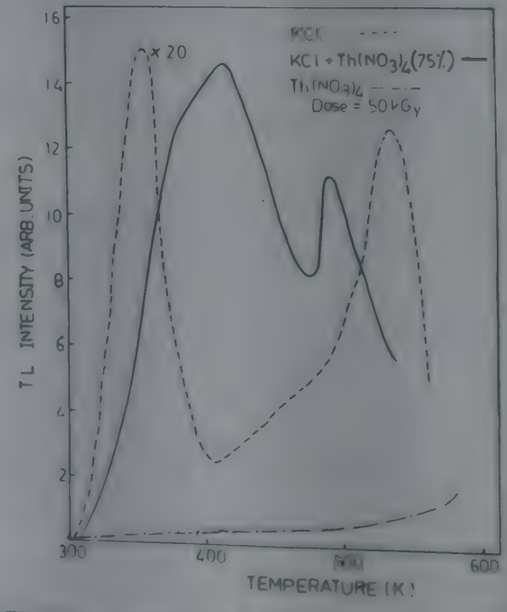

Fig. 5—TL-Glow curves for KCl and its binary mixture with 75% $Th(NO_3)_4$ irradiated at an absorbed dose of 50 kGy.

halides[11,12,20], oxides[9], sulphates and carbonates[14] act as medium for energy transfer in the decomposition process. It has been proposed that the energy transfer process may take place in terms of electron migration[33,34] or by exciton transfer[35]. Since a minimum of ~ 4 eV is required to cause dissociation of nitrate ion, only matrix materials having higher energy gap will be effective in causing the energy transfer. In the present studies on the radiolysis of binary mixtures of thorium nitrate with halides both self-irradiation (internal α-irradiation) and external gamma irradiation are operative. However, the contribution of internal α-irradiation has been eliminated by applying appropriate blank correction.

It is observed that the extent of enhancement of $G(NO_2^-)$ by halides is much smaller in higher dose region. Kalkar *et al.*[36] have suggested the role of colour centres in energy transfer. On γ-irradiation alkali halides give rise to V- and F-centres and species such as X_3^-, X_2^- and X_2. Presumably, the colour centres and radical species may react with the intermediates of NO_3^- in the binary mixture in following manner:

Primary process

$KX \rightsquigarrow (X_2^-, V)$ and (F-centres e^-) etc.

$NO_3^- \rightsquigarrow {}^{\bullet}NO_3^*, NO_3^{2-}, {}^{\bullet}NO_2$ etc.

Secondary process

$$NO_3^- + X_2^- \rightarrow {}^{\bullet}NO_3 + 2X^-$$

$${}^{\bullet}NO_3^* + NO_3^{2-} \rightarrow 2NO_2^- + O_2$$

$${}^{\bullet}NO_3^* + e^- \rightarrow NO_2^- + 1/2\,O_2$$

$${}^{\bullet}NO_3^* + h\nu \rightarrow {}^{\bullet}NO_2 + O$$

It is not clear from EPR spectral evidence (Fig. 2), as to what is the role of O_2^- and O_3^- formed during γ-radiolysis of $Th(NO_3)_4$. It is evident from Fig. 3 that somewhat separate mechanisms seem to be operating at different compositions of binary mixtures. In the case of 75% KX compositions (specially with KBr) $G(NO_2^-)$ values are higher than that for thorium nitrate suggesting that radical species which accelerate the decomposition are composition-dependent. It means that at lower (or even higher) composition of the binary mixtures with halides the backward reaction ($NO_2^- + O \rightarrow NO_3^-$) may become predominant lowering the rate of formation of NO_2^-.

Therefore, efficiency of energy transfer resulting in enhanced decomposition of thorium nitrate is dependent on the nature of additive, its concentration and absorbed dose. This is essentially due to the interaction of colour centres and the radical species formed during γ-irradiation.

Acknowledgement

Our sincere thanks are due to the authorities of the Nagpur University for the award of a research studentship and to the CSIR, New Delhi for an SRF award to one of us (NGJ). Grateful thanks are due to Drs M.D. Sastry and V. Natarajan, Radiochemistry Division, BARC, Bombay for EPR measurements and to Prof. G.K. Mehta, Director, NSC, New Delhi for permission to use Pelletron. We also wish to thank one of the referees for his helpful comments in improving the manuscript.

References

1 Johnson E R, *The radiation induced decomposition of inorganic molecular ions* (Gordon and Breach Science Publishers, New York), 1970.
2 Batra R J & Garg A N, *Radiochem Radioanal Lett*, 53 (1982) 177.
3 Kulkarni S P & Garg A N, *Indian J Chem*, 23A (1984) 712.
4 Kulkarni S P & Garg A N, *J radioanal nucl Chem Lett*, 153 (1991) 211.
5 Garway D G, Parwate D V & Garg A N, *Indian J Chem*, 27A (1988) 708.
6 Johnson E R, *J Am chem Soc*, 80 (1958) 4460.
7 Chen T H & Johnson E R, *J phys Chem*, 66 (1962) 2249.
8 Nevostruev V A, Zakharov Yu A & Kirov S M, *Politokh Inst Tomsk Kinet Katal*, 8 (1967) 210.
9 Patil S F, Bhoite S A & Bedekar A G, *J radioanal nucl Chem Lett*, 93 (1984)133.
0 Kulkarni S P & Garg A N, *Int J Radiat Phys Chem*, 32 (1988) 609.
11 Srivastava S B, Sarpotdar A S & Shankar J, *Indian J Chem*, 8 (1970) 426; 9 (1971) 144.
12 Batra R J & Garg A N, *J radioanal nucl Chem Art*, 129 (1989) 335.
13 Zhukova T N, Ershov B G & Pikaev A K, *Khim Vys Energy*, 6 (1972) 376.
14 Kulkarni S P, Batra R J & Garg A N, *Radiat Effects and Defects Solids*, 113 (1990) 315.
15 Jones A R, *J chem Phys*, 35 (1961) 751.
16 Joshi N G & Garg A N, *J radioanal nucl Chem, Art*, 142 (1990) 515.
17 Gupta B L, Bhat R M, Narayan G R & Nilekani S R, *Int J Radiat Phys Chem*, 26 (1985) 647.
18 Shinn M B, *Ind Engng Chem Anlyt Edn*, 13 (1941) 33.
19 Kershaw N F & Chamberlin N S, *Ind Engng Chem Analyt Edn*, 14 (1942) 312.
20 Khare M & Johnson E R, *J phys Chem*, 74 (1970) 4085.
21 Muhammad D & Maddock A G, *J chem Soc Faraday Trans I*, 74 (1978) 919.
22 Atkins P W & Symons M C R, *Structure of inorganic radicals* (Elsevier Publishers, Amsterdam) 1967.
23 Silver B L, Koresh J, Schhick S & Luz Z, *Molec Phys*, 22 (1971) 225.
24 Tagaya K, *Japan J appl Phys*, 24 (1985) 75.

25 Bennett J E, Ingram D J E, Symons M C R, George P & Griffith J S, *Phil Mag*, 46 (1955) 443.
26 Furukawa K & Ohno S, *Bull chem Soc Japan*, 58 (1958) 1831.
27 Franklin M L, Hisatune J C & Miller W W, *Radiat Effec*, 82 (1984) 199.
28 Hersh H N, *J chem Phys*, 2 (1957) 1330.
29 Robinson V J & Chandratillake M R in *Radiation chemistry: Principles and applications*, edited by Farhataziz and M A J Rodgers (VCH Publishers, New York) 1987, 437.
30 Dhoble S J, Sahare P D & Moharil S V, *J Phys C Condens Matter*, 3 (1991) 1189.
31 Mariani D F & Alvarez Riwas J L, *J Phys C Solid State Phys*, 11 (1978) 3499.
32 Delgado L & Alvarez Riwas J L, *J Phys C Solid State Phys*, 13 (1980) 1185.
33 Sagert N H & Robinson R W, *Can J Chem*, 72 (1968) 2075.
34 Wong P K & Willard J E, *J phys Chem*, 72 (1968) 2623.
35 Rabe J E, Rabe B & Allen A O, *J phys Chem*, 70 (1966) 1098.
36 Kalkar C D, Khare V H & Patil V, *Appl Radiat Isot*, 39 (1988) 237.

Indian Journal of Chemistry
Vol. 31A, December 1992, pp. 921-928

Conversion of methanol over metal salts of 12-molybdophosphoric acid

Fikry M Ebeid, Laila I Ali*, Nabil H Amin & Fawzia F Abd-Alla
Chemistry Department, Faculty of Education, Ain-Shams University, Heliopolis, Cairo, Egypt

Received 30 May 1991; revised 3 February 1992; accepted 1 April 1992

The effect of ionic size of the counter cation and its electronegativity on the conversion of methanol to dimethyl ether and methane over sodium, calcium, magnesium and zinc salts of dodecamolybdophosphoric acid has been studied. The reaction has been carried out in a flow system. It has been found that the zinc salt which has the highest electronegativity and the smallest cation radius is the most active catalyst. The higher activity observed at lower calcination temperatures may be explained by the concept of pseudo liquid phase. The results indicate that methane is formed by a consecutive reaction. The effect of pyridine on both products has also been studied. It is found that the formation of ether is more inhibited by pyridine than methane. Ether formation follows a second order equation of Langmuir-Hinshelwood type, whereas methane formation follows a first order equation.

The dehydration of methanol to dimethyl ether is a well known reaction catalysed by solid acidic oxides[1,2], while its conversion into hydrocarbons on heteropoly compounds has been reported only during the last decade[3-8]. Ono *et al.*[9,10] found that copper(II) and silver(I) salts of dodecatungstophosphoric acid and dodecatungstosilicic acid are active catalysts for the conversion of methanol into dimethyl ether and hydrocarbons. It was found[3,8,11] that dimethyl ether is a precursor for hydrocarbons and that the weakly acidic sites may be sufficient to catalyze the formation of the ether. The active sites are assumed[3] to be Brönsted acid sites. The catalytic activity of tungstophosphoric acid and its salts is proportional to acid strength[8,12,13].

The acidity of the salts of heteropoly acids[14-17] is due to: (i) the dissociation of the water coordinated to metal cation (M^{n+}), (ii) proton generation from H_2 or H by the reduction of metal cations like Ag^+ and Cu^{2+}, and (iii) protons are formed by the partial hydrolysis of anions in the preparation process. The acidic properties of molybdophosphoric acid and tungstophosphoric acid, i.e., the amount of acidity, its type (Brönsted or Lewis) and its strength were studied by many authors[18-21]. From IR spectra of adsorbed pyridine it was found[18,21] that pyridine is present in the form of the pyridinium ion. Number of surface acidic protons on heteropoly acids is comparable with the number of Brönsted acid sites on silica-alumina[22] and heteropoly acids are stronger in acidity[18] than Al_2O_3-SiO_2. The changes in the calcination conditions may alter both the number and strength of the acidic sites[3]. The acidity of salts of dodecamolybdophosphoric acid is strongly affected by the electronegativity of the cation as well as its amount[23,24]. Salts of cations with lower electronegativity are less acidic whereas the most electronegative cation has the maximum activity.

The aim of this work is to study the activity of the catalyst with time, the effect of calcination temperature, to compare the catalytic activity of Na, Ca, Mg and Zn salts of 12-molybdophosphoric acid towards the conversion of methanol, the effect of pyridine on ether and methane formation and to throw some light on the reaction mechanism.

Materials and Methods

The procedure, apparatus and catalyst preparation have been given elsewhere[10,25]. The particle size of the catalysts used is 0.2-0.3 mm except with the calcium salt ($\leqslant$0.1 mm) which was difficult to obtain in the required particle size. Each catalyst specimen was activated by heating at 400°C in a stream of pure and dry H_2 for 4 hrs before measurements, then the temperature was lowered to the desired reaction temperature. A series of ether and methane standards in argon were prepared to determine the amount of the ether and methane produced. The effect of pyridine (5% and 19% v/v in the alcohol feed) on the formation of both ether and methane at constant temperature and constant argon flow was studied. The reaction products were analysed chromatographically using 3700 Varian Gas Chromatograph with flame ionisation detector. The column used was packed with 10% squalane supported on chromosorb. All the chemicals used in this study were pure grade as indicated by chromatographic analysis.

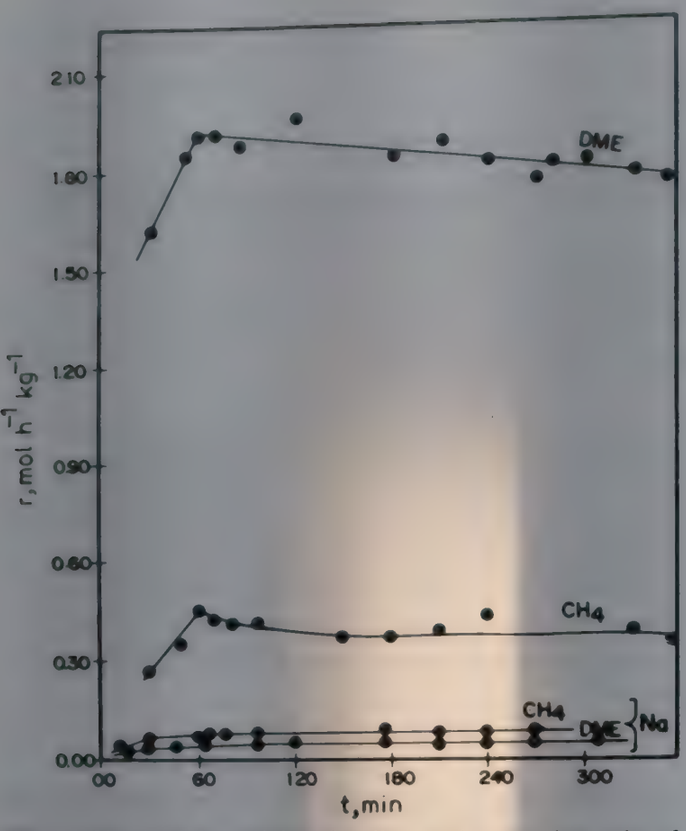

Fig. 1—Check of the activity of sodium and magnesium salts of molybdophosphoric acid towards the formation of dimethyl ether and methane at different time intervals. [$^{p}CH_3OH = 102$ torr, temp. = 300°C.]

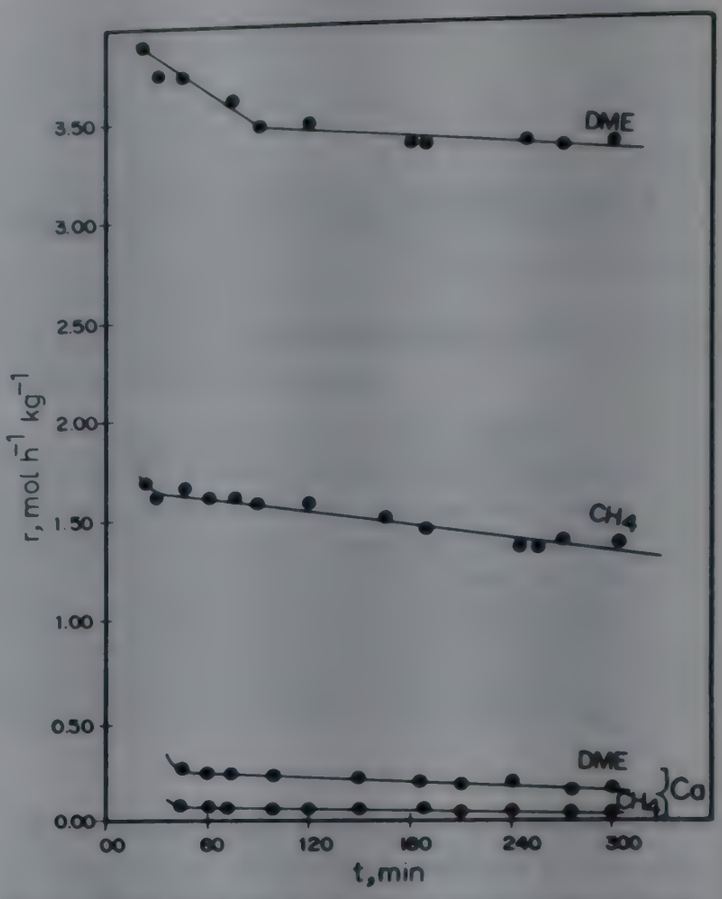

Fig. 2—Check of the activity of calcium and zinc salts of molybdophosphoric acid towards the formation of dimethyl ether and methane at different time intervals. [$^{p}CH_3OH = 102$ torr; temp. = 300°C.]

Results

Catalyst activity with time

The activities of all the catalysts used towards the conversion of methanol were determined in terms of the rate formation of both the products. The activity was checked at different time intervals under fixed experimental conditions. It was observed with Na salt catalyst (Fig. 1) that the activity towards ether and methane formation increases with time from the beginning of the run and reaches a constant value after 90 min for ether and 75 min for methane, then it remains constant for about 3½ hrs. The activity of Mg salt catalyst towards ether formation reaches after 6 hrs to 91% of the steady state value obtained after one hr from start of the run. The activity towards methane formation reaches the steady state after one hr and then remains nearly constant for 5 hrs. It was observed that the activity of Ca and Zn salts towards ether formation decreases to 62% and 87% of the original activity whereas methane formation decreases to 51% and 80% of its original value respectively (Fig. 2).

Effect of calcination temperature on the catalyst selectivity towards dimethyl ether and methane formation

Formation of ether and methane was studied over Zn salt pretreated at 250, 300 and 400°C in H_2 atmosphere for 4 hrs. The reaction temperature was in the range 110-392°C and the partial pressure of methanol was kept fixed at 102 torr. The results (Fig. 3) show that ether formation proceeds at a very low rate up to 110°C, then increases sharply until a maximum is reached at 250°C for both samples pretreated at 250° and 300°C, whereas a shift in the temperature of the maximum to 360°C was observed with the sample pretreated at 400°C. It was also observed that higher calcination temperature inhibits greatly ether formation and has little effect on methane formation.

Effect of partial pressure of methanol on the rate of dimethyl ether and methane at different temperatures

The rates of ether and methane formation were measured at 280, 300 and 320°C at partial pressure of methanol ranging from 30-485 torr over calcium, magnesium and zinc salts of molybdophosphate. With sodium salt the reaction was investigated in the temperature range 300, 320 and 340°C. The results obtained are given in Table 1. It was observed that the rate of ether and methane formation is propor-

Table 1—Effect of partial pressure of methanol on dimethyl ether and methane formation at different temperatures over four catalysts pretreated at 400°C

P_{CH_3OH} torr	r.mol.h^{-1}.kg^{-1}					
	280°		300°		320°	
	DME	CH_4	DME	CH_4	DME	CH_4
			Ca Salt			
31	0.063	0.013	0.165	0.062	0.266	0.153
58	0.109	0.021	0.208	0.079	0.319	0.183
102	0.179	0.030	0.285	0.087	0.390	0.204
211	0.183	0.040	0.333	0.111	0.552	0.241
397	0.185	0.041	0.353	0.109	0.585	0.273
485	0.211	0.043	0.357	0.120	0.574	0.281
			Mg Salt			
31	0.581	0.122	0.984	0.303	1.407	0.624
58	0.994	0.172	1.476	0.396	2.169	0.761
102	1.265	0.190	1.800	0.452	2.742	0.899
211	1.386	0.211	2.109	0.481	2.922	0.843
397	1.530	0.234	2.169	0.468	3.134	0.874
485	1.540	0.250	2.290	0.499	3.194	0.888
			Zn Salt			
31	1.864	0.765	2.043	1.054	2.990	2.025
58	2.043	0.807	2.534	1.354	3.826	2.413
102	2.382	0.938	3.635	1.627	4.377	2.630
211	2.927	0.934	4.571	1.703	6.261	3.030
397	3.142	0.963	4.769	1.762	6.660	2.957
485	3.259	0.957	4.893	1.772	6.969	3.023
			Na Salt			
	300°		320°		340°	
	DME	CH_4	DME	CH_4	DME	CH_4
31	0.0006	0.0047	0.004	0.0058	0.006	0.009
58	0.0020	0.0058	0.009	0.0080	0.015	0.013
102	0.0030	0.0074	0.011	0.0110	0.024	0.018
211	0.0080	0.0086	0.021	0.0120	0.035	0.019
397	0.0110	0.0083	0.025	0.0130	0.046	0.022
485	0.0130	0.0080	0.028	0.0135	0.045	0.021

tional to partial pressure of methanol until a saturation value is reached. The saturation partial pressure was increased as the reaction temperature increased.

Effect of temperature on catalyst selectivity towards ether and methane formation

The catalytic reaction was investigated at different temperatures varying between 100-400°C at constant partial pressure of methanol (102 torr) over four catalysts. It was observed that the rate of ether formation increased with reaction temperature until a maximum value at about 360°C after which it decreased. However, methane was formed at a very slow rate in the beginning then increased gradually and sharply as the reaction temperature increased up to about 386°C. With Na salt the ether formation begins at higher temperature than the other catalysts (above 260°C) and increased gradually with temperature up to 300°C, then increases sharply until 398°C (Fig. 4). It was observed that at higher reaction temperatures the rate of methane formation increased as the rate of ether decreased (Fig. 5). This may be explained by the decomposi-

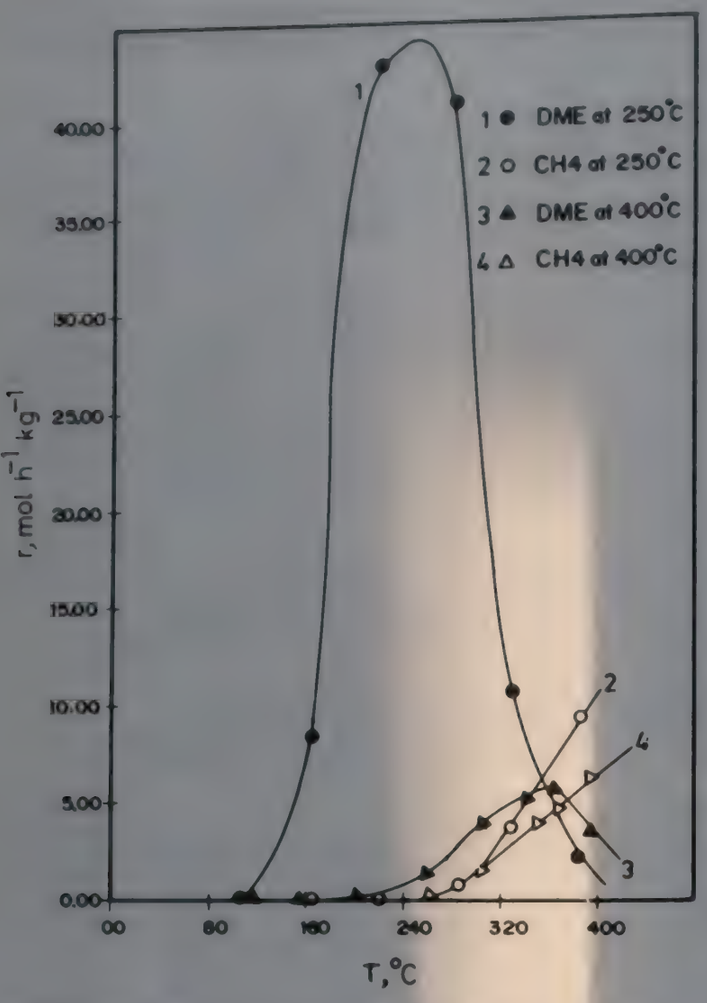

Fig. 3—Effect of temperature on the rate of formation of dimethyl ether and methane over zinc molybdophosphate pretreated at 250° and 400°C. [P_{CH_3OH} = 102 torr]

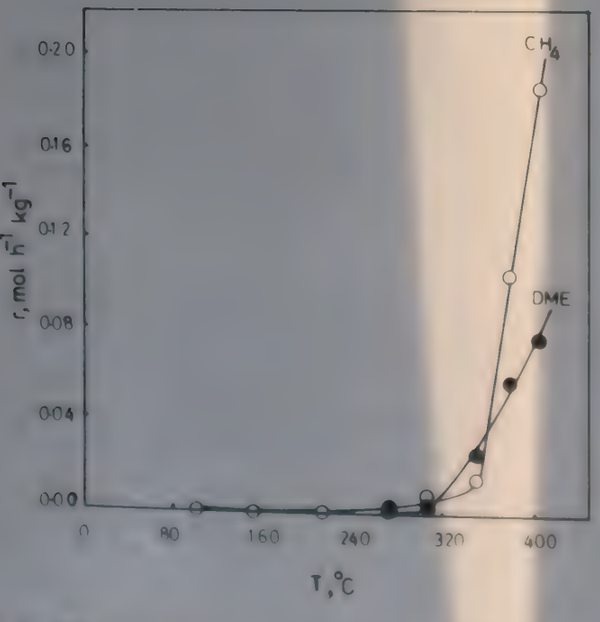

Fig. 4—Effect of temperature on the rate of formation of dimethyl ether and methane over sodium molybdophosphate pretreated at 400°C. [P_{CH_3OH} = 102 torr]

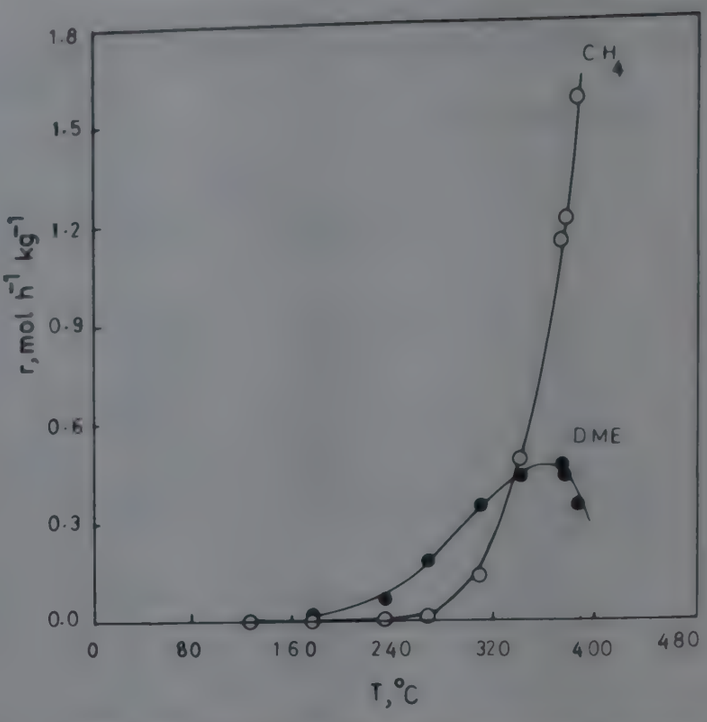

Fig. 5—Effect of temperature on the rate of formation of dimethyl ether and methane over calcium molybdophosphate pretreated at 400°C. [P_{CH_3OH} = 102 torr]

tion of ether to methane in a consecutive manner. The result is in agreement with the conclusion of several authors[3,8,11].

Formation of dimethyl ether and methane from preadsorbed methanol

The rate of ether and methane formation from preadsorbed methanol as a function of time was measured at 320°C over Ca, Mg and Zn salts under constant argon flow 0.195 mol/h. The results indicate that both ether and methane disappear from the reaction mixture after a few minutes from stopping the alcohol feed to the reactor (Fig. 6). The Na salt was not investigated because of its very low activity under non-steady state conditions.

Effect of pyridine on the formation of dimethyl ether and methane

The poisoning effect of pyridine on Zn salt catalyst towards ether and methane formation was investigated. The catalyst was previously pretreated at 400°C in H_2 for 4 hrs and the study was carried out at 349°C. The flow rate of argon was kept constant at 0.195 mol/h. The concentrations of pyridine in alcohol feed were 5% and 19% (v/v). The results show that 5% pyridine inhibits the catalyst activity towards ether and methane formation by about 5% and 2% of the original value, whereas 19% pyridine decreases the rate by about 19% and 10% respectively.

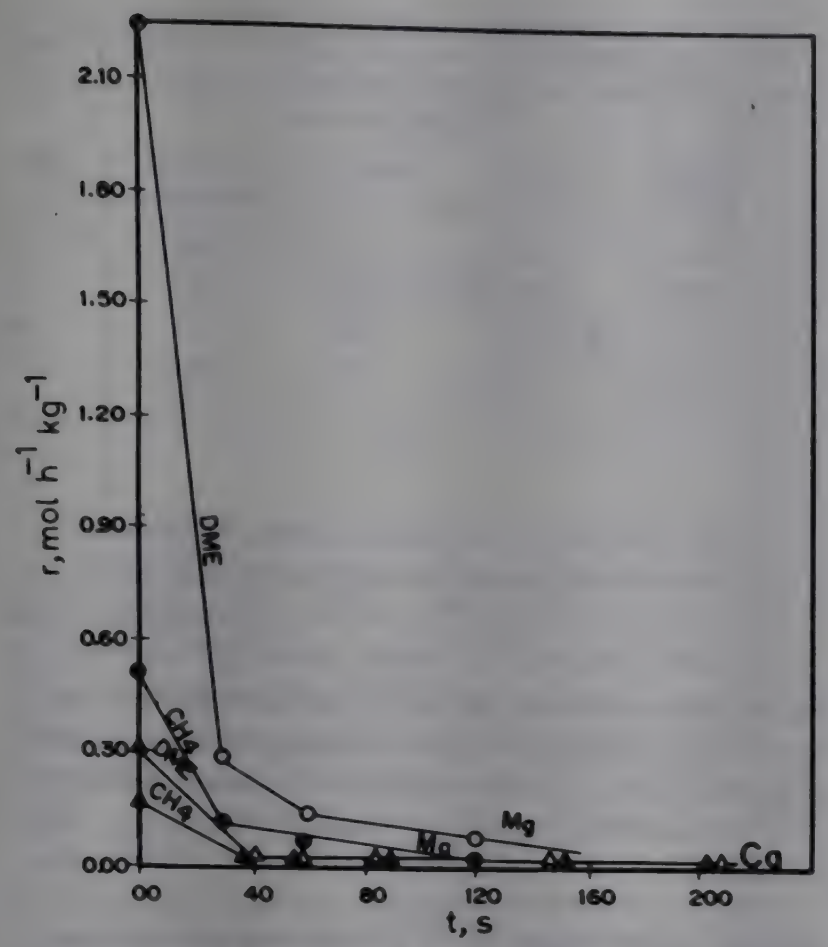

Fig. 6—Rate of formation of dimethyl ether and methane at 320°C from preadsorbed methanol over calcium and magnesium molybdophosphate pretreated at 400°C

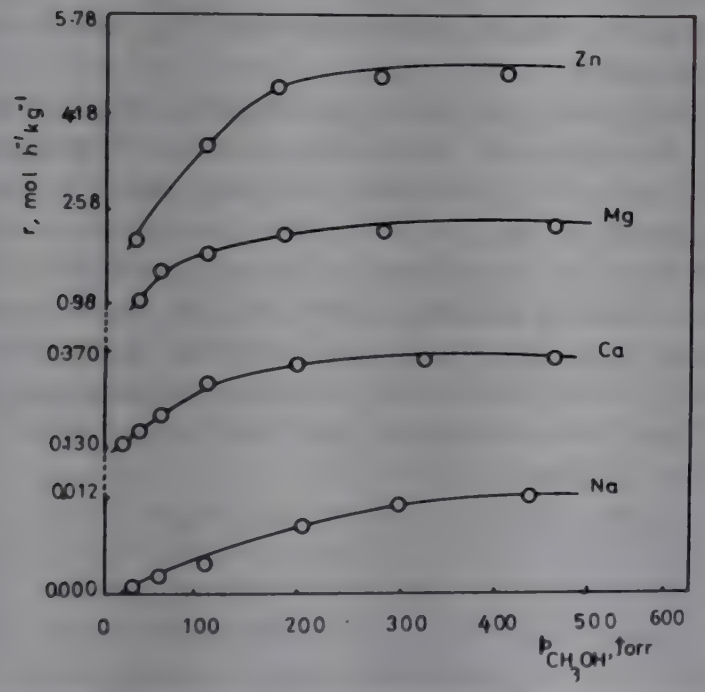

Fig. 7—Effect of partial pressure of methanol on the rate of formation of dimethyl ether at 300°C

Effect of counter cation on dimethyl ether and methane formation

The comparison between the activity of the four salts in terms of the reaction rate towards ether and methane formation at constant temperature 300°C and partial pressure of methanol 300 torr is given in Figs 7 and 8. It is observed from Fig. 7 that the ratio

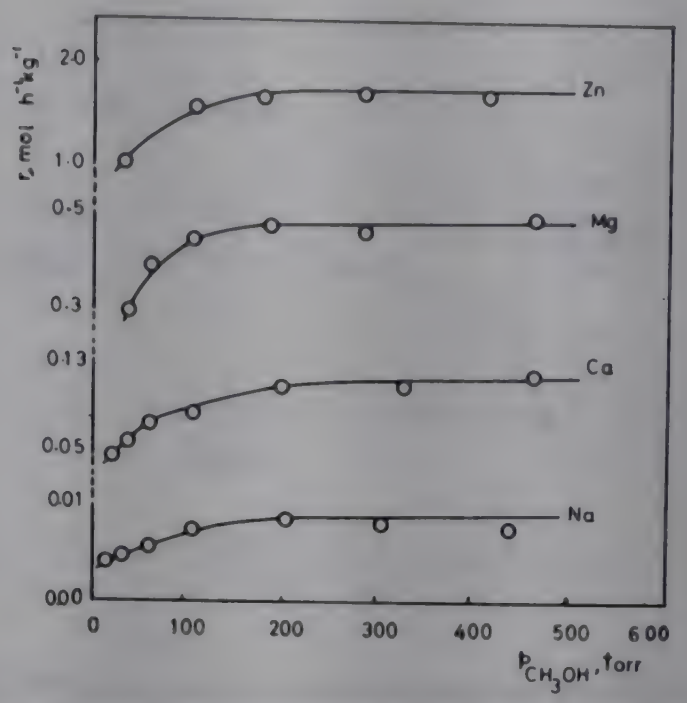

Fig. 8—Effect of partial pressure of methanol on the rate of formation of methane at 300°C

between the activities for ether formation over Na, Ca, Mg and Zn salts is 1:35:220:478 respectively. For methane formation (Fig. 8) the activity is 1:14:57:207 over the four catalysts respectively.

Test for the validity of Langmuir-Hinshelwood mechanism

The kinetics of ether and methane formation was tested by the validity of Langmuir-Hinshelwood Eqs (1) and (2).

$$r = \frac{kK_A P}{1 + K_A^P} \qquad \ldots (1)$$

$$r = k\left[\frac{K_A P}{1 + K_A P}\right]^2 \qquad \ldots (2)$$

Plots of 1/r against 1/P (for model 1) and $1/\sqrt{r}$ versus 1/P (for model 2) are linear. From these plots the values of the adsorption coefficient, K_A, and the rate constant, k, for ether and methane formation were calculated. By comparing the theoretical values of ether and methane formation with those obtained experimentally, a suitable model was concluded. It was found that ether over Zn salt at 320°C approaches the second order equation Fig. 9. The activation energy over Na, Ca, Mg and Zn salts were found to be 13.4, 10.0, 10.6 and 11.5 kcal/mol respectively. It is observed from Fig. 10 that the experimental values for methane formation are in a good agreement with model (1). The activation energies were 19.4, 29.3, 20.7 and 20.5 kcal/mol respectively. It was observed that the higher activation energy for ether formation over Na salt agrees with its

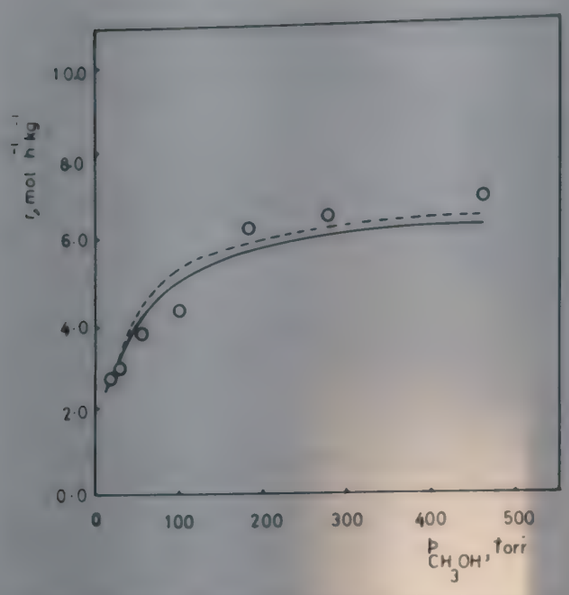

Fig. 9—The variation of rate of dimethyl ether formation over zinc molybdophosphate at 320°C with the high partial pressures of methanol. [○○, Experimental values; —, values calculated from model (1); --, values calculated from model (2)]

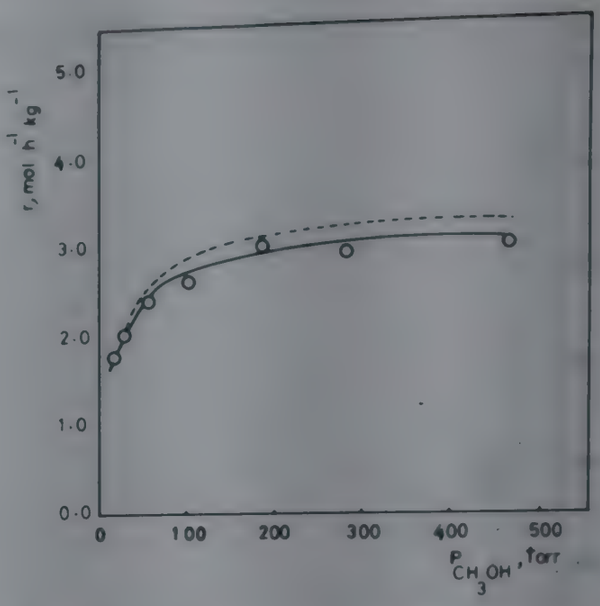

Fig. 10—The variation of the rate of methane formation over zinc molybdophosphate at 320°C with the high partial pressures of methanol. [○○, Experimental values; —, values calculated from model (1); --, values calculated from model (2)]

low activity whereas the other values are comparable and reflect their activity. For methane formation the activation energy are nearly the same except the Ca salt because its particle size was efficient ($\leqslant 0.1$ mm).

Discussion

The observed increase in the catalyst activity with time (Fig. 1) may be explained by adopting the induction period concept, i.e., the reaction requires some time to generate new active centers through catalytic process. The decrease in the activity of Ca and Zn salt towards ether and methane formation (Fig. 2) may be explained by the irreversible consumption of the active centers and/or the partial blocking of Brönsted centers by carbon deposits[26] which is evident from the dark colour of the catalyst observed at the end of the run.

Decrease in the rate of ether formation with the increase in calcination temperature may be explained by adopting the conclusion of Matsuda *et al*[27]. They concluded that at lower calcination temperature where the catalyst surface has more Lewis acidity, higher activity towards ether formation is observed, whereas at higher calcination temperature the amount of Lewis acid centers decreases and consequently the rate of ether formation decreases greatly. This may explain the important role of Lewis acidity in ether formation. Besides, as methane formation decreases slightly by increasing the calcination temperature from 250 to 400°C. The higher activity observed at lower calcination temperatures may also be explained by adopting the concept of pseudo liquid phase[16,20,28,29]. This concept assumes that at lower calcination temperature the water produced during the dehydration reaction is adsorbed in the bulk thus increasing the reaction zone. This probably increases the proton acidity which increases the catalyst activity towards the conversion of methanol.

The relation between the reaction temperature and the rates of ether and methane formation (Fig. 5) may be explained by assuming that ether is a precursor for methane[8,11]. This conclusion is evident from the sharp increase in methane formation after injecting dimethyl ether into the feed under steady state conditions. The increase in methane formation may be also due to the direct formation of methane from methanol and the degradation of higher hydrocarbons[3].

The disappearance of both products from the reaction mixture after one minute from stopping the alcohol feed to the reactor may be explained by: (1) the existence of a weakly adsorbed methanol species required for the formation of ether and methane, (2) the rapid conversion of the preadsorbed species to products, (3) in absence of alcohol feed to the reactor, no water is produced which is necessary for promoting the conversion of the adsorbed species.

The inhibition of ether and methane by pyridine may be explained by assuming that the acid centers participating in the formation of both products are poisoned. It is observed that ether formation is more inhibited than methane in the presence of 5% and 19% pyridine in the feed of methanol. This result may be explained by assuming that the active cen-

Table 2—Effect of cation radius, and electronegativity on the rate of formation of dimethyl ether and methane at 102 torr methanol and 300°C

Cation	Electro-negativity	Ionic radius (Å)	r_{DME}, mol.h.$^{-1}$kg^{-1}	r_{CH_4}, mol.h.$^{-1}$kg^{-1}
Na	1.01	—	0.004	0.007
Ca	1.04	1.06	0.285	0.09
Mg	1.23	0.78	1.800	0.45
Zn	1.66	0.69	3.640	1.64

ters involved in ether formation are strongly affected by pyridine rather than the those involved in methane formation. However, it may also be assumed[13] that methane is mainly formed in the bulk which is not accessible to the bulky molecules of pyridine. Pyridine adsorbed on heteropoly compounds exists as pyridinium ion (as evident from IR spectra) as a result of interaction with Brönsted acid centers[18,19,30]. These Brönsted acid centers are proposed to participate in methane formation by a carbenium ion mechanism[3,8,31,32]. It is assumed by Hayashi and others[3,8,12,13,33] that the activity towards hydrocarbon formation is influenced by the concentration and strength of Brönsted acid sites.

The results given in Table 2 indicate that the activity of the catalyst is affected by the ionic size of the counter cation and its electronegativity. It is observed that as the ionic radius increases the activity towards both ether and methane formation decreases. Zinc salt, the most active catalyst among the three catalysts studied, has the smallest cation radius. The Na salt was not considered in this comparison since it is a monovalent cation. It is shown from the data given in Table 2 that Zn cation being the most electronegative has the maximum activity towards ether and methane formation. This result is in a good agreement with the following equation[27].

$$M_n[PMo_{12}O_{40}]\cdot H_2O \rightarrow [M-OH^-]H^+[PMo_{12}O_{40}]$$

The higher the electronegativity of the element the stronger is its tendency to attract the OH^- anion thus producing a strongly acidic site by increasing the protonic nature of H^+.

From the results obtained in this study the proposed mechanism for the conversion of methanol may be given as in Scheme 1:

According to Scheme 1, ether molecule may be formed from the participation of two adjacent surface alkoxide groups whereas methane formation requires a surface alkoxide and a carbenium ion. Ether formation follows a second order equation of Langmuir-Hinshelwood type whereas methane formation obeys a first order equation of the same type.

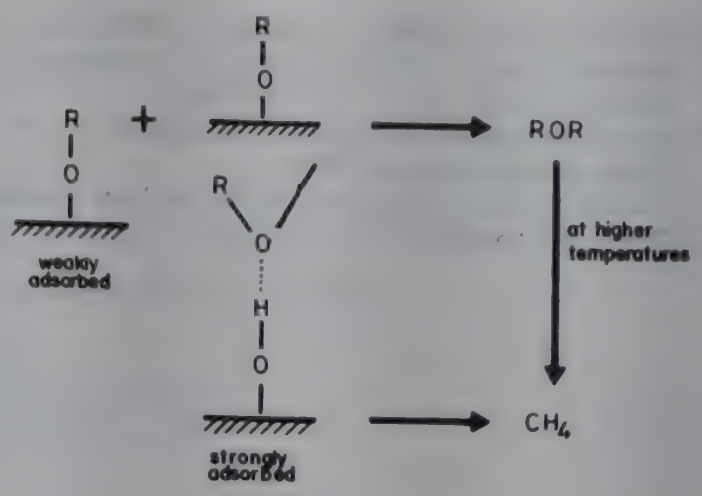

Scheme 1

References

1 Soma Y, Onishi T & Tamoru K, *Trans Faraday Soc*, 65 (1988) 2215.
2 Schmitz G, *J chim Phys*, 75 (1978) 650.
3 Hayashi H & Moffat J B, *J Catal*, 77 (1982) 473.
4 Ono Y, *Mekhanizm Kataliza, Novosibirsk (USSR)*, (1984) 192.
5 Misono M & Okuhara T, *Kenkyu Hokoku-Asahi Garasu Kogyo Gijutu Shoreikoi*, 45 (1984) 115.
6 Zhiyun W, Zhonggiong Z, Min J, Kai L & Qiang Z, *Proc Int Conf Rare Earth Dev Appl*, 1 (1985) 630.
7 Makatun V N, Chuvaev V F, Solovei O M & Shestakov V L, *Dokl Akad Nauk SSSR*, 287 (1986) 282.
8 Hayashi H & Moffat J B, *J Catal*, 81 (1983) 61.
9 Ono Y, Mori T & Keii T, *Preprints of 7th International Congress on Catalysis*, C 12, Tokyo, 1980.
10 Ono Y, Baba T, Sakai J & Keii T, *J chem Soc Chem Commun*, (1981) 400.
11 Ebeid Fikry M & Ali Laila I, *Surface Technology*, 20 (1981) 287.
12 Highfield J B & Moffat J B, *J Catal*, 88 (1984) 177.
13 Highfield J B & Moffat J B, *J Catal*, 89 (1984) 185.
14 Niiyama H, Saito Y & Echigoya E, *Proceedings 7th International congress on catalysis, Tokyo*, 1980 *Kondansha, Tokyo*, (Elsevier, Amsterdam) 1981 p 1416.
15 Baba T, Watanabe H & Ono Y, *J phys Chem*, 87 (1983) 2406.
16 Okuhara T, Hayakawa N, Kasai A, Misono M & Yoneda Y, *J Catal*, 83 (1983) 121.
17 Katamura K, Nakamura T, Sakata K, Misono M & Yoneda Y, *Chem Lett*, 89 (1981).
18 Misono M, Mizuno N, Katamura K, Kasai A, Konishi Y, Sakata K, Okuhara T & Yoneda Y, *Bull chem Soc Japan*, 55 (1982) 400.
19 Furuta M, Sakata K, Misono M & Yoneda Y, *Chem Lett*, (1979) 31.
20 Misono M, Sakata K, Yoneda Y & Lee W Y, *Proc 7th International congress on catal, Tokyo*, 1980 *Kondansha, Tokyo*, (Elsevier, Amsterdam) 1981, p 1047.
21 Furuta M, Okuhara T, Misono M & Yoneda Y, *44th Symposium on catalysis, Fukuoka*, 1979, 4 R 11.
22 Matsubara T, Take J & Yoneda Y, *Shokubai*, 20 (1978) 202.
23 Ai M, *J Catal*, 71 (1981) 88.
24 Tanaka K & Ozaki A, *J Catal*, 8 (1967) 1.
25 Ebeid Fikry M & Pasek J, *Collh Czech chem Commun*, 35 (1970) 2166.

26 McMonagle J B & Moffat J B, *J Catal*, 91 (1985) 132.
27 Matsuda T, Sato M, Kanno T, Miura H & Sugiyama K, *J chem Soc Faraday Trans* 1, 77 (1981) 3107.
28 Misono M, Sakata K & Yoneda Y, *The CSJ/ACS Chemical Congress Honolulu*, April, 1979.
29 Okuhara T, Kasai A, Hayakawa N, Misono M & Yoneda Y, *Chem Lett* (1981) 391.
30 Okuhara T, Hashimoto T, Hibi K & Misono M, *J Catal*, 93 (1985) 224.
31 Hayashi H & Moffat J B, *J Catal*, 83 (1983) 192.
32 Ono Y & Mori T, *J chem Soc Faraday Trans* 1, 77 (1981) 2209.
33 Baba T, Sakai J & Watanabe H, *Bull chem Soc Japan*, 55 (1982) 2555.

Indian Journal of Chemistry
Vol. 31A, December 1992, pp. 929-936

X-ray K-absorption spectral studies of some copper (II) mixed ligand complexes with glycine as primary ligand

B D Shrivastava*, A Mishra & S K Joshi†
School of Studies in Physics, Vikram University, Ujjain-456 010

and

S N Mandloi††
School of Studies in Chemistry, Vikram University, Ujjain-456 010
Received 3 December 1991; revised and accepted 9 June 1992

X-ray K-absorption spectra of some structurally important copper (II) mixed ligand complexes have been recorded using a Cauchois type bent crystal X-ray spectrograph of 0.4m radius. The spectra have been recorded using both solid complexes as well as their aqueous solutions. The observed X-ray absorption parameters e.g., chemical shift, edge-width, shift of the principal absorption maximum and structure of the K-edge have been used to explain the structure of the complexes and also these parameters have been correlated with chemical studies. The changes in the structure of the complexes as they form aqueous solutions have also been interpreted in terms of the X-ray absorption parameters. Further the average metal-ligand bond distances have been estimated from the extended X-ray absorption fine structure (EXAFS). It has been found that the average metal-ligand bond distance increases in the aqueous solution state as compared to that in the solid state.

The study of X-ray absorption edges, the near edge structure (XANES) and extended fine structure (EXAFS) associated with them, provides valuable information[1-3] on the electronic structure and chemical bonding in various types of materials. The X-ray absorption spectral studies have been reported on transition metal complexes by various workers but very few comparative studies have been made on the complexes in solid state as well as in their aqueous solution forms. The present paper reports the results of our X-ray spectroscopic studies on six mixed ligand copper complexes in solid form as well as in aqueous solution form. The complexes are Cu(Gly)(Val), Cu(Gly)(GlyGly), Cu(Gly)(Abu), Cu(Gly)(Thr), Cu(Gly)(Ser) and Cu(Gly)(Ala), where glycine (Gly) has been used as primary ligand and valine (Val), glycylglycine (GlyGly), α-amino butyric acid (Abu), threonine (Thr), serine (Ser) and alanine (Ala) as the secondary ligands.

Materials and Methods

Preparation of complexes

The complexes Cu(Gly)(Ser) and Cu(Gly)(Ala) were prepared using standard methods[4]. The other complexes, Cu(Gly)(Val), Cu(Gly)(GlyGly), Cu(Gly)(Abu) and Cu(Gly)(Thr), were prepared as follows.

An equimolar (0.025 *M*) aqueous solution of different ligands was heated on a water bath with an excess of freshly precipitated copper (II) hydroxide for an hour or two as required. Still hot solution were filtered. The filterate containing the ternary complex was concentrated and a small amount of absolute alcohol (Bengal Chemical grade) was added to the hot filtrate to affect the precipitation and crystallization of the complex. The solutions were allowed to stand overnight for better crystallization, then filtered and washed four or five times with alcohol and ether respectively. All the six complexes studied were intense blue coloured crystals which were quite distinguishable from the crystals of their binary complexes, leading to the conclusion that only ternary complexes were crystallized. The complexes were dried in oven for an hour at 50°C.

All the solutions were prepared in doubly distilled water. The ligands used were either analytical grade reagents or chromatographical homogeneous BDH biochemical grade reagents.

Elemental analysis of the complexes

The chemical formulae for the complexes are listed in Table 1. In the dried complexes, carbon, hydrogen

†Present address: Govt. Arts and Science College, Ratlam 457 001.
††Present address: Govt. College, Dhar 454001.

and nitrogen were estimated by G.P.R. microanalyser. The percentage of carbon, hydrogen and nitrogen found and calculated for the complexes lead to the conclusion that the present ternary complexes are in pure state. Further support for their purity, has been obtained from distinguishable colour of the binary complexes. A good agreement within the experimental limits, has been found between experimental and calculated data supporting the assumed formulae of the complexes.

The general structure of all the complexes is represented in Fig. 1.

X-ray spectrometric set up

A Machlett sealed X-ray tube with a tungsten target operating at 18 kV and 10mA was used as the source of continuous radiation. A 0.4m bent crystal spectrograph having (100) reflection planes of muscovite mica for the analyser was employed to record the spectra on Agfa-Curix Ml X-ray films. In the present investigation, the absorption screens were prepared by spreading uniformly the powdered sample on 1sq.cm area of cellophane tape. Another piece of cellophane tape was put over it, sealing off the substance in between. The screens which gave the best spectra were found to have generally the thickness of the order of 15 to 30mg/cm^2 in the case of copper complexes. The absorption screen of aqueous solution was prepared by using a perspex sheet as done by earlier workers[5] of dimension 5cm × 5cm × 0.2cm with a circular hole of 1.5cm diameter at its centre for filling the solution. One side was covered with cellophane tape and then solution was filled inside the hole. The other side was closed with another piece of cellophane tape. Care was taken such that no air bubble is left inside the solution. The

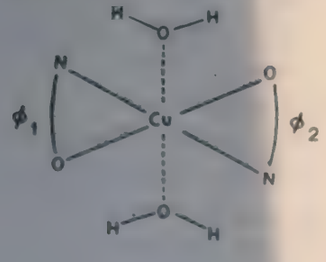

ϕ_1 = Primary glycine ligand

ϕ_2 = Other amino-acid ligand forming mixed-ligand complex with ϕ_1. The ligands ϕ_2 are : Val (Valine), GlyGly (Glycylglycine), Abu (Alpha aminobutyric acid), Thr (Threonine), Ser (Serine), Ala (Alanine).

Fig. 1—Strucutre of Cu(II) mixed ligand complexes with glycine(Gly) as primary ligand

aqueous solution was prepared by dissolving 25mg to 30mg powder in doubly distilled water. Sometimes the solution was heated upto 60°C for dissolving the powder into water. The concentration of aqueous solution was 100 mg/cm^3. The exposure time varied from 4 to 12h. The $L\beta_4$, $L\eta$ and $L\alpha_2$ emission lines of tungsten ^{74}W were used as reference lines. For each sample several microphotometer records were taken on a Carl-Zeiss GII microphotometer, coupled with a Carl-Zeiss GIBI recorder, with magnification 100x and 8.33x for edge position and extended fine structure measurements respectively. The other details of the experimental procedure have been described earlier[6].

Results

In Table 1 the results of the chemical studies[7] e.g., IR, UV and electronic spectra have been reproduced for the six copper complexes both in solid state as well as in aqueous solution form. The infrared spectra of metal chelates can be divided into two broad regions: the high frequency (4000cm^{-1} to 667cm^{-1} and the low frequency (667cm^{-1} to 50cm^{-1}). In some of the complexes new bands appear in the lower frequency region at 420 and 480 cm^{-1}, they may be assigned to Cu-O and Cu-N bands respectively and may be taken to suggest bonding between nitrogen atom of amino group[8-10] and oxygen of the carboxylate group[11] of the metal ion.

The results of the electronic spectra indicate that there is an asymmetric absorption band at around 16000 cm^{-1}. Because the absorption band is at much higher frquency than that for tetrahedral geometry (8000-11500 cm^{-1}), this suggests[12-15] that the complexes may have distorted octahedral geometry. Furthermore, the observed lower values (about 50) of molar extinction coefficient ε support that the complexes possess tetragonally distorted octahedral geometry. The spectra taken in UV region (200nm to 360 nm) with Beckman's spectrophotometer show that there is a band at about 230nm, (with $\varepsilon > 10^3$) which may be taken as a charge transfer band[16].

The polarographic characteristic of these ternary complexes are also reproduced in Table 1.

The copper K-absorption edges in the six complexes studied in solid and aqueous solution forms, alongwith the extended fine structure associated with them are represented in Figs 2 and 3. In these figures the successive curves have been displaced vertically for the convenience of representation.

In Table 2 are presented the results on the wavelengths and corresponding energies of the K-absorption edge (λ_K, E_K) and energies of the

Table 1—IR spectral data, electronic spectral data, ultraviolet spectral data for copper (II) mixed ligand complexes

In solid form	IR spectra			Electronic spectra			UV spectra		Polarographic characteristics in aqueous solution form					
				in aqueous solution form			solution form							
	$-NH_2$ broad absorption band (cm^{-1})	Cu-O absorption band (cm^{-1})	Cu-N absorption band (cm^{-1})	ν_{max} (cm^{-1})	ε	(nm) $\Delta\nu$ (cm^{-1})	ν_{max} (nm)	ε	Temp. (0°C)	i_d (μA)	% Temp. co-efficient of i_d	$E_{\frac{1}{2}}$	Q_e kcal/ mole	Q_D kcal/ mole
Cu(Gly)(Val)	3200 3500	—	465 B	16180	45	50	230	7000	25 35 45 55	4.8 5.4 6.0 6.8	— 1.2 1.4 1.1	0.231 0.227 0.224 0.221	2.9	3.5
Cu(Gly)(GlyGly)	3260 Sh 3280 S	440 S	545 S	15750	180	−125	No absorption max. in UV region observed.	—	25 35 45 55	7.9 8.8 9.8 10.4	— 1.0 1.0 0.6	0.272 0.270 0.269 0.267	2.7	3.5
Cu(Gly)(Abu)	3200 3500	—	470Vw	16130	55	30	224	7400	25 35 45	7.5 8.4 9.4	— 1.1 1.1	0.227 0.222 0.218	6.8	4.4
Cu(Gly)(Thr)	3200 3400	425	485 B,W	16000	50	−130	232	8600	25 35 45	3.4 3.9 4.3	— 1.5 1.3	0.247 0.236 0.226	5.8	4.0
Cu(Gly)(Ser)	3200 3500	420 S	470 S	16000	50	−40	232	5700	30 40 50 60	5.0 6.0 6.8 7.2	— 1.8 1.2 0.6	0.240 0.234 0.215 0.183	5.9	4.3
Cu(Gly)(Ala)	3200 3500	410	465 B,W	16130	50	30	232	12000	30 40 50 60	5.4 5.9 6.5 7.3	— 0.9 1.0 1.2	0.254 0.243 0.223 0.223	6.4	4.7

S = Sharp, W = Weak, Sh = Shoulder, St = Strong, B = Broad, V = Very; NH^+_3 absorption band at $\simeq$ 2564, $\simeq$ 2100, $\simeq$ 1630 and $\simeq$ 500 were absent in all complexes; in i_d = diffusion current; $E_{\frac{1}{2}}$ = half wave potential; Q_e = activation energy of electrode process; and Q_D = activation energy of diffusion.

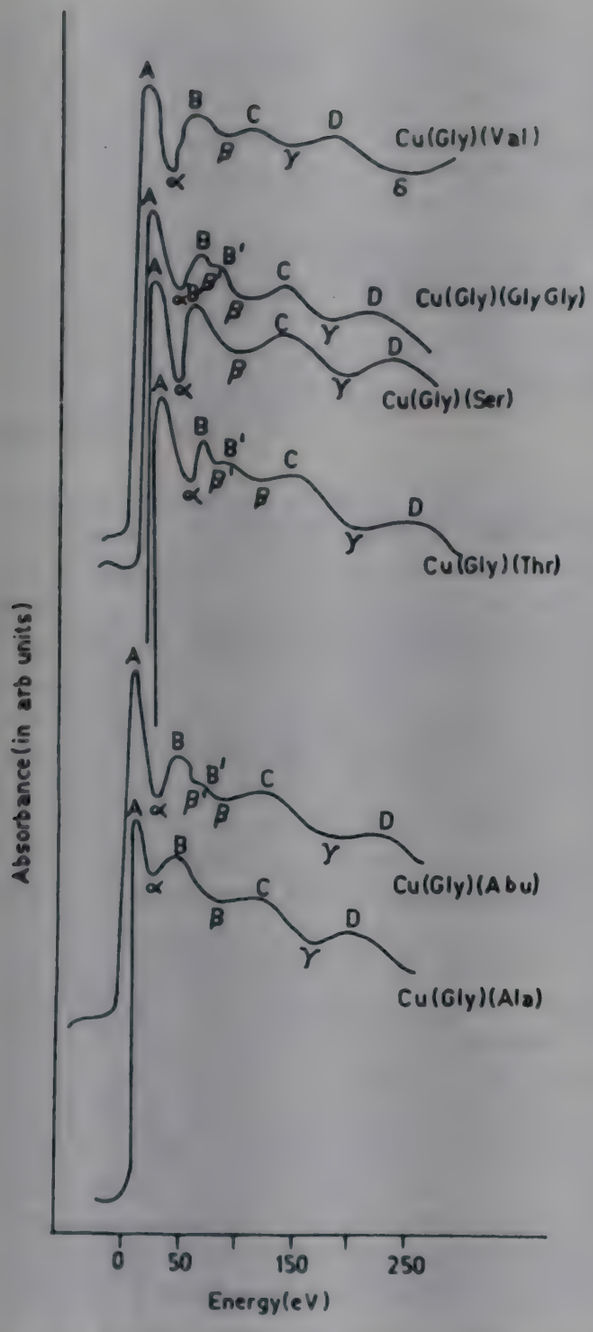

Fig. 2—EXAFS at the K-absorption edges of copper in its Cu(II) mixed ligand complexes in solid form.

principal absorption maximum A (E_A) of copper in metal and its six complexes in solid form and aqueous solution form. The chemical shift of the K-edge and also the shift in the principal absorption maximum (in eV) in the complexes are given in Table 2.

Discussion

(*i*) *Chemical shifts*

The shift of the X-ray absorption edge i (i = K, L, M ...) of an element is written as

$\Delta E_i = E_i$ (compound) - E_i (element).

In the present work the K-absorption edge of copper has been found to be shifted to the higher energy side in solid form as well as the solution form,

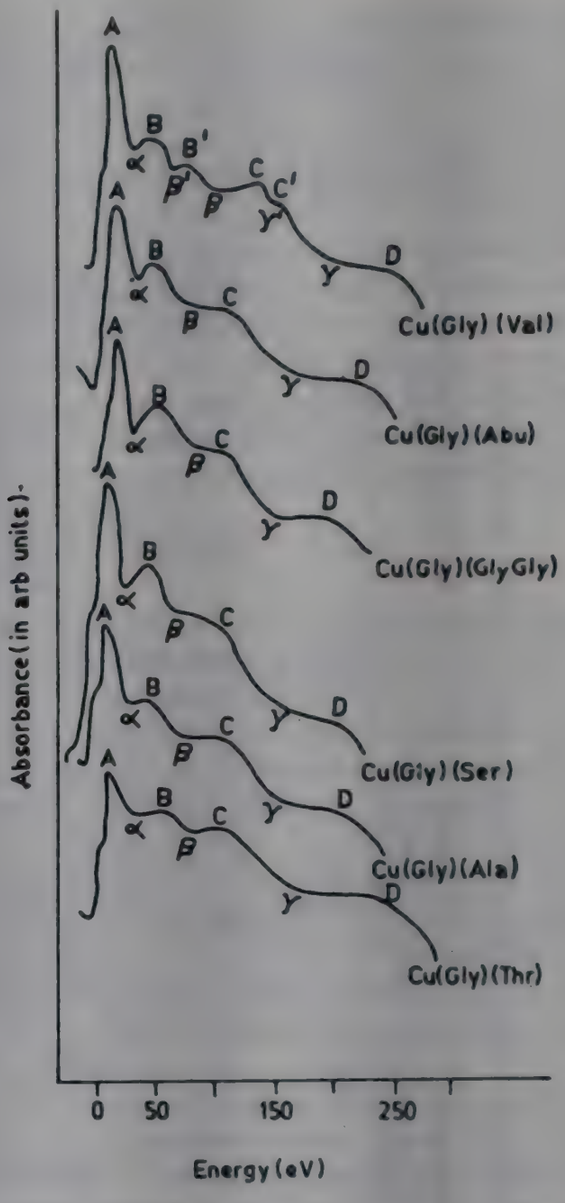

Fig. 3—EXAFS at the K-absorption edges of copper in its Cu(II) mixed ligand complexes in aqueous solution form.

i.e., the chemical shift ΔE_K is positive. In the solid form it ranges from 8.3eV to 13.4eV, while in the solution form it ranges from 6.2eV to 9.0eV. For each complex, the solid form shows larger chemical shift as compared to the solution form.

The position of the X-ray K-absorption edge has been shown to depend on the valency of the absorbing ion, the effective charge on the central metal ion[17-19] and upon the geometry of the complex ion[20-21].

Agarwal *et al.*[22] have suggested an empirical rule for ΔE : In general the chemical shift is towards the high energy side of the metal edge, it increases progressively with increase in the valence of the cation, unless the shift is either suppressed by the covalent character of the bond or enhanced by the formation of a metal-metal bond.

In the present case all the six complexes studied have valency +2. The observed changes in the chemical shift values will be dependent only on the

Table 2—Chemical shifts of K-absorption edges of copper(II) complexes in solid form and in aqueous solution form

Complex		λ_K edge ±0.05XU	E_K edge (eV)	E_A (eV)	Chemical shift ΔE_K (eV)	Shift of the principal absorption maximum (eV)	Edge-width (E_A-E_K) (eV)
Copper metal		1377.73 1377.79[a]	8980.4	9001.2	—	—	20.8
Cu(Gly)(Val)	Solid	1376.46	8988.6	8996.8	8.3	16.5	8.2
	Solution	1376.78	8986.3	9004.0	6.2	23.9	17.7
Cu(Gly)(GlyGly)	Solid	1376.34	8989.4	9001.3	9.0	20.9	11.9
	Solution	1376.57	8987.9	9002.3	7.5	21.9	14.4
Cu(Gly)(Abu)	Solid	1376.20	8990.3	9004.5	10.0	24.2	14.2
	Solution	1376.68	8987.1	9002.9	6.8	22.6	15.8
Cu(Gly)(Thr)	Solid	1375.90	8992.3	9001.4	11.6	20.7	9.1
	Solution	1376.60	8987.6	9003.6	7.2	23.2	16.0
Cu(Gly)(Ser)	Solid	1375.84	8992.7	9003.7	12.3	23.3	11.0
	Solution	1376.50	8988.4	9003.7	8.0	23.3	15.3
Cu(Gly)(Ala)	Solid	1375.67	8993.8	9003.8	13.4	23.4	10.0
	Solution	1376.35	8989.4	9003.7	9.0	23.3	14.3

a = Value adopted by Cauchois Y & Senemaud C, *Wavelengths of X-ray emission lines and absorption edges* (Pergamon Press, Oxford) 1978.

relative ionic character of the complexes. Larger chemical shifts in solid form as compared to the corresponding solution form in each case, shows that the complexes are more ionic in character in solid form than in the solution form. Similar observation have been reported earlier by Nigam *et al.*[23] in solutions of metallic soaps of cobalt in benzene. As there are not many similar reports in aqueous forms, the present work is an attempt in this direction.

The IR spectra show that for all the free amino acids sharp absorption bands are observed around 1600cm^{-1} (ν_{as}) and 1400cm^{-1} (ν_s) indicating the presence of ionized carboxylate group[24]. These bands show shifts upto considerable extent when the ligand undergoes complexation to metal ion. According to Nakamoto[25], on complexation of carboxylate group, its asymmetric stretching frequencies increase while symmetric frequencies decrease. The values $\Delta\nu$ (difference between asymmetric and symmetric stretching frequencies) are less than 225cm^{-1}; this suggests that the nature of Cu-O band is essentially ionic[16]. The other pertinent bands are given in Table 1.

It is clear from the data in Table 2 that the chemical shift is largest for Cu(Gly)(Ala) complex in the solid state followed in order by Cu(Gly)(Ser), Cu(Gly)(Thr), Cu(Gly)(Abu), Cu(Gly)(GlyGly) and Cu(Gly)(Val). As the shift can be taken to be proportional to ionic character[18,19,26], the above sequence represents the ionic character of the complexes in decreasing order. The order of the complexes according to chemical shift in the aqueous solution form is in general the same as in the solid form with the lone exception of Cu(Gly)(Gly Gly). It implies that, in general, the degree of covalency changes to the same extent while going from solid state to solution form in the complexes in the present series. Interestingly, Cu(Gly)(GlyGly) in solution, which shows a different behaviour in this series in X-ray absorption studies, has been found to show anamalous behaviour in IR, electronic spectra and UV studies also (Table 1). It did not give any absorption maximum in UV region and in electronic spectra it gave a very different value of ν_{max}, $\Delta\nu$ and ε. In IR spectra Cu(Gly)(GlyGly) gave uncertain values of absorption bands Cu-O and Cu-N.

(ii) Edge-widths

Nigam and coworkers[27-31] have suggested that the edge-width of the K-absorption edge increases with the increase of covalent character of metal-ligand bonds, provided other factors, like

molecular symmetry etc. remain the same. The experimental data of edge-width of Cu(II) complexes (Table 2) in solid form show that the edge-width decreases as follows: Cu(Gly)(Abu) > Cu(Gly)(GlyGly) > Cu(Gly)(Ser) > Cu(Gly)(Ala) > Cu(Gly)(Thr) > Cu(Gly)(Val). The edge-width data sequence of Cu(II) complexes (Table 2) in aqueous solution form is Cu(Gly)(Val) > Cu(Gly)(Thr) > Cu(Gly)(Abu) > Cu(Gly)(Ser) > Cu(Gly)(GlyGly) > Cu(Gly)(Ala). The order in the solid form is thus not found to match with the order in solution form. Also these orders do not match with the order according to chemical shifts. This is so because the edge-widths do not solely depend on those factors which are responsible for the chemical shifts.

(*iii*) *Shift of the principal absorption maximum*

The shift of principal absorption maximum depends upon the type of overlap between metal atom and the ligand orbitals. The greater the overlap of the metal and the ligand orbital, the more stable are bonding molecular orbitals and hence more unstable the antibonding orbitals[32]. Since transitions of principal absorption maxima occur from 1*s* to the unoccupied antibonding orbitals ($1s \rightarrow T^*_{1n}$) in octahedral complexes[33], the principal absorption shifts to the high energy side. According to Glen *et al.*[32] the overlap between the metal and oxygen will be less than that between metal and nitrogen. In the mixed ligand complexes studied here, the overlap is between Cu-N. Thus the shifts in the absorption maxima are found to be quite large in all the complexes as seen from Table 2.

It is to be noticed here that the values of shifts of the principal absorption maxima are lower in solid form as compared to the aqueous solution form with the lone exception of Cu(Gly)(Abu). The order is same as that due to chemical shifts with only a few exceptions. The exceptions are Cu(Gly)(GlyGly) and Cu(Gly)(Abu) in solid form and Cu(Gly)(Val) in aqueous solution form.

The order of values of the shift of principal absorption maximum in solid form are the same as the order of values of activation energy of diffusion Q_D and the values of activation energy of electrode process Q_e (Table 1) as obtained from the polarographic studies on these complexes. The values of Q_e and shift of principal absorption maximum in Cu(Gly)(Abu) are highest and the value of half wave potential $E_{\frac{1}{2}}$ is lowest in the same complex because it might be attributed to the smaller size of α-butyric acid causing steric effect.

(*iv*) *Splitting of main edge*

None of the complexes in solid form showed any splitting of the K-absorption edge. It is in-line with the octahedral structure of all these complexes. Van Nordstrand[34] has investigated the structure of the K-absorption edges of transition metals in variety of solids and has suggested a criterion of coordination symmetry based on the edge structure. Cotton and Hanson[35] have reported that the low energy absorption occurs prominently in the complexes having tetrahedral or lower symmetry and no such absorption is noticed in octahedral complexes. Sinha and Mande[36] have also explained the absence of the low energy absorption in case of octahedral complexes. The initial absorption rise (called K_1) arises from transitions to the state of *s-p-d* admixed symmetry, and the second absorption rise (called K_2) from transitions to the Laporte-allowed states of nearly pure 4*p* symmetry. The inflection point on K_1 locates the Fermi level E_F. Above E_F, the *s-p-d* admixed states first acquire pure *s* symmetry and finally pure 4*p* symmetry around the inflection point of K_2. The kink arises because the transition probability suddenly decreases for the pure *s* character of states and this causes a decrease of the absorption. The splitting of the main edge has also been explained by many workers[37-38] on the basis of mixed valency.

The complexes in aqueous solution form show splitting of the K-absorption edge. This is due to the fact that these mixed ligand complexes may have distorted octahedral geometry, because the absorption band is at much higher frequency than that for tetrahedral geometry. In fact when two *trans*-ligands in an octahedral complex (for example those along z-axis) are moved either towards or away from the metal ion the resulting complex is said to be tetragonally distorted. The John-Teller effect favours such a distortion. The best evidence for the presence of John-Teller effect in transition metal compounds comes from structural studies of Cu(II) complexes. The electronic configuration for bivalent state of copper is (Ar) $3d^9$. Thus, it is expected to form distorted octahedral complexes.

Furthermore, the lower values of molar extinction coefficient ε (Table 1) observed for all the complexes in solution form support that these complexes possess tetragonally distorted octahedral geometry. Therefore, the complexes in aqueous solution form show structure (K_1,K_2).

(*v*) *Extended X-ray absorption fine structure (EXAFS)*

Well marked EXAFS features on the high energy side of the K-absorption edge, upto several hundred eV, have been observed in the copper metal and its complexes. From the knowledge of the EXAFS, we

have estimated the average metal-ligand bond lengths for the copper metal as well as for the complexes with the help of graphical method proposed by Lytle, Sayers and Stern[39].

The EXAFS of copper metal and its complexes in solid and in aqueous solution forms are shown in Figs 2 and 3. The positions of EXAFS maxima and minima are given in Table 3 for the metal and also for the complexes in solid and in aqueous solution forms. The results of the average metal-ligand bond lengths of the metal and the complexes have been tabulated in Table 4.

The theoretical values calculated by Sanderson's method[40] are found to lie between 2.12 and 1.92Å. These values have been calculated by adding the atomic radii with the ionic radii between Cu-O and Cu-N respectively. The agreement in the values of bond-lengths obtained by LSS method[39] and the theoretical values is thus found to be reasonable.

Usually a comparison of the EXAFS of an ion in a solid form with that in solution form shows two salient features: (a) the positions of the EXAFS maxima and minima with respect to the edge remain unchanged[41-43] and (b) the EXAFS in ionic solution are faint i.e. the intensity fluctuations are smaller. In the present work (a) the aqueous solution EXAFS did not coincide with the solid EXAFS and (b) the intensity fluctuations were slightly pronounced in the EXAFS in solid forms and were certainly not as faint as in aqueous solutions. The observation of clear EXAFS in the solutions shows the existence of the short-range order. Interestingly the nature of these results are same as reported earlier by Nigam *et al.*[23] for some complexes. From Table 4 it is seen that bond lengths are slightly greater in aqueous solutions than in solids, which is an expected result.

Table 4—Average values of metal-ligand bond lengths (in A) estimated by LSS method[39] for copper(II) mixed ligand complexes in solid form and in solution form

Complex	Solid	Aqueous solution
Copper metal	2.53	—
Cu(Gly)(Val)	2.00	2.02
Cu(Gly)(GlyGly)	1.86	2.09
Cu(Gly)(Abu)	1.94	1.97
Cu(Gly)(Thr)	1.94	2.01
Cu(Gly)(Ser)	1.96	2.04
Cu(Gly)(Ala)	1.97	1.99

References

1 Bonnelle C & Mande C, *Advances in X-ray spectroscopy*, (Pergamon Press, New York) 1981.
2 Hasnain S, *X-ray absorption fine structure* (Ellis Harwood, London) 1991.
3 Meisel A, Leonhardt G & Szargan R, *X-ray spectra and chemical binding*, (Springer-Verlag, Berlin) 1989.
4 Åblov A V, Chapurina L F and D'yakon I A, *Zh Neorg Khim*, 20 (1975) 722.
5 Koul P N, Padalia B D, *X-ray Spectrometry*, 12 (1983) 128.
6 Shrivastava B D, Joshi S K & Pandeya K B, *X-ray Spectrometry*, 17 (1988) 127.
7 Mandloi S N, Ph D Thesis (1984) Vikram University, Ujjain (Unpublished).
8 Pawl D B, *J chem Soc*, (1956) 4495.
9 Nakamoto K, *Infrared spectra of inorganic and coordination compounds* (Wiley Interscience, New York) 1970, p 236.
10 Shimamouchi T & Nakagawa J, *Spectrochim Acta*, 18 (1962) 89.
11 Condrate R A & Nakamoto K, *J chem Phys*, 42 (1965) 2590.
12 Nichollas N & Karburton B A, *J inorg nucl Chem*, 33 (1971) 1941.

Table 3—Data in(eV) for EXAFS maxima and minima at the K-absorption edge of copper metal and also copper(II) mixed ligand complexes in solid form and in aqueous solution form

Structure designation	Copper metal / (present work)	Cu(Gly)(Val)		Cu(Gly)(GlyGly)		Cu(Gly)(Abu)		Cu(Gly)(Thr)		Cu(Gly)(Ser)		Cu(Gly)(Ala)	
		Solid	Solution	Solid	Solution	Solid	Solution	Solid	Solution	Solid	Solution	Solid	Solution
A	20.8	8.2	17.7	11.9	14.4	14.2	15.8	9.1	16.0	11.0	15.3	10.0	14.3
α	36	37	47	41	52	46	42	38	45	42	40	39	41
B	47	64	60	60	72	72	71	61	64	66	69	62	63
β′	58	—	66	84	—	79	—	70	—	—	—	—	—
B′	63	—	76	91	—	85	—	78	—	—	—	—	—
β	70	103	100	110	109	110	109	100	104	101	102	103	97
C	93	125	144	146	139	150	146	143	152	154	139	149	136
γ′	—	—	155	—	—	—	—	—	—	—	—	—	—
C′	—	—	163	—	—	—	—	—	—	—	—	—	—
γ	121	150	203	198	176	215	211	215	204	218	197	199	183
D	155	203	253	252	253	258	259	258	256	252	248	250	251
δ	179	256	—	—	—	—	—	—	—	—	—	—	—
E	227	—	—	—	—	—	—	—	—	—	—	—	—

13 Symal A, *J Indian chem Soc*, 45 (1968) 374.
14 Gilland N S & Nyholm R S, *J chem Soc*, (1959) 3997.
15 Bhagwat V, Khadikar P V, Kekre M G & Sharma V, *J inorg nucl Chem*, 36 (1974) 442.
16 Swayer D & Paulson P, *J Am chem Soc*, 80 (1958) 1597, 82 (1960) 4191.
17 Becker M V, *Naturwissenschaften*, 51 (1964) 633.
18 Ovsyannikova I A, Batsanov S S, Nosonova L I, Batsanova L R & Nakrasova E A, *Bull Acad Sci USSR Phys Ser*, 31 (1967) 936.
19 Barinskii R L, *J struct Chem, USSR*, 8 (1967) 805.
20 Meisel A & Keilacker H, *Z phys Chem, (Leipzig)*, 247 (1971) 32.
21 Heintz D, Dissertation, Munich University (1969).
22 Agarwal B K & Verma L P, *J Phys C*, 3 (1970) 535.
23 Nigam A N, Rajput O P & Shrivastava B D, *X-ray spectrometry*, 14 (1985) 136.
24 Kogal R J, Greenstein J P, Birnbayn S N, Wintzs M & McCallum R A, *J Am chem Soc*, 77 (1955) 5708.
25 Nakamoto K, *J Am chem Soc*, 83 (1963) 6528.
26 Nadzhakov E G & Barinskii R L, *Sov Phys Dokl*, 4 (1960) 1319.
27 Srivastava U C & Nigam H L, *Coord chem Rev*, 9 (1973) 275.
28 Nigam H L & Srivastava U C, *Chem Commun*, 14 (1971) 761.
29 Prasad J, Krishna V & Nigam H L, *J chem Soc (Dalton)* (1976) 2413.
30 Srivastava U C & Nigam H L, *Indian J pure appl Phys*, 9 (1970) 63.
31 Krishna V, Prasad J & Nigam H L, *Inorg Chem Acta*, 20 (1976) 193.
32 Glen G L & Dodd C G, *J appl Phys*, 39 (1968) 5372.
33 Obashi M, *Japan J appl Phys*, 16 (1977) 167.
34 Van Nordstrand R A, *Advances in catalysis*, (Associated Press, New York), 12 (1960).
35 Cotton F A & Hanson H P, *Developments in applied spectroscopy*, 2 (1963) p 254.
36 Sinha K P & Mande C, *Indian J Phys*, 37 (1963) 257.
37 Vishnoi A N, *J Phys C*, 2 (1970) 227.
38 Nigam H L & Srivastava U C, *Can J Chem*, 49 (1971) 3229.
39 Lytle F W, Sayers D E & Stern E A, *Phys Rev*, B11 (1975) 2795.
40 Sanderson R T, *Inorganic chemistry* (East-West Press, New Delhi), 1971.
41 Cauchois Y, *C R Acad Sci*, 224 (1947) 1556; 227 (1948) 65.
42 Kiyono S, *Sci Rep Tohoku Univ*, 36 (1952) 236; 37 (1953) 249.
43 Ray B B, Das S R & Bagchi N, *Indian J Phys*, 13 (1940) 37.

Indian Journal of Chemistry
Vol. 31A, December 1992, pp. 937-942

Hydrazones derived by the condensation of 4-methoxybenzoyl hydrazide with salicylaldehyde, *o*-hydroxyacetophenone and diacetylmonoxime as ligands for cobalt (II & III)

Kamalendu Dey*, Kripasindhu Mandal & Debasish Bandyopadhyay
Department of Chemistry, University of Kalyani, Kalyani 741 235

Received 22 July 1991; revised 17 January 1992; accepted 25 March 1992

Reactions of salicylaldehyde 4-methoxybenzoyl hydrazone, (H_2)SMBHON, *o*-hydroxyacetophenone 4-methoxybenzoyl hydrazone, (H_2)OHAPMBHON, and diacetylmonoxime 4-methoxybenzoyl hydrazone (H_2)DAMMBHON with $Co(OAc)_2.4H_2O$, $CoCl_2.6H_2O$, $Co(NO_3)_2.6H_2O$ and $Co(acac)_2.2H_2O$ under varied reaction conditions have been studied and many new mono-nuclear and di-nuclear complexes of cobalt(II) and cobalt(III) have been isolated. The complexes isolated have been characterised by elemental analyses, molar conductance values, magnetic susceptibilities and spectroscopic (UV-visible and IR) data. It has been concluded that formation of these complexes involves tridentate ONO donor ligands either in the monobasic form or in the dibasic form.

Various hydrazone ligands possess strong bactericidal, herbicidal, insecticidal and fungicidal properties[1-6]. In addition hydrazones have analytical applications[7-10] also, besides other uses[11]. Hydrazones have interesting ligational properties due to the presence of several potential coordination sites[12], and both transition and non-transition metal complexes of these ligands have been synthesised earlier.

Although metal complexes of many aroylhydrazones have been studied in recent years[12], no such work on the metal complexes of the hydrazones derived by the condensation of 4-methoxybenzoyl hydrazide with salicylaldehyde (abbreviated to (H_2)SMBHON), *o*-hydroxyacetophenone (abbreviated to (H_2)OHAPMBHON) and diacetylmonoxime (abbreviated to (H_2)DAMMBHON) is available. We have therefore, studied the reactions of these three hydrazone ligands (I) with different metal salts and the present paper describes the results obtained in the case of cobalt (II & III).

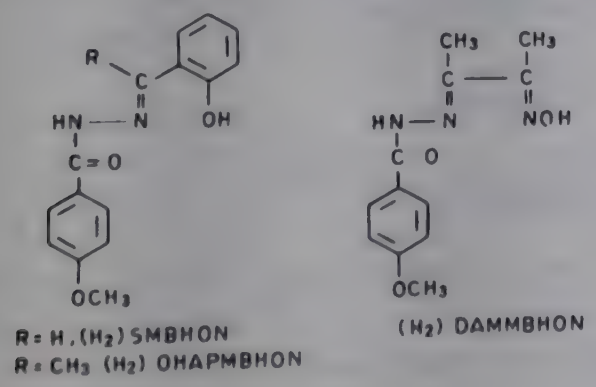

R = H, (H_2) SMBHON
R = CH_3 (H_2) OHAPMBHON

(H_2) DAMMBHON

Although some scanty reports on the Co(II) complexes of (H_2)SMBHON and (H_2)OHAPMBHON have been reported[13], detailed and systematic studies are lacking.

Materials and Methods

Physicochemical data were collected as described in our earlier publication[14]. Satisfactory elemental analyses were obtained for all the complexes. Analysis for carbon, hydrogen and nitrogen were performed at the RSIC, CDRI, Lucknow.

Synthesis of 4-methoxybenzoyl hydrazide, (H)MBHIN

4-Methoxybenzoyl hydrazide was prepared via the preparation of 4-methoxymethyl benzoate followed by treatment with hydrazine hydrate (85%) as reported[15,16].

Synthesis of hydrazones, (H_2)SMBHON, (H_2)OHAPMBHON, and (H_2)DAMMBHON

Salicylaldehyde, *o*-hydroxyacetophenone or diacetylmonoxime was heated under reflux with the hydrazine (H)MBHIN (0.01 molar, 1:1 ratio) in ethanol (40 ml) for 4h, 9h and 11h respectively in the cases of (H_2)SMBHON, (H_2)OHAPMBHON and (H_2)DAMMBHON. The resulting solution on concentration at reduced pressure yielded the title hydrazones (H_2)SMBHON, (H_2)OHAPMBHON and (H_2)DAMMBHON respectively in satisfactory yields.

Synthesis of the complexes

The preparative methods used were almost similar. One representative example is given below. The experimental details for the complexes are shown in three reaction schemes below.

$[Co^{II}(SMBHON)H_2O]$, (*1*)

The solution of the ligand (H_2)SMBHON (0.001 mol) in EtOH (20 ml) was added to the suspension of $Co(OAc)_2.4H_2O$ (0.001 mol) in EtOH (20 ml) under nitrogen atmosphere. Yellowish orange solution (*p*H ~ 6) alongwith a small amount of yellow solid was formed immediately, which was heated under reflux for an hour. The yellow compound was filtered off after cooling and washed thoroughly with hot EtOH and dried *in vacuo*; yield 65%.

Results and Discussion

The reactions of (H_2)SMBHON, (H_2)OHAPMBHON and (H_2)DAMMBHON with $CoCl_2.6H_2O$, $Co(OAc)_2.4H_2O$ and $Co(acac)_2.2H_2O$ under varied reaction conditions yielded coloured cobalt (II & III) complexes of the types $[Co^{II}(SMBHON)\ H_2O]$, (**1**), $[Co^{II}_2\ \{(H)OHAPMBHON\}_2(OHAPMBHON)\ H_2O]$, (**2**), $[Co^{III}\ \{(H)DAMMBHON\}\ (DAMMBHON)]\ H_2O$, (**3**), $[Co^{II}\ \{(H)SMBHON\}\ 3H_2O]X$, $[X = NO_3^-$, (**4**), $X = Cl^-$, (**5**)], $[Co^{II}_2$ (OHAPMBHON)$_2$] H_2O, (**6**), $[Co^{III}(OHAPMBHON)\ (NH_3)_2\ H_2O]Cl$, (**7**), $[Co^{III}\ (SMBHON)\ (NH_3)_2(OAc)]$, (**8**), $[Co^{III}\ (SMBHON)\ (NH_3)_2(H_2O)]Cl$, (**9**), $[Co^{III}\ (SMBHON)\ (NH_3)_3]\ NO_3$, (**10**), $[Co^{III}_2\ (SMBHON)_2\ (NH_3)_4]Cl_2$, (**11**), $[Co^{II}\{(H)SMBHON\}_2]$, (**12**), $[NH_4]\ [Co^{III}\ (SMBHON)_2].H_2O$, (**13**), $[Co^{III}\ \{(H)\ SMBHON\}(SMBHON)]$, (**14**), $[Co^{III}\ \{(H)OHAPMBHON\}\ (OHAPMBHON)]$, (**15**), and $[Co^{II}\{\ (H)\ DAMMBHON\}_2]$, (**16**), shown in the Schemes 1 to 3. The yields of the compounds varied between 50 and 75%.

All the isolated compounds were found to be stable and were characterised on the basis of elemental analyses, molar conductance values, magnetic moments (Table 1) and spectroscopic data. The stoichiometry of the complexes fits well the proposed formulations. Most of the compounds are insoluble in common organic solvents but are soluble in coordinating solvents like DMSO, DMF and py. However, the compounds (**7**)-(**11**) and (**13**) are also soluble in EtOH, CH_3OH and other common organic solvents. The results of present synthesis show that the enolisation and the final basicity of the ligands are dependent on the *p*H of the solution and also on the nature of the cobalt salts/compounds used as reactants.

The ligands (H_2)SMBHON, (H_2)OHAPMBHON and (H_2)DAMMBHON in the complexes

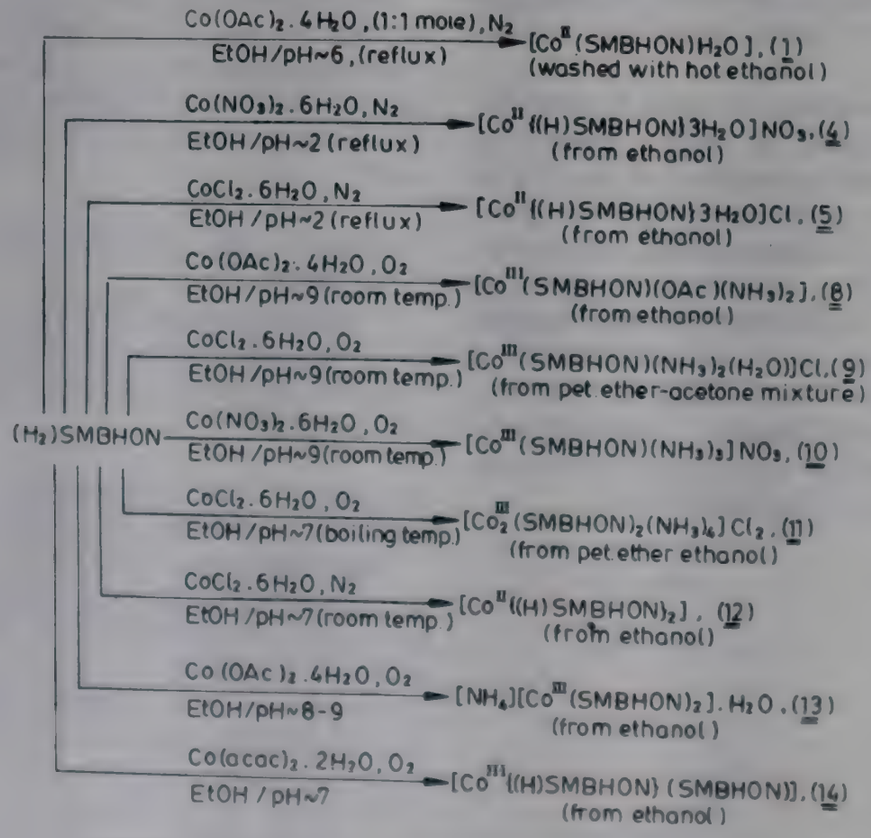

Scheme 1 : [Alcoholic NH_4OH solution (30%) was used to raise the pH of the reaction media]

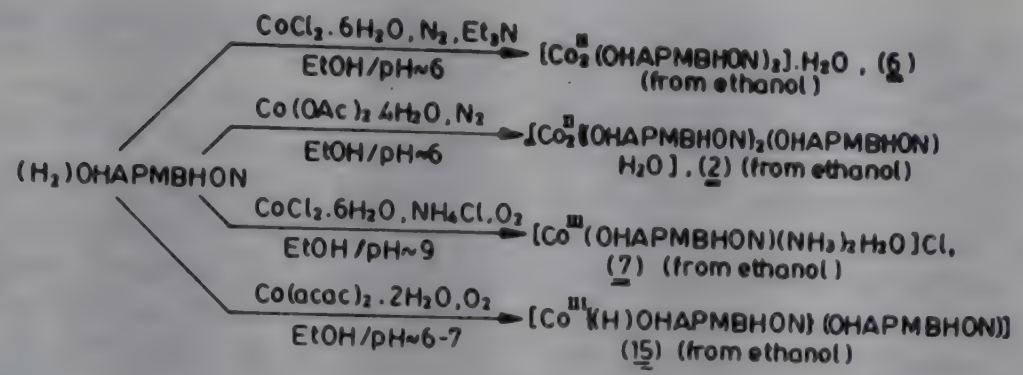

Scheme 2

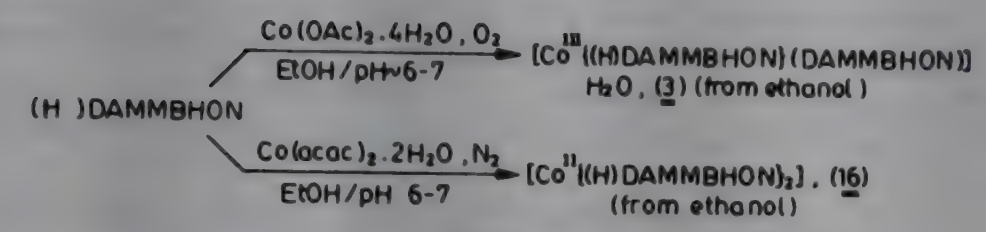

Scheme 3

(**1**), (**6**)-(**11**) and (**13**) function in the dibasic tridentate manner and in the compounds (**4**), (**5**), (**12**) and (**16**) in monobasic tridentate fashion. It is interesting to note that the ligands in the compounds (**2**), (**3**), (**14**) and (**15**) show dual character, i.e., in each compound two moles of the ligands are present one of which functions as a monobasic tridentate and the other as a dibasic tridentate ligand.

The molar conductance data of the compounds are recorded in Table 1. The compounds (**1**)-(**3**), (**6**), (**8**), (**12**) and (**14**)-(**16**) are found to be non-electrolytes[17,18] in DMSO (Λ_M of 10^{-3} *M* solution at room temperature varies between 8 and 12 cm^2 ohm^{-1} mol^{-1}). On the other hand, (**4**), (**5**), (**9**) and (**13**) show conductance values of 43.83, 39.67 cm^2 ohm^{-1} mol^{-1} (both in DMSO), 46.43, 52.44 and 52.5 cm^2 ohm^{-1} mol^{-1} (all in EtOH) respectively at room temperature indicating their 1:1 electrolytic nature[17,18]. The conductance value of 98.03 cm^2 ohm^{-1} mol^{-1} (in EtOH) for the compound (**11**) indicates its 1:2 electrolytic nature[17,18] in solution. However, the solutions of compounds (**2**), (**3**), (**6**), (**14**) and (**15**) on prolonged standing showed somewhat higher values of molar conductance. This may be due to some sort of solvolysis, which we could not study in detail.

The room temperature magnetic moment values of all the isolated complexes are recorded in Table 1. The observed magnetic moment value of 4.4 B.M. for complex (**1**) indicates tetrahedral geometry[6,13], which is also supported by the electronic spectral data. The observed magnetic moment values of 5.19, 4.98, 4.94 and 4.92 B.M. for the complexes (**4**), (**5**), (**12**) and (**16**) respectively suggest octahedral geometry for the complexes. The room temperature magnetic moment value of 3.79 B.M. obtained for the complex (**6**) is slightly lower than the usually observed value for a tetrahedral cobalt(II) compound, which is slightly higher than values for square-planar or spin-paired octahedral cobalt(II) species. However, this lower value may be explained on the basis of a tetrahedral dimeric structure[13,19-21](II). This is also substantiated by molecular weight determination of the complex (Rast's method).

The complex (**2**) shows magnetic moment value

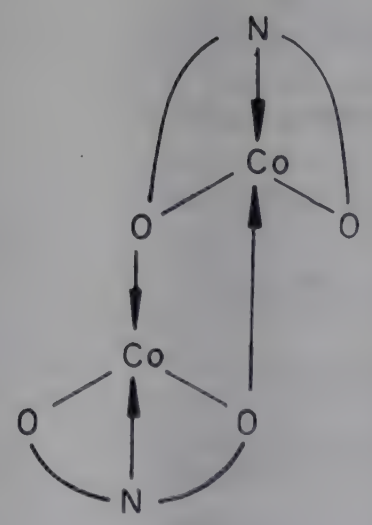

(II)

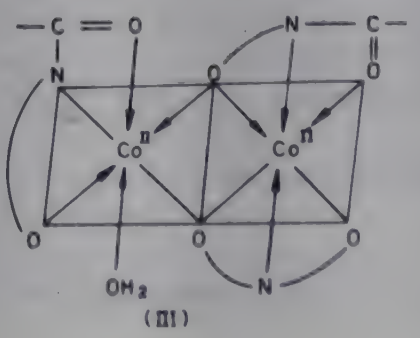

(III)

of 3.15 B.M. at room temperature which is much below the expected range of tetrahedral or high spin octahedral complexes. The stoichiometry of the complex suggest an octahedral geometry around cobalt(II) ion in this complex, which is also substantiated by electronic spectral data (see later discussion). It may attain a dinuclear structure (III) in the solid state, which is also supported by the molecular weight determination of the complex (Rast's method).

Similar observations were earlier made by other workers[22].

Electronic spectra

The electronic spectra of cobalt(II & III) complexes (**1**)-(**16**) were recorded in solution. The visible spectra of cobalt(II) complexes with ligands having N_2O_4 donor sets are known[12,13,23] to show two bands in the region 20,000-17,390 cm^{-1} and 10,000-8,330 cm^{-1} corresponding to the transi-

Table 1 – Analytical, magnetic moment and molar conductivity data of cobalt (II & III) complexes

Complexes (Colour)	m.p. (°C)	Found (Calc.), %				$\mu_{eff.}$ (B.M.)	Λ_M ($cm^2ohm^{-1}mol^{-1}$)
		C	H	N	Co		
$[Co^{II}(SMBHON)H_2O]$, (**1**) (Yellow)	290-293(d)	52.05 (52.17)	4.15 (4.05)	7.92 (8.11)	17.5 (17.1)	4.48	8.1[a]
$Co^{III}_2\{(H)OHAPMBHON\}_2$ $(OHAPMBHON)]H_2O]$, (**2**) (Brown)	> 310	59.00 (58.50)	4.78 (4.67)	8.08 (8:53)	12.09 (11.99)	3.45	12.5[a]
$[Co^{III}\{(H)DAMMBHON\}$ $(DAMMBHON)]H_2O$, (**3**) (Orange-yellow)	150-152	50.40 (50.34)	5.08 (5.06)	14.48 (14.68)	10.02 (10.30)	Dia	11.7[a]
$[Co^{II}\{(H)SMBHON\}3H_2O]NO_3$, (**4**) (Red-violet)	200-208(d)	40.35 (40.54)	4.58 (4.28)	9.59 (9.46)	13.34 (13.28)	5.19	43.83[a]
$Co^{II}\{(H)SMBHON\}3H_2O]Cl$, (**5**) (Orange-red)	216-218	43.74 (43.11)	4.23 (4.55)	7.08 (6.71)	14.50 (14.13)	4.98	39.67[a]
$Co^{II}_2(OHAPMBHON)_2].H_2O$, (**6**) (Reddish brown)	> 250	55.50 (54.85)	4.19 (4.28)	8.21 (8.00)	16.99 (16.85)	3.79	10.5[a]
$Co^{III}(OHAPMBHON)(NH_3)_2H_2O]Cl$, (**7**) (Brown)	> 250	45.20 (44.8)	5.30 (5.13)	13.10 (13.06)	13.29 (13.76)	Dia	74.4[b]
$[Co^{III}\{SMBHON)(NH_3)_2(OAc)]$, (**8**) (Light brown)	156-158	47.75 (48.50)	4.98 (4.75)	11.29 (11.97)	14.97 (14.01)	Dia	9.5[a]
$[Co^{III}(SMBHON)(NH_3)_2(H_2O)]Cl$, (**9**) (Brown)	198-200	43.76 (43.42)	4.72 (4.82)	13.05 (13.51)	14.60 (14.23)	Dia	46.43[b]
$Co^{III}(SMBHON)(NH_3)_3]NO_3$, (**10**) (Brown)	210-215	40.81 (40.90)	4.88 (4.77)	19.08 (19.09)	13.38 (13.40)	Dia	52.44[b]
$[Co^{III}(SMBHON)_2(NH_3)_4]Cl_2$, (**11**) (Brown)	> 300	45.36 (45.30)	4.75 (4.54)	13.88 (14.12)	14.50 (14.88)	Dia	98.03[b]
$Co^{II}\{(H)SMBHON\}_2]$, (**12**) (Orange-yellow)	> 300	60.2 (60.3)	4.42 (4.35)	9.19 (9.38)	10.02 (9.88)	4.94	9.59[a]
$[NH_4][Co^{III}(SMBHON)_2]H_2O$, (**13**) (Light brown)	> 250	57.10 (57.05)	4.70 (4.75)	11.00 (11.09)	9.10 (9.35)	Dia	52.5[b]
$[Co^{III}\{(H)SMBHON\}(SMBHON)]$, (**14**) (Orange-yellow)	> 300	59.80 (60.30)	4.35 (4.10)	8.72 (9.39)	10.14 (9.88)	Dia	11.67[a]
$[Co^{III}\{(H)OHAPMBHON\}$ $(OHAPMBHON)]$, (**15**) (Dark)	> 310	60.92 (61.44)	4.40 (4.80)	8.76 (8.96)	9.60 (9.44)	Dia	10.26[a]
$[Co^{II}\{(H)DAMMBHON\}_2]$, (**16**) (Orange)	280(d)	51.30 (51.80)	5.14 (5.04)	14.98 (15.13)	10.23 (10.60)	4.92	11.34[a]

[a] 10^{-1} *M* solution in DMSO at room temperature; [b] 10^{-3} *M* solution in EtOH at room temperature.

tion $^4T_{1g}(F) \rightarrow {}^4T_{1g}(P)$ and $^4T_{1g}(F) \rightarrow {}^4T_{2g}$ in the octahedral geometry. The visible spectra of the present cobalt(II) compounds (**2**), (**4**), (**5**), (**12**) and (**16**) show bands in the region 21,000-17,420 cm^{-1} supporting thereby the pseudo-octahedral geometry of the present cobalt(II) complexes.

On the other hand, the complexes (**1**) and (**6**) show bands in the region 16,190-16,000 cm^{-1} corresponding to the transition $^4A_2(F) \rightarrow {}^4T_1(P)$ suggesting tetrahedral geometry for these complexes[13]. However, due to limitation of the instrumental facilities we could not detect the other important transition (i.e. $^4A_2(F) \rightarrow {}^4T_1(F)$) usually observed in a tetrahedral cobalt(II) compound.

Cobalt(III) complexes (**7**)-(**11**), (**14**) and (**15**), on the other hand, show bands at 21,000-17,420 cm^{-1} corresponding to the transition $^1A_{1g} \rightarrow {}^1T_{1g}$. This observation also suggests pseudo-octahedral nature of these complexes[12,13,23].

The bands observed in the region 30,000-28,000 cm^{-1} in all the present cobalt complexes are very strong and may be due to charge transfer[6,13,23].

Infrared spectra

The infrared spectra of the ligands (H_2)SMBHON, (H_2)OHAPMBHON and (H_2)DAMMBHON and their cobalt(II & III) complexes have been measured in KBr phase.

The spectra of the ligands show medium to strong bands in the range 3200-3280 cm^{-1} assignable to ν_{OH} in the case of (H_2)SMBHON and (H_2)OHAPMBHON and a band at 3,000-3,400 cm^{-1} assignable to $\nu_{OH(oxime)}$ in the case of ligand (H_2)DAMMBHON. The broad nature of the bands suggests hydrogen bonding[24-26]. The free ligands also show bands at 3020-3080 and 1640-1650 cm^{-1} assignable to ν_{NH} and $\nu_{C=O}$ modes. The $\nu_{C=N(hydrazone\ linkage)}$ in the ligands appeared at 1610-1615 cm^{-1}. The $\nu_{C=N(oxime\ linkage)}$ mode in the free ligand (H_2)DAMMBHON is possibly submerged by the strong band at 1610 cm^{-1}.

The ν_{N-O} mode for the ligand (H_2)DAMMBHON is observed as a strong band[27] at 940 cm^{-1}. The bands observed at 1515-1545 cm^{-1} and at 1260 cm^{-1} are assignable to amide-II and amide-III. The C−O stretch (phenolic) of the ligands (H_2)SMBHON and (H_2)OHAPMBHON is observed around 1520 cm^{-1}, while the amide-III bands of all the ligands are observed around 1575 cm^{-1}. These data suggest that the free ligands exist in the keto form[24-26].

The infrared spectra of the compounds (**4**), (**5**) and (**12**) exhibit ν_{NH} at 3000-3040 cm^{-1} alongwith the following changes in amide group vibrations; amide-II increases in frequency (1530-1545 cm^{-1}) and amide-III splits into two components at 1205-1215 cm^{-1} and 1375-1385 cm^{-1}. These changes in amide group vibrations suggest amide oxygen coordination to metal ion as well as coordination of ligands in keto form[26,28]. The coordination of amide oxygen is supported by the appearance of a band at 415-420 cm^{-1} which may be assigned[26] to ν_{Co-O}. The disappearance of the band due to ν_{OH} at 3200-3280 cm^{-1} in the compounds (**4**), (**5**) and (**12**) indicates the involvement of phenolic oxygen in coordination after deprotonation. The appearance of a new band at 480-910 cm^{-1} suggests metal-oxygen (phenolic) coordination[26,29]. The band observed at 450-470 cm^{-1} is assigned to ν_{Co-N} vibration[29]. In the complexes (**4**), (**5**) and (**12**) $\nu_{C=N}$ is lowered by ~20 cm^{-1} suggesting coordination of nitrogen of the azomethine group to the metal atom. It is, therefore, inferred that the ligands in the complexes (**4**), (**5**) and (**12**) coordinate as monobasic tridentate ligand. The bands at 3300-3600 and 840-860 cm^{-1} in the chelates (**2**), (**4**) and (**5**) indicate the presence of coordinated water molecule[24].

The bands at 800, 1025 and 1045 cm^{-1} indicate the presence of NO_3^- in the compound (**4**)[24,30].

The infrared spectra of the compound (**2**), (**3**), (**14**) and (**15**) are complicated. On complexation, the ν_{NH} bands of the above ligands lose both sharpness and intensity. Sharp, strong bands in the infrared spectra of the complexes at 1600-1610 cm^{-1} have been assigned[31] to the (C=N−N=C) skeleton and the $\nu_{C=O}$ (amide-I) band. The phenolic ν_{C-O} shows an upward shift ($\Delta\nu = 30\ cm^{-1}$). All these indicate that the two ligands are attached to the metal ion in two forms[32]. One of the ligands is attached as a dibasic tridentate ONO donor[33], and the other as a monobasic ONO donor in the keto form.

Dramatic changes are observed in the spectra of the complexes (**1**), (**6**)-(**11**) and (**13**) which do not show any characteristic band of amide and amino groups suggesting that the ligand is coordinated in 'enol' form assigned to the skeleton[31] C=N−N=C. The disappearance of a band due to ν_{OH} at 3200-3280 cm^{-1} in all the said complexes indicates the involvement of phenolic oxygen in coordination through deprotonation. It is, therefore, suggested that the ligands in the complexes (**1**), (**6**)-(**11**) and (**13**) coordinate in dibasic tridentate fashion. The bands observed at 1540-1545 and 1300-1305 cm^{-1} indicate the presence of phenolic oxygen bridging[26] in the compound (**6**) and (**11**). The bands observed at 3200-3500 and 850 cm^{-1} indicate the presence of coordinat-

ed NH_3 molecule[24,34] in the chelates (**7**)-(**11**). The bands observed at 3060-3580 and 1410 cm^{-1} indicate the presence of NH_4^+ ion in the compound (**13**)[24,35]. The bands at 1640 and 1330 cm^{-1} in the compound (**8**) indicate the presence of coordinated acetato group[24].

The presence of water molecule in the complexes (**1**) to (**9**) and (**13**) complicates the band assignments (see above). Heating of these complexes at 115 ± 2°C indicated the presence of non-coordinated water in the complexes (**3**), (**6**) and (**13**), and coordinated water in rest of the complexes.

The above discussion corroborates the structural features of the Co(II & III) complexes depicted in the Schemes 1 to 3.

Acknowledgement

We gratefully acknowledge the financial help from the UGC and CSIR, New Delhi. Two of us (K.S.M. & D.B.) are thankful to the UGC and CSIR for a Teacher Fellowship and a Senior Research Fellowship respectively. Analytical services from RSIC, Madras IIT and CDRI, Lucknow are also acknowledged.

References

1 Hoyle W & Howarth G A, *Chem Abstr*, 78 (1973) 1608h.
2 Dilworth J R, *Coord Chem Rev*, 21 (1976) 29.
3 Alcock J P, Baker H J & Diamautis A A, *Aust J Chem*, 25 (1972) 289.
4 Sahni S K, Gupta S P, Sangal S K & Rana V B, *J inorg nucl Chem*, 39 (1977) 1098.
5 Foye W O & Duvall R N, *J Am pharm Assoc Sci Edut*, 47 (1958) 285.
6 Sing N K, Aggarwal R C & Aggarwal N, *Indian J Chem*, 23A (1984) 1011.
7 Katyal M & Dutty, *Talanta*, 22 (1975) 151.
8 Hett M L & Ryan D E, *Anal chim Acta*, 34 (1966) 407.
9 Jenson R E & Ptvaum R T, *Anal chim Acta*, 37 (1967) 397.
10 Dey K, Ray S B, Bhattacharya P K, Gangopadhyay A, Bhasin K K & Verma R D, *J Indian chem Soc*, 62 (1985) 809.
11 Farag A B, Morsi M A & Ibrahim S A, *Indian J Chem*, 25A (1980) 882.
12 Dutta R L & Hossain M, *J scient Ind Res*, 44 (1985) 635.
13 Rastogi D K, Sahni S K, Rana V B & Dua S K, *Indian J Chem*, 16A (1978) 86.
14 Dey K, Bandyopadhyay D & Bhar J K, *Synth React inorg met-org Chem*, 18 (1988) 849.
15 Vogel A I, *A text book of practical organic chemistry*, 3rd Edn (Longman, London) 1959, 780.
16 Fox H H & Gibas C T, *J org Chem*, 17 (1952) 165.
17 Geary W J, *Coord Chem Rev*, 7 (1971) 11, 110.
18 Sinn E & Harris C M, *Coord Chem Rev*, 4 (1969) 391.
19 William D J, Smith D W & Stoufer R C, *Inorg Chem*, 6 (1967) 590.
20 Stoufer R C, Smith D W, Clevanger E A & Morris T N, *Inorg Chem*, 5 (1966) 1167.
21 Melson G A & Busch D M, *J Am chem Soc*, 86 (1964) 4830.
22 Carlin R L, *Transition Met Chem*, 1 (1956) 1.
23 Lever A B P, *Inorganic electronic spectroscopy* (Elsevier, New York) 1968.
24 Nakamoto K, *Infrared spectra of inorganic and coordination compounds*, 2nd Edn (John Wiley & Sons, Inc, New York) 1963, 143-150.
25 Nonayama N, Tomit S & Yamasaki K, *Inorg chim Acta*, 12 (1975) 33.
26 Rastogi D K, Dua S K & Sahni S K, *J inorg nucl Chem*, 42 (1980) 323.
27 Mostafa M M, Ibrahim K M & Moussa M N H, *Transition Met Chem*, 9 (1984) 243.
28 Rastogi D K, Sahni S K, Rana V B, Dua K & Dua S K, *J inorg nucl Chem*, 41 (1979) 21.
29 Gillard R D, Silver H G & Wood J L, *Spectrochim Acta*, 20 (1964) 63.
30 Miners J C, Coles R B & Harris C M, *J chèm Soc Dalton Trans*, (1972) 1149.
31 Sayed L-El & Iskander M F, *J inorg nucl Chem*, 33 (1971) 435.
32 Dutta R L & Das B R, *Indian J Chem*, 22A (1983) 207.
33 Dutta R L & Hossain M, *Indian J Chem*, 21A (1982) 985.
34 Archer R D & Costoradi B P, *Inorg Chem*, 4 (1965) 1584.
35 Gosavi R K & Rao C N R, *J inorg nucl Chem*, 29 (1967) 1937.

Indian Journal of Chemistry
Vol. 31A, December 1992, pp. 943-946

The stoichiometry and kinetics of oxidation of 1,4-benzenediol by diaquotetrakis(2,2′-bipyridine)-μ-oxodiruthenium(III) cation in perchlorate medium

J Femi Iyun*
Department of Chemistry, Ahmadu Bello University, Zaria (Nigeria)
and
G Adefikayo Ayoko*
Department of Chemistry, University of Papua, New Guinea, P.O. Box 320, University, NCD, (Papua New Guinea)
and
H Muda Lawal
Chemistry Department, Abubakar Tafawa Balewa University, Bauchi, (Nigeria)

Received 30 December 1991; revised 2 June 1992; accepted 5 August 1992

The stoichiometry and kinetics of oxidation of 1,4-benzenediol (hydroquinone, H_2Q) by the oxo-bridged dimer, diaquotetrakis(2,2′-bipyridine)-μ-oxodiruthenium(III) cation ($[Ru_2O]^{4+}$) has been investigated in aqueous perchloric acid. At $[H^+]=0.05$ mol dm^{-3}, $I=1.0$ mol dm^{-3} ($NaClO_4$) and $T=25.0\pm0.1$°C, the reaction conforms to an overall equation,

$$2[Ru_2O]^{4+} + H_2Q = 2[Ru_2O]^{3+} + Q + 2H^+$$

The experimental result is consistent with a second-order rate law,

$$-\tfrac{1}{2}\, d[Ru_2O^{4+}]/dt = k_2[Ru_2O^{4+}][H_2Q]$$

with $k_2=(12.4\pm1.1)\times10^{-2}$ mol^{-1} dm^3 s^{-1}. Added Li^+, Na^+, Pb^{2+}, Mg^{2+} and Mn^{2+} have no effect on the rate of the reaction while Cl^-, Br^- and NO_3^- catalyze the reaction. Rate of the reaction is independent of change in [acid] of the reaction medium in the range $0.05\leqslant1.0$ mol dm^{-3} and is not affected by changes in ionic strength in the range $0.25\leqslant I\leqslant2.0$ mol dm^{-3}. On the basis of the results of this investigation, the absence of both spectroscopic and kinetic evidence of complex formation prior to electron-transfer and the non-conformity of our results with the Michaelis-Menten equation, it is suggested that the oxidation of hydroquinone by $[Ru_2O]^{4+}$ most probably proceed by an outer-sphere mechanism.

Meyer *et al.*[1] reported that the μ-oxobridged complexes of ruthenium(III) displayed some properties quite different from analogous monomeric ruthenium(II) and ruthenium(III) complexes and attributed them to an extensive metal-metal electronic interaction across the oxide linkage. Such properties as displayed by these ruthenium(III) oxobridged dimers[1], like their relatively high energy transfer ability, has provided a basis for the design of artificial systems used in the splitting of water with solar energy[2] and for the use of their higher oxidation state forms as oxidative catalysts[3]. We have recently shown some interest[4-7] in the substitution and electron-transfer reactions of some of these μ-oxobridged complexes. In this paper, we report the stoichiometry and kinetics of the oxidation of 1,4-benzenediol by diaquotetrakis(2,2′-bipyridine)-μ-oxodiruthenium(III) cation in acidic medium. It is our hope that these series of studies will highlight the effect of the cross-bridge electronic interaction of the ruthenium centres on the wet chemistry of the μ-oxobridged dimers.

Materials and Methods

Diaquotetrakis(2,2′-bipyridine)-μ-oxo-diruthenium(III) perchlorate, $[(bipy)_2H_2ORuORuH_2O(bipy)_2](ClO_4)_4$ was prepared and characterized as reported by Meyer *et al.*[1] ($\varepsilon_{max}^{658}=25{,}000$). The solution of the dimer in aqueous media was very stable and was kept in the freezer when not being used. The dimer showed enhanced absorbance in aqueous acidic solutions when compared to aqueous solutions of the same concentration, although it

was equally stable. The enhancement in absorbance, which was independent of the acid concentration in the range, $0.05 \leqslant [H^+] \leqslant 1.0$ mol dm^{-3} suggested a possible protonation of the oxo-bridged dimer. The concentrations of the dimer solutions were determined spectrophotometrically before kinetic runs. Hydroquinone (M & B) was recrystallized from ethanol, washed with ether[8] and its purity confirmed by its melting point[9]. All other reagents (analar grade) were used as supplied. All solutions were prepared with doubly distilled water.

The stoichiometry was determined by spectrophotometric titration using the mole ratio method. The concentration of $[Ru_2O]^{4+}$ was kept constant at 1.87×10^{-5} mol dm^{-3} and that of H_2Q varied from 1.0×10^{-5} mol dm^{-3} to 1.0×10^{-2} mol dm^{-3} at $[H^+] = 0.05$ mol dm^{-3}, $I = 1.0$ mol dm^{-3} ($NaClO_4$) and $T = 25.0 \pm 0.1$°C.

The rate of the reaction was monitored on a Corning colorimeter 253 with a Perkin-Elmer 56 recorder attached, by following the decrease in absorbance of the oxobridged dimer at $\lambda = 658$ nm. The rates were monitored under pseudo-first order conditions with $[H_2Q]$ at least 100-fold in excess over the [dimer]. The ionic strength was maintained constant at 1.0 mol dm^{-3} ($NaClO_4$). Temperature was kept constant at 25.0 ± 0.1°C for all runs.

Results and Discussion

The stoichiometry of the reaction was found to be in the ratio 2.0:1. The overall equation for the reaction of $[Ru_2O]^{4+}$ by H_2Q can therefore be written as,

$$2[Ru_2O]^{4+} + H_2Q \rightarrow 2[Ru_2O]^{3+} + Q + 2H^+ \quad \ldots (1)$$

This suggests that $[Ru_2O]^{4+}$ undergoes a one-electron reduction. A similar stoichiometry was reported for the oxidation of hydroquinone[10,11] by Ce(IV), Fe^{3+} and Co^{3+}.

Acrylamide (0.001-0.015 mol dm^{-3}) was added to partially oxidised reaction mixtures of the dimer and hydroquinone at $[H^+] = 0.05$ mol dm^{-3} and at 1.0 mol dm^{-3}. We did not observe any gel formation even on addition of a large excess of methanol. This does not however rule out the possibility of the formation of the semiquinone radical in this reaction. Earlier reports on the reaction of hydroquinone with Fe^{3+}, Ce(IV) and Co(III) which are one-electron oxidizing agents showed that the rate-determining step in these reactions[12] is the formation of the semiquinone radical. However, Baxendale and Hardy[13] have suggested that the semiquinone radical is so reactive in most systems that it is difficult to observe it experimentally. This may be one reason why we did not observe it in this investigation. The oxidation of hydroquinone by multi-electron oxidants like Cr(IV) usually takes place in a single two-electron step to form *p*-quinone[12] although such oxidations can also pass through the semiquinone radical[14].

The UV spectrum of the product of this reaction had a maximum at $\lambda = 485$ nm. This is the same as the λ_{max} we observed in the reaction of $[Ru_2O]^{4+}$ with Fe^{2+} and ascorbic acid[5] and with I^- (ref. 6). We suspect that this is due to the $[Ru_2O]^{3+}$ product of these reactions.

The electronic spectra of the reaction mixture containing $[Ru_2O]^{4+} = 1.87 \times 10^{-5}$ mol dm^{-3}, $[H_2Q] = 0.01$ mol dm^{-3}, $[H^+] = 0.05$ mol dm^{-3} and $I = 1.0$ mol dm^{-3} ($NaClO_4$) was run after one and two minutes respectively and compared with that of the same concentration of the dimer alone at the same $[H^+]$ and ionic strength. There was no shift in the λ_{max} of 658 nm characteristic of the oxobridged dimer[1]. The addition of H_2Q to a solution of $[Ru_2O]^{4+}$ also did not result in any enhancement of the absorbance of the oxobridged dimer. Although this does not completely negate the formation of an intermediate complex, it suggests that if any intermediate complex is formed at all, it must have a very small formation constant.

The linearity of the pseudo-first order plots of $\ln(A_t - A_\infty)$ versus time (A_t and A_∞ are the absorbances of the reaction mixture at time t and at the end of the reaction respectively) up to more than 80% reaction suggests a first order dependence of the reaction rate on $[Ru_2O]^{4+}$. A plot of $\log k_1$ (k_1 is the pseudo-first order rate constant obtained from the slope of the pseudo-first order plots) versus $\log[H_2Q]$ at $[H^+] = 0.05$ mol dm^{-3}, $I = 1.0$ mol dm^{-3}, gave a slope of 0.98 ± 0.06 indicating that the reaction is first order in $[H_2Q]$. At $[H^+] = 0.05$ mol dm^{-3}, the reaction is overall second order and can be represented as in Eq. (2).

$$-\tfrac{1}{2} d[Ru_2O^{4+}]/dt = k_2[Ru_2O^{4+}][H_2O] \quad \ldots (2)$$

The second order rate constants, k_2 determined as $k_1/[H_2Q]$ are presented in Table 1. At $[H^+] = 0.05$ mol dm^{-3} the average value of k_2 was obtained as $(12.4 \pm 1.1) \times 10^{-2}$ mol^{-1} dm^3 s^{-1}. The second order kinetics observed in this investigation is similar to that observed in the reaction of hydroquinone with Mn^{3+} and Fe^{3+} (ref. 10).

Cr(VI)[15] and also in the copper complex catalysed aerobic oxidation of hydroquinone[16].

The second order rate constant was determined as a function of [acid] in the range $0.05 \leqslant [H^+] \leqslant 1.0$ mol dm^{-3} and the results are presented in Table 1. The rate constant was insensitive to the changes in $[H^+]$ in the acid range investigated. This result correlates some earlier acid-dependence studies involving hydroquinone. For example, no hydrogen ion dependence was observed in the reaction of hydroquinone with 12-tungstocobaltate(III) ion[11] and with Ce(IV)[10]. The lack of acid dependence of this reaction might not be unconnected with the very low acid dissociation constant of hydroquinone. The pK_a for the formation of the hydroquinone anion is 10.35[17] in the acid range investigated at 25°C. It is therefore most probable that the native form of the hydroquinone predominates over the acid range investigated. In some earlier reactions, the dependences of hydroquinone reactions on $[H^+]$ have been attributed to either the hydrolysis or the protonation capabilities of the metal ions involved[18].

On the basis of our results and the results of earlier investigations[6,7] we are proposing the mechanism in Scheme 1 for the oxidation of H_2Q by $[Ru_2O]^{4+}$.

$$[Ru_2O]^{4+} + H_2Q \overset{K_3}{\rightleftharpoons} [Ru_2O]^{4+} \cdot H_2Q \quad \ldots (3)$$

$$[Ru_2O]^{4+} \cdot H_2Q \overset{k_4}{\rightarrow} [Ru_2O]^{3+} + H^+ + HQ \quad \ldots (4)$$

$$[Ru_2O]^{4+} + HQ \overset{k_5}{\rightarrow} [Ru_2O]^{3+} + H^+ + Q \quad \ldots (5)$$

Scheme 1

With Eq. (4) as the rate-determining step, the rate equation is,

$$-\tfrac{1}{2}\, d[Ru_2O^{4+}]\,/dt = k_4[Ru_2O^{4+} \cdot H_2Q] \quad \ldots (6)$$

Substituting for $[Ru_2O^{4+} \cdot H_2Q]$ from Eq. (3) gives the rate of reaction as,

$$-\tfrac{1}{2}\, d[Ru_2O^{4+}]\,/dt = k_4 K_3[Ru_2O^{4+}][H_2Q] \quad \ldots (7)$$

Equation (7) is similar to Eq. (2) with

$$k_2 = k_4 K_3 \quad \ldots (8)$$

Hence the proposed mechanism agrees with experimental results.

The results in Table 1 show that changes in ionic strength has no effect on the oxidation of H_2Q by $[Ru_2O]^{4+}$. Similar results have been reported for some reactions of hydroquinone[18,19]. The observed zero Bronsted-Debye[20] salt effect is consistent with the undissociated or unprotonated hydroquinone as the reactant.

Table 1 – Pseudo-first order and second order rate constants for the reaction of $[Ru_2O]^{4+}$ and H_2Q. $[Ru_2O]^{4+} = 1.87 \times 10^{-5}$ mol dm^{-3}, T = 25.0 ± 0.1°C, λ = 658 nm

$10^2 \times [H_2Q]$ (mol dm^{-3})	$10^2 \times [H^+]$ (mol dm^{-3})	I (mol dm^{-3})	$10^4\, {}^xk_1$ (s^{-1})	$10^2\, {}^xk_2$ (mol^{-1} dm^3 s^{-1})
0.2	5	1.0	2.8	13.8
0.5	5	1.0	6.4	12.8
1.0	5	1.0	13.4	13.4
2.0	5	1.0	22.2	11.1
3.0	5	1.0	37.6	12.5
5.0	5	1.0	55.0	11.0
10.0	5	1.0	132.0	13.2
20.0	5	1.0	234.0	11.7
1.0	5	1.0	11.9	11.9
1.0	5	1.0	11.5	11.5
1.0	20	1.0	11.2	11.2
1.0	30	1.0	12.3	12.3
1.0	50	1.0	11.5	11.5
1.0	70	1.0	11.9	11.9
1.0	100	1.0	12.3	12.3
1.0	5	0.25	12.0	12.0
1.0	5	0.50	12.2	12.2
1.0	5	0.75	12.8	12.8
1.0	5	1.0	11.8	11.8
1.0	5	1.25	11.5	11.5
1.0	5	1.50	13.0	13.0
1.0	5	1.75	12.5	12.5
1.0	5	2.0	11.9	11.9

As the results of Table 2 show, the addition of different concentrations of Li^+, Na^+, Pb^{2+} and Mn^{2+} had no effect on the reaction rate. The rate of the reaction was however enhanced by added Cl^-, Br^- and NO_3^-. The enhancement in rate was in the order $Br^- > Cl^- > NO_3^-$ in the range $0.01 \leqslant (X^-) \leqslant 0.1$ *M* (where X = Br, Cl, NO_3). The plot of the anion-dependent second order rate constant ${}^xk_2$ versus $[X^-]$ fitted an equation,

$${}^xk_2 = p + q[X^-] \quad \ldots (9)$$

with $p(Br^-) = (12.1 \pm 0.2) \times 10^{-2}$ mol^{-1} dm^3 s^{-1},
$q(Br^-) = 1.67 \pm 0.20$ mol^{-2} dm^6 s^{-1},
$p(Cl^-) = (12.4 \pm 0.1) \times 10^{-2}$ mol^{-1} dm^3 s^{-1},

Table 2 – The effect of anions and cations on the second order rate constants for the $[Ru_2O]^{4+} + H_2Q$ reaction. $[Ru_2O]^{4+} = 1.87 \times 10^{-5}$ mol dm^{-3}, $[H_2Q] = 0.01$ mol dm^{-3}, $[H^+] = 0.05$ mol dm^{-3}, $I = 1.0$ mol dm^{-3}, ($NaClO_4$), T = 25.0 ± 0.1°C, $\lambda = 658$ nm.

X	$10^2 \times [X]$ (mol dm^{-3})	$10^4 \times k_1$ (s^{-1})	$10^2 \times k_2$ (mol^{-1} dm^3 s^{-1})
Li^+	1.0	12.5	12.5
	5.0	12.1	12.1
	10.0	12.3	12.3
Na^+	1.0	12.2	12.2
	5.0	11.8	11.8
	10.0	11.8	11.8
Pb^{2+}	1.0	11.9	11.9
	5.0	12.2	12.2
	10.0	12.1	12.1
Mg^{2+}, Mn^{2+}	1.0	12.5	12.5
	5.0	12.4	12.4
	10.0	12.1	12.1
Cl^-	1.0	13.9	13.9
	3.0	15.3	15.3
	5.0	17.7	17.7
	7.0	19.8	19.8
	10.0	24.4	24.4
Br^-	1.0	18.5	18.5
	3.0	22.8	33.8
	5.0	24.1	24.1
	7.0	28.9	28.9
	10.0	33.0	33.0
NO_3^-	1.0	13.7	13.7
	5.0	16.3	16.3
	7.0	17.9	17.9
	10.0	21.5	21.5

$q(Cl^-) = 1.16 \pm 0.18$ mol^{-2} dm^6 s^{-1}, $p(NO_3^-) = (12.2 \pm 0.2) \times 10^{-2}$ mol^{-1} dm^3 s^{-1} and $q(NO_3^-) = 0.90 \pm 0.17$ mol^{-2} dm^6 s^{-1} at $[H^+] = 0.05$ mol dm^{-3}, $I = 1.0$ mol dm^{-3}.

The anion catalysis suggests that this reaction most probably proceeds by an outer sphere mechanism. Anion catalysed reactions are thought to be characteristic of outer sphere reactions[21,22]. That the oxidation of H_2Q by $[Ru_2O]^{4+}$ proceeds by the outer sphere mechanism is further supported by the absence of either kinetic or spectroscopic evidence of complex formation. Similar observations and deductions were made in the reaction of hydroquinone with IO_4^- and with Cr(VI) (ref. 14).

The plot of $1/k_1$ versus $1/[H_2Q]$ was linear and passed through the origin suggesting the absence of any precursor complex formation prior to the electron-transfer step. As in the reaction of Co(III) with 1,2-aromatic diols[23] and that of 12-tungstocobaltate(III) with hydroquinone[11], we are proposing that the oxidation of H_2Q by $[Ru_2O]^{4+}$ proceed by the outer sphere mechanism.

References

1 Weaver T R, Meyer T J, Adeyemi S A, Brown G M, Eckberg W E, Hatfield W E, Johnson E C, Murray R W & Unterker D, *J Am chem Soc*, 97 (1975) 3039.

2 (a) Bolleta F, Joris A, Moesln M & Sandrini D, *Inorg Chim Acta* 44 (1980) 175.
(b) Taqui Khan M M, Ramachandraiah & Prakash Rao, *Inorg Chem*, 25 (1986) 665.
(c) Creutz C & Sutin N, *Proc Natl Acad Sci, USA*, 72 (1975) 2858.

3 (a) Chi-Ming C, Kwok Y N, Wai-Ho L & Chung-Kwong P, *Inorg Chem*, 25 (1986) 345.
(b) Meyer T J, Sipe K B & Meyer B A, *Inorg Chem*, 20 (1981) 1475.
(c) Meyer T J, *J Electrochem Soc*, 7 (1984) 221.
(d) Gersten S W, Samuels G J & Meyer T J, *J Am chem Soc*, 104 (1982) 4029.
(e) Gilbert J A, Gersten S W & Meyer T J, *J Am chem Soc*, 104 (1982) 6872.
(f) Thompson M S & Meyer T J, *J Am chem Soc*, 104 (1982) 4106.
(g) Thompson M S & Meyer T J, *J Am chem Soc*, 104 (1982) 5070.
(h) Thompson M S, DeGiovani W F, Moyer B A & Meyer T J, *J org Chem*, 49 (1984) 4972.

4 Iyun J F & Adegite A, *J chem Soc, Nigeria*, 14 (1981) 11.

5 Iyun J F & Adegite A, *Bull chem Soc, Ethiopia*, 4 (1990) 27.

6 Iyun J F, Ayoko A & Lawal H M, *Transition met Chem.* in press.

7 Iyun J F, *J chem Soc Nigeria*, in press.

8 Brodovitch J C, McAuley A & Oswald T, *Inorg Chem*, 21 (1982) 3442.

9 Roberts J D & Caserio M C, *Basic principles of organic chemistry*, (W A Benjamin, New York) (1965) pp. 902.

10 Wells C F & Kuritsyn L V, *J chem Soc A*, (1969) 2575.

11 McAuley A, Amjad Z & Brodovitch Z, *Can J Chem*, 55 (1977) 3581.

12 Pelizzetti E, Mentasti E & Saini G, *J chem Soc Dalton Trans*, (1973) 2605.

13 Baxendale J H & Hardy H R, *Trans Faraday Soc*, 47 (1951) 963.

14 Ghosh S K, Bose R N & Gould E S, *Inorg Chem*, 27 (1988) 1620.

15 Sullivan J C & French J E, *J Am chem Soc*, 87 (1965) 538.

16 Frey J W, Klein J & Klesper E, *Makromol Chem*, 188 (1987) 821.

17 *Handbook of chemistry and physics*, edited by R C Wiest (Chemical Rubber Publishing Co., Cleveland, Ohio) (1972).

18 Wells C F & Kuritszn L V, *J chem Soc A* (1979) 676.

19 Kaiser E T & Weidman S W, *J Am chem Soc*, 87 (1964) 4354.

20 Bronsted J N, *Z Phys Chem*, 102 (1922) 160.

21 Adegite A, Iyun J F & Ojo J F, *J chem Soc Dalton Trans*, (1977) 115 and the references therein.

22 Przystas T J & Sutin N, *J chem Soc*, 95 (1973) 5545.

23 Pelizzetti E, Mentasti E & Pramauro E, *Inorg Chem*, 15 (1976) 2898.

Indian Journal of Chemistry
Vol. 31A, December 1992, pp. 947-950

Studies on electrode kinetics of schiff bases in aqueous and DMF media

A S Madhava, G Ramachandraiah† & D N Vyas*
University Department of Chemistry, Bhavnagar University, Bhavnagar 364 002

Received 24 September 1991; revised 3 March 1992; accepted 1 July 1992

Electrochemical reduction of schiff bases, viz., salicylidene-2-hydroxyaniline (**1**), acetophenonidene-2-hydroxyaniline (**2**), 4-hydroxyacetophenonidene-2-hydroxy aniline (**3**) and 4-hydroxyacetophenonidene-2-hydroxy-5-chloroaniline (**4**) using techniques of cyclic voltammetry, chronoamperometry and chronopotentiometry in buffer solutions of different *p*H and in 100% DMF at HMDE have been carried out. The kinetic parameters have been determined and the mechanism for electrochemical reduction of these schiff bases has also been proposed.

Although the preparation, structural and spectral characterisation and the coordination chemistry of schiff bases have been studied extensively[1,2], yet little is reported on the polarographic studies and their metal complexes[3]. Recently, studies on schiff bases derived from salicylaldehyde, acetophenone and 4-hydroxy acetophenone with *o*-aminophenol and its chloro derivative using voltammetric, potentiometric and spectrophotometric techniques have been reported[4]. In continuation of our earlier work, an attempt is made to study the kinetic parameters for the reduction of these schiff bases **1-4** at HMDE in aqueous and DMF media by cyclic voltammetry, chronoamperometry and chronopotentiometry.

Materials and Methods

The cyclic voltammograms of schiff bases (solutions) were recorded with PARC model 384 B Polarographic analyser equipped with a Houstan DMP-40 digital plotter and PAR 303 A cell assembly as described earlier[4]. The chronoamperometric and chronopotentiometric results were recorded with PAR 175 universal programmer connected to PAR 306 and PAR 176 current voltage converter. A cup shaped cell provided with model PAR 303 SMDE/HMDE, containing platinum wire (auxillary) and SCE (reference) electrodes was used throughout the study. The effective area of the working electrode employed was 0.017 cm^2.

The schiff bases **1-4** were prepared according to the procedure described earlier[4]. Stock solutions (0.1 *M*) of the schiff bases were prepared in DMF and the ionic strength and varying *p*H values of solutions were maintained as mentioned previously[4]. The schiff bases **1-4** were also studied in 100% DMF with tetrabutyl ammonium perchlorate (TBAP) (0.1 *M*) in final volume of 5 ml. The ligand solutions were deaerated with nitrogen. The characteristic $i \rightarrow E$, $i \rightarrow t$ and $E \rightarrow t$ plots were recorded under specific conditions as mentioned in the respective Tables.

Results and Discussion

Cyclic voltammetry

All the schiff bases **1-4** at *p*H 8, show one cathodic peak and its anodic counterpart in the potential range −0.5 V to −0.4 V versus Ag/AgCl. A representative diagram for schiff base **1** at *p*H 8 has been given (Fig. 1A). The reduction and oxidation steps of all the schiff bases have been earlier explained on the basis of reversible 2 electron exchange[4]. The electrode process in all the cases is found to be coupled with protons of the medium. The peak currents are almost constant in the *p*H range 5.0-7.5 and found decreasing on either side of it. The ratio of anodic to cathodic currents is always less than unity at lower scan speeds and the difference between the cathodic and anodic peak potentials, ΔE_p, is greater than 0.3 V. Further, the peak potentials are also dependent on scan speeds. Similar results are obtained at all *p*H values in the range 1-10. These observations clearly indicate that the two electron reduction of schiff bases **1-4** at HMDE is not totally reversible. The plots of $i p_c$ versus $\nu^{1/2}$ are linear and pass through origin at all the *p*H values. This shows that the electrode process is controlled by diffusion in all the cases. Table 1 presents the cyclic voltammetric data of schiff bases **1-4** at two selected *p*H (3.5/5.2 and 8) values where they ex-

†Coordination Chemistry & Homogeneous Catalysis Division, CSMCRI, Bhavnagar 364 002

Table 1 – Cyclicvoltammetric data for schiff bases **1-4** at different *p*H and in DMF
[μ = 0.1 *M* TBAP; conc. = 1 m*M*; W.E. = HMDE; R.E. = Ag/AgCl]

Schiff base	*p*H/DMF	Scan rate V/sec	i_{p_c} μA	i_{p_a} μA	i_{p_a}/i_{p_c}	$-E_{p_c}$ V	$-E_{p_a}$ V	E_p V
1	3.5	0.05	0.53	0.35	0.65	0.150	0.090	0.060
		0.10	0.75	0.50	0.67	0.160	0.090	0.070
	8.0	0.05	0.58	0.42	0.72	0.400	0.340	0.060
		0.10	1.85	1.30	0.70	0.410	0.340	0.070
	DMF	0.05	1.09	1.00	0.92	0.760	0.630	0.130
		0.10	1.65	1.50	0.91	0.770	0.630	0.140
2	5.2	0.05	1.40	0.65	0.47	0.284	0.200	0.084
		0.10	2.06	0.95	0.46	0.286	0.200	0.086
	8.0	0.05	0.50	0.32	0.63	0.436	0.371	0.065
		0.10	1.60	1.10	0.64	0.440	0.375	0.065
	DMF	0.05	1.16	1.10	0.95	0.908	0.780	0.128
		0.10	1.81	1.76	0.94	0.926	0.780	0.146
3	3.5	0.05	0.50	0.31	0.62	0.162	0.097	0.065
		0.10	0.71	0.45	0.63	0.169	0.099	0.070
	8.0	0.05	0.58	0.39	0.67	0.493	0.425	0.068
		0.10	1.64	1.15	0.70	0.498	0.426	0.072
	DMF	0.05	1.00	0.91	0.91	0.875	0.760	0.115
		0.10	1.40	1.25	0.89	0.880	0.760	0.120
4	3.5	0.05	0.48	0.30	0.62	0.085	0.017	0.068
		0.10	0.75	0.52	0.69	0.090	0.018	0.072
	8.0	0.05	0.55	0.37	0.67	0.452	0.387	0.065
		0.10	1.46	0.95	0.65	0.458	0.383	0.075
	DMF	0.05	1.20	1.07	0.89	0.855	0.720	0.135
		0.10	1.80	1.63	0.90	0.860	0.720	0.140

ist as a single component viz. either protonated or the free form[4].

The cathodic and anodic processes of schiff bases **1-4** in DMF appear in the potential region −0.95 V-0.6 V and the difference in peak potentials, ΔE_p, is always greater than 0.1 V which indicates that the reduction process is not the same as that in the aqueous medium. However, the plots of $^{i}p_c$ versus $\nu^{1/2}$ are linear and pass through the origin (Fig. 1.C). The cyclic voltammograms for the schiff base **1** in DMF is given in Fig. 1B. The peak potentials and peak currents data of all the four schiff bases are given in Table 1.

Chronoamperometry

The diffusion coefficients of the schiff bases in different solvents were studied by chronoamperometry. The chronoamperograms of the schiff bases **1-4** in both aqueous and DMF media are well defined at their respective peak potentials or beyond that. In each case, the plots of $it^{1/2}$ versus t are horizontal showing that the charge transfer process is diffusion controlled. The linear portion of these plots are extrapolated to zero time to obtain $(it^{1/2})_{t=0}$. This quantity is used to evaluate the coefficients of the corresponding schiff bases with Cottrell equation[5] (1),

$$i = \frac{nFA\, D_{ox}^{1/2}\, C_{ox}^{*}}{\pi^{1/2}\, t^{1/2}} \qquad \ldots (1)$$

where t = time in seconds, i = instantaneous currents in microamperes, C_{ox}^{*} = concentration of schiff base in millimoles per litre.

The data obtained are presented in Table 2 and the plot of $it^{1/2}$ versus t for the schiff base **1** in DMF is given in Fig. 1 D.

Chronopotentiometry

In order to verify the diffusion coefficient data of the schiff bases in different solvent media and to evaluate electrode kinetic parameters, chronopotentiometric study was also undertaken. The typical E → t plots for the schiff bases **1-4** in aque-

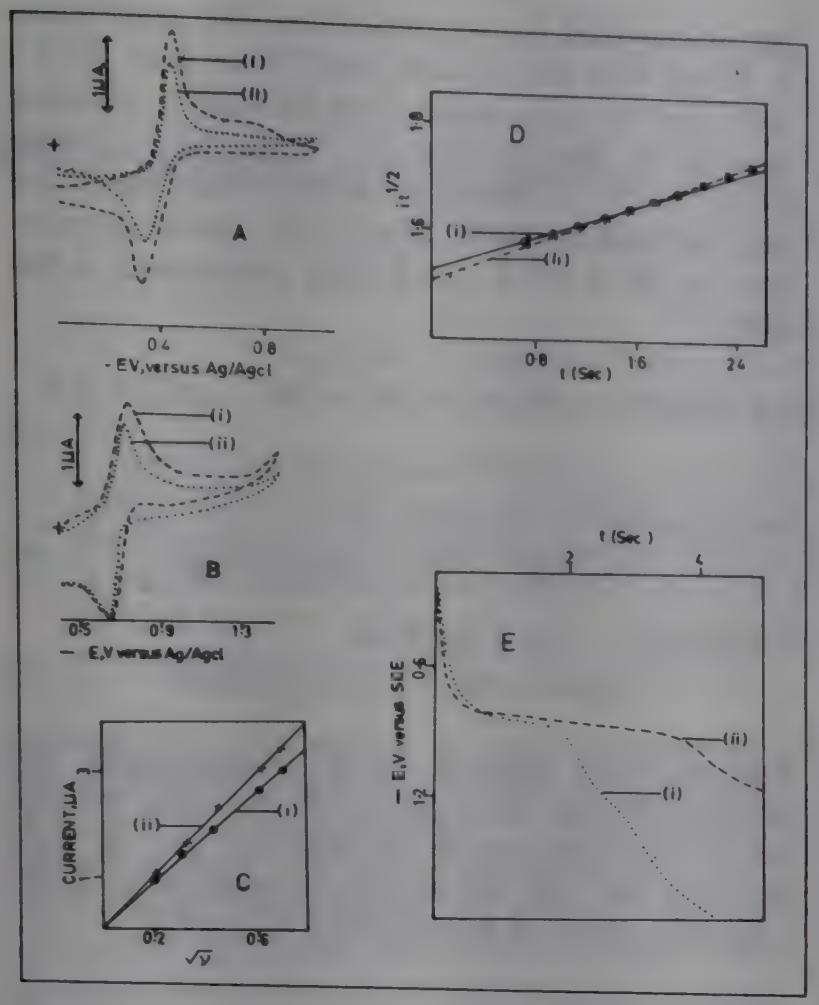

Fig. 1(A) – Cyclic voltammogram of schiff base **1** at *p*H 8.0 scan speed, ν, (i) 0.2 V/sec and (ii) 0.1 V/sec. conc. = 1 m*M*; W.E. = HMDE. (B) Cyclic voltammogram of schiff base **1** in 100% DMF scan speed, ν, (i) 0.2 V/sec (ii) 0.1 V/sec; conc. = 1 m*M*; W.E. = HMDE; supporting electrolyte TBAP. (C) Plots of i_p versus $\nu^{1/2}$ for schiff base **1** (i) and schiff base **2** (ii) in 100% DMF. (D) Plots of $it^{1/2}$ versus t for the reduction of schiff base **1** in 100% DMF at applied voltage (i) −0.85 V (ii) −0.90 V vs SCE, Conc. = 1 m*M*, (E) Chronopotentiograms of schiff base **1** (i) and schiff base **2** (ii) in DMF at applied current 2 μA; supporting electrolyte TBAP; conc. = 1 m*M*

ous and DMF media were obtained by applying the current densities in the range 1-3 μA. They were well defined and the transition times, τ, obtained were in the range 0.5 to 3 seconds for aqueous solutions and 0.5 to 6.7 seconds for DMF solutions. The $i\tau^{1/2}$ values (Table 2) for each schiff base were found fairly constant but they were different from each other. The consistancy in the result indicates that the reduction process involved in each schiff base is diffusion controlled. The chronopotentiograms of the schiff bases **1** & **2** in DMF are given in Fig. 1E. With the help of chronopotentiometric data, the diffusion coefficients of schiff bases **1-4** have been calculated using equation[6] (2),

$$\tau^{1/2} = \frac{\pi^{1/2} n F A D_{ox}^{1/2} C_{ox}}{2i} \quad \ldots (2)$$

Table 2 – Chronopotentiometric data of schiff bases **1-4** in aqueous and DMF media

Conc.: 1 m*M*

Schiff base	*p*H/DMF	Current applied μA	Transition time, τ, sec	$it^{1/2}$
1	3.5	1.5	1.31	1.72
	8.0	2.0	1.20	2.19
	DMF	1.5	3.14	2.66
		2.0	1.57	2.51
2	5.2	1.5	0.66	1.22
	8.0	2.0	1.10	2.10
	DMF	1.5	6.70	3.88
		2.0	3.35	3.66
3	3.5	1.5	1.17	1.62
	8.0	2.0	0.97	1.97
	DMF	1.5	3.00	2.59
		2.0	1.60	2.52
4	3.5	1.5	1.10	1.57
	8.0	2.0	0.90	0.90
	DMF	1.5	3.10	2.64
		2.0	1.59	2.52

and the values are reported in Table 3. The values so obtained in two different media are in good agreement with those obtained from chronoamperometric data.

Kinetic studies

The peak separation values, ΔE_p, were used to calculate the standard reaction rate constant k_s^0 for the reduction of each schiff base in aqueous and DMF media using Eq. (3) of Nicholson[7]

$$\psi = \frac{\gamma^{\alpha} k_s^0}{(\pi(nF/RT)D_{ox})^{1/2}} \quad \ldots (3)$$

Here ψ is the function of ΔE_p, γ is the ratio of the diffusion coefficients of the reduced and oxidised forms of the electroactive species ($D_{red}/D_{ox} \simeq 1$), α is the transfer coefficient and all other symbols have their usual meanings.

The potential, E_t at a definite time, t, expressed by Eq. (4),

$$E_t = \frac{RT}{\alpha n_a F} \ln\left(\frac{nFAC_{ox} K_m^0}{i}\right) + \frac{RT}{\alpha n_a F} \ln[1-(t/\tau)^{1/2}] \quad \ldots (4)$$

is utilised by plotting E_t versus $\log[1-(t/\tau)^{1/2}]$, as it satisfies the condition of linear diffusion[8] at this

Table 3 – Kinetic parameters for the reduction of schiff bases **1-4** at different *p*H

[Conc. = 1.0 m*M* (aqueous and DMF media); $\mu = 0.1$ *M* (TBAP); scan speed (ν) = 0.1 V/sec; W.E. = HMDE; R.E. = Ag/AgCl/SCE]

Schiff	*p*H/DMF	$D \times 10^6$ cm/sec		$^*\alpha n_a$	$^*k_{fh}^0 \times 10^{14}$ cm/sec	ψ	$^{**}k_s^0 \times 10^2$ cm/sec
		*CP	**CA				
1	3.5	0.32	0.49	0.85	0.410	2.63	0.910
	8.0	0.62	0.78	0.90	0.450	2.63	1.150
	DMF	0.75	0.67	0.69	0.782	0.16	0.064
2	5.2	0.29	0.29	0.87	0.220	0.95	0.250
	8.0	0.31	0.30	0.93	0.240	25.12	1.410
	DMF	1.53	1.12	0.71	0.245	0.23	0.120
3	3.5	0.26	0.43	0.82	0.380	2.63	0.850
	8.0	0.55	0.70	0.91	0.420	2.20	0.910
	DMF	0.75	0.63	0.73	0.537	0.36	0.143
4	3.5	0.24	0.41	0.80	0.250	2.20	0.690
	8.0	0.52	0.67	0.83	0.290	1.66	0.670
	DMF	0.75	0.61	0.73	0.614	0.16	0.193

*Calculated from chronopotentiometric (CP) data

**Calculated by cv using the diffusion coefficients from chronoamperometric (CA) data

potential. By using intercept and slope values of various plots, the forward rate constant k_{fh}^0 and αn_a of the schiff bases in aqueous and DMF media have been calculated. The values of k_s^0, k_{fh}^0 and αn_a so obtained are presented in Table 3. The values of k_s^0 suggest that the electrode process in both aqueous and DMF media are not reversible[9]. The k_s^0 values in DMF are almost ten times less than those in aqueous media which indicates that electrode processes in DMF are relatively more irreversible. The k_s^0 values in aqueous medium are found higher in the basic range of *p*H than in the acidic range. Among all the four schiff bases studied it is marked that the schiff base **2** is quickly reduced and is less irreversible in acidic medium and schiff base **4** in basic medium.

Mechanism of the electrode processes

Our earlier findings[4] showed that the formal potentials of the single redox couple in **1-4** are *p*H dependent. The anodic shifts of peak potentials (Table 1) with decreasing *p*H suggest the resultant effect of protons in the electron transfer rate steps. Earlier potentiometric data[4] had shown the protonation of the schiff bases **1-4** in acidic *p*H. It can thus be concluded that the schiff bases **1**, **3** and **4** at *p*H 3.5 and schiff base **2** at *p*H 5.2 fully exist in protonated form through a chemical reaction at the nitrogen of $-C(R)=N-$ (where R = N or CH_3). However, all the schiff bases **1-4** exist as such at *p*H 8. Hence, the electrode reactions at *p*H 3.5/5.2 and 8.0 are considered as follows:

$$-C(R)=N- + H^+ \rightleftharpoons -C(R)=\overset{+}{N}H-\ (pH\ 3.5/5.2) \quad \ldots (5)$$

$$-C(R)=\overset{+}{N}H- + 2e + 2H^+ \rightleftharpoons -C(R)H-\overset{+}{N}H_2-\ (pH\ 3.5/5.2) \quad \ldots (6)$$

$$-C(R)=N- + 2e + 2H_2O \rightleftharpoons -C(R)H-NH- + 2OH^-\ (pH\ 8) \quad \ldots (7)$$

The electrode reaction (6) is comparatively less irreversible than the reaction (7). In DMF, the following electrochemical reaction (8) can be proposed as the rate of electrolytic reaction in DMF is less than those of the reactions (6) and (7),

$$SB + 2e \rightleftharpoons (SB)^{2-} \quad \ldots (8)$$

Based on the experimental data in Table 3, the electron transfer rates in aqueous and DMF media were found in the order, reaction (8) < reaction (6) < reaction (7).

Acknowledgement

We are thankful to the Department of Chemistry, Bhavnagar University and CSMCRI, Bhavnagar, for library and other facilities. One of us (ASM) is thankful to Gujarat Government for financial support.

References

1 Boucher L J, *J inorg nucl Chem*, 36 (1974) 531.
2 Varshney A K, Verma P S & Varshney S, *Synth React Inorg Met Org Chem*, 19 (1989) 75.
3 Trivedi T, Patel M S & Vyas D N, *J Indian chem Soc*, LV (1978) 980.
4 Seshu Madhava A, Patil C J, Vyas D N & Ramachandraiah G, *Bull Electrochem*, 7 (1991) 283.
5 Adems R N, *Electrochemistry at solid electrodes* (Marcel Dekker, New York) 1966.
6 Sand H J S, *Philmag*, 1 (1901) 45.
7 Nicholson R S, *Analyt Chem*, 37 (1965) 1351.
8 Gelus Z, *Fundamentals of electrochemical analysis* (Ellie Marwood Ltd, Chichester) 1976, 243.
9 Matsuda H & Ayabe Y, *Z Electrochem*, 59 (1955) 494.

Indian Journal of Chemistry
Vol. 31A, December 1992, pp. 951-953

Physicochemical investigation of the reactions of some organo-phosphine derivatives with cyanogen halides

Habib A Aughsteen[†]
Department of Chemistry, College of Science, University of Salahaddin, Erbil - Iraq
Received 18 March 1992; revised and accepted 25 June 1992

The organo-phosphines $CH_3P(C_6H_5)_2$, $(CH_3)_2PC_6H_5$ and $[(C_2H_5)_2N]_3P$ react with CNX(X = I and Br) in methyl cyanide solution to give two adducts, a 1:1 of ionic nature and 2:1 non-electrolyte, namely R_3PCNI and $R_3P(CN)_2$ respectively with CNI, whereas cyanogen bromide gives only one type of adduct of composition R_3PCNBr. Conductometric titration studies and molar conductance measurements show that the 1:1 adducts are very strong electrolytes. In contrast, the 2:1 adduct formed in the case of CNI is a non-electrolyte.

Although the preparation of new phosphorous compounds of the type $R_3P(CN)X$ (R = alkyl or aryl, X = Br or I) have been reported[1-5], the reaction of cyanogen halides with group VB elements has not been thoroughly investigated. By analogy with the reactions of halogens and inter-halogens with phosphines which give conducting species in aprotic solvents[6-8], it is of interest to study similar systems using pseudo-halogen halides instead of halogens. In view of the success achieved in the previous work from studying different phosphine-halogen systems by conductometric titration[9,10] a similar technique is used to study the behaviour of $CH_3P(C_6H_5)_2$, $(CH_3)_2PC_6H_5$ and $[(C_2H_5)_2N]_3P$ - CNX systems.

Materials and Methods

Methyl cyanide (Fluka, Puriss P.a.) was purified by somewhat modified method as described by Goetzee *et al.*[11]. The solvent was successively treated with NaOH, $CaCl_2$, and P_2O_5. After refluxing, the solvent was distilled to collect the middle cut during each distillation, dried and further distilled on the vacuum line to remove traces of any drying agent left over. This solvent was used for conductance measurements. For spectroscopic purposes, Fluka spectroscopic grade was used after drying over molecular sieve and then freeze dried.

Cyanogen iodide (CNI) (Fluka) was recrystallized twice from chloroform (mp. 146-147°C). Cyanogen bromide (CNBr) (Fluka) was always redistilled before use (mp.51-52°C).

Adduct preparations

The adducts $R_1R_2R_3P(CN)X$ (X = Br,I) were prepared by addition of solutions of cyanogen halides dissolved in petroleum ether (7-10 ml) to solution of $R_1R_2R_3P$ in a 1:1 mole ratio of CNX:phosphine. The resulted coloured oils were triturated with dry ether. The crystals obtained were washed with dry ether and then vacuum dried. All adducts decomposed in the range of 120-130°C during the determination of their melting points. The adducts $R_1R_2R_3P(CN)_2$ were isolated as white crystals when pet.ether solutions of CNX (X = Br,I) were added to $R_1R_2R_3P$ in 2:1 mole ratio of CNX:phosphines dissolved in pet.ether. The adducts prepared by similar methods were $CH_3P(C_6H_5)_2(CN)_2$, $(CH_3)_2PC_6H_5(CN)_2$, $[(C_2H_5)_2N]_3P(CN)_2$ and their respective mps were 108-110°, 103-104° and 114-115°C. Fluka ampuled samples of phosphines were used without any further purifications. The results of the elemental micro analyses of the various adducts (Alfred Bernhardt, West Germany) are given in Table 1.

For avoiding contact with moisture, all the work was carried out in dry box (P_2O_5). Dry nitrogen was flushed frequently so as to maintain an inert atmosphere.

A conductometric cell was placed in the dry box, on a magnetic stirrer, and was fitted with a dropping burette. The conductance of the solution, placed in the cell, was measured by using a Wayne Kerr B641 Autobalance Universal Bridge. The bridge was placed outside the dry box. The titrations were performed by varying the molar ratios of the reactants and the conductance values were recorded.

Infra-red spectra were recorded on Pye Unicam SP1000 infrared spectrophotometer. Ultraviolet spectra were recorded on Perkin-Elmer spectrophotometer, Hitachi 2000.

[†] Present address: Department of Chemistry, College of Education, Taiz, P.O. Box 6803, Yemen.

Table 1—Elemental analyses of the adducts

Adduct	Found				Calc.			
	%C	%H	%N	%P	%C	%H	%N	%P
$CH_3P(C_6H_5)_2CNI$	47.02	3.96	4.08	9.02	47.59	3.68	3.96	8.78
$CH_3P(C_6H_5)_2CNBr$	54.26	4.02	4.81	10.72	54.90	4.25	4.58	10.13
$(CH_3)_2PC_6H_5CNI$	37.81	3.84	4.62	11.03	37.24	3.79	4.83	10.69
$(CH_3)_2PC_6H_5CNBr$	44.80	4.19	5.98	13.08	44.26	4.51	5.74	12.70
$[(C_2H_5)_2N]_3PCNI$	39.13	7.39	14.61	8.03	39.00	7.50	14.00	7.75
$[(C_2H_5)_2N]_3PCNBr$	44.05	8.86	15.98	9.01	44.19	8.50	15.86	8.78
$CH_3P(C_6H_5)_2P(CN)_2$	70.99	5.21	11.49	12.43	71.43	5.16	11.11	12.31
$(CH_3)_2PC_6H_5(CN)_2$	63.83	6.01	14.39	15.98	63.16	5.78	14.73	16.14
$[(C_2H_5)_2N]_3P(CN)_2$	56.81	10.11	23.08	10.59	56.19	10.03	23.41	10.37

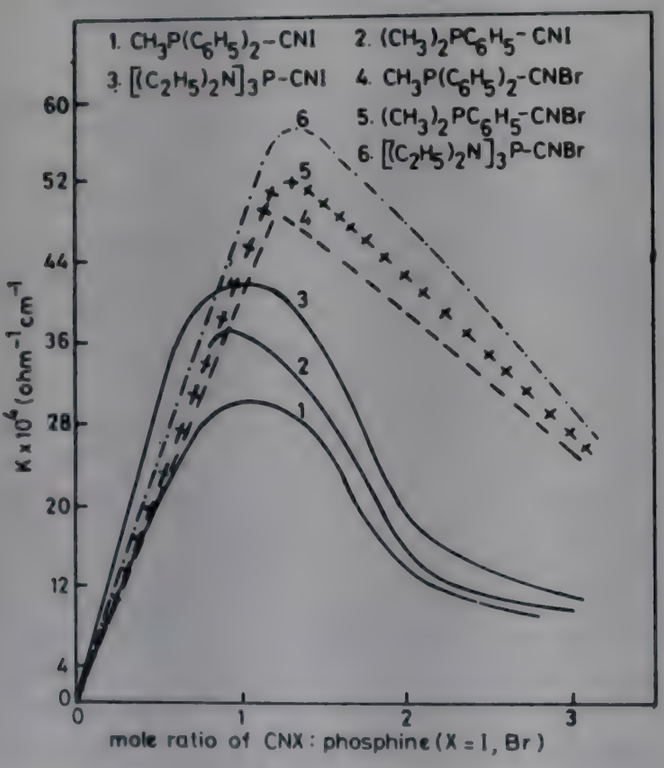

Fig. 1—Conductometric titration graphs

Table 2—Molar conductance values calculated at 1:1 and 2:1 breaks (Fig.1)

Curve	(ohm^{-1} Λ_m cm^2 mol^{-1})	C_m($mol.l^{-1}$)
	1:1 breaks	
1	92.12	0.0315
2	99.31	0.0365
3	104.06	0.0372
4	115.39	0.0416
5	119.82	0.0430
6	127.73	0.0441
	2:1 breaks	
1	38.0762	0.0326
2	49.1306	0.0420
3	57.7284	0.0462

$\Lambda_m = \frac{10^3 K}{C}$, K = Specific conductance in ohm^{-1} cm^{-1}

C_m = Concentration in $mol.l^{-1}$

Results and Discussion

The interaction of $CH_3P(C_6H_5)_2$, $(CH_3)_2PC_6H_5$ and $[(C_2H_5)_2N]_3P$ with CNX, X = Br and I, in methyl cyanide was investigated by conductometric titration technique. The conductance graphs obtained are shown in Fig.1. Curves show two inflections around 1:1 and 2:1 mole ratios of CNI:phosphines, and one break only close to 1:1 mole ratio of CNBr:phosphines.

These breaks clearly indicate that the two systems behave differently after the 1:1 mole ratio in methyl cyanide solution.

The molar conductance measured at the observed breaks in the conductometric titration graphs are given in Table 2. Thus it is evident that both adducts (of CNI and CNBr) formed in solution at 1:1 mole ratio are strong electrolytes. Hence, Eq.(1) might explain the formation of such adducts, and their electrolytic behaviour.

$$R_1R_2R_3P + CNX \rightarrow R_1R_2R_3P(CN)X \rightleftarrows R_1R_2R_3\overset{+}{P}CN. + X^- \quad \ldots(1)$$

The above mode of ionization is supported by electrolysis experiment[2] where the halogen was generated at the anode compartment giving pale yellow coloration in case of cyanogen bromide adduct and orange coloration in case of cyanogen iodide adduct. UV spectral studies for solutions of phosphines and cyanogen halide in methyl cyanide in rather similar mole ratios to those used in conductometric titration studies gave no indication for the presence of any trihalide ions.

Furthermore, adduct preparation at mole ratios similar to the breaks indicated by conductometric graphs, resulted in the isolation of two compounds $R_1R_2R_3P(CN)X$ (X = Br and I) by using equimolar

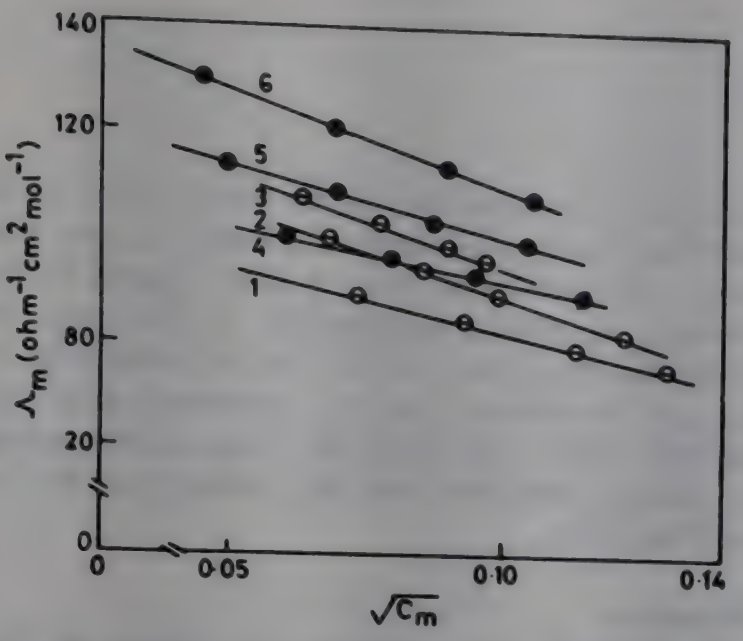

Fig. 2—Electrolytic conductance of cyanogen halide adduct

Table 3—Molar conductance at 0.1 *M* (Fig.2)

Compound	Molar conductance (ohm^{-1}cm^{2}mol^{-1})
$CH_3P(C_6H_5)_2CNI$	81.5
$(CH_3)_2PC_6H_5CNI$	88.0
$[(C_2H_5)_2N]_3PCNI$	93.0
$CH_3P(C_6H_5)_2CNBr$	92.5
$(CH_3)_2PC_6H_5CNBr$	100.5
$[(C_2H_5)_2N]_3PCNBr$	110.5

amounts of reactants. Their molar conductances at different concentrations, at 25°C (Fig.2) and at 0.1 *M* concentration (Table 3) indicate that these adducts are strong electrolytes and hence support the previously suggested mode of ionization.

These isolated 1:1 adducts were confirmed by elemental analysis as well as infrared spectral studies. The observed sharp strong absorption band at ca. 2174 cm^{-1} was assigned to the CN stretching frequency in $R_1R_2R_3P(CN)I$[12,13].

However, after the 1:1 mole ratio the system in which CNBr was used behaved differently from the CNI system. The latter system gave further break close to the 2:1 mole ratio of CNI:phosphine whereas the former did not show any indication for such break.

From the conductance value (Table 2) calculated at 2:1 mole ratio of CNI:phosphine and that of the isolated adduct (Table 4) it is obvious that this adduct is non-electrolyte. The isolated adduct showed an absorption band (very sharp) at ca. 2165 cm^{-1} in its infrared spectrum which was attributed to the stretching mode of the CN group[12,13]. From this and elemental analysis, the above isolated adduct was

Table 4—Values for molar conductance of 2:1 adducts

Compound	(ohm^{-1} Λ_m cm^2 mol^{-1})	C_m (mol l^{-1})
$CH_3P(C_6H_5)_2(CN)_2$	2.13	0.0061
$(CH_3)_2PC_6H_5(CN)_2$	2.37	0.0058
$[(C_2H_5)_2N]_3P(CN)_2$	2.71	0.0053

suggested to have the constitution of $R_3P(CN)_2$. Its UV spectrum in methyl cyanide solution exhibited an absorption band of λ_{max} 460. This is due to the presence of free iodine in solution. Therefore reaction (2) may well represent its formation in solution.

$$R_3P(CN)I + CNI \rightarrow R_3P(CN)_2 + I_2 \quad \ldots (2)$$
(1:1 mole ratio)

The higher value of conductance found for such adduct when formed during the conductometric titration graph (Fig.1, graphs 1,2 and 3) could be due to the formation of the 1:1 adduct of strong electrolyte behaviour prior to the 2:1 adduct.

In view of results obtained from molar conductance measurements (Table 3) it is clear that there is a steady increase in the electrolytic behaviour of the cyanogen iodide and bromide adducts on the exchange of organic groups of phosphines by others of stronger electron donating nature due to the change in the basicity of the phosphine which is effected by inductive and resonance effects as well as steric effects. Also, the cyanogen bromide adduct was found to be a stronger electrolyte than cyanogen iodide one (Table 3).

References

1 Aughsteen H A, *Zanco* (1983) 88.
2 Aughsteen H A, Ph.D. thesis, University of St. Andreus, (1975).
3 Steinkopf W & Wolfarm A, *Ber*, 54 (1951) 848.
4 Clune J E & Cohn K, *Inorg Chem*, 7 (1968) 2067.
5 Horrier L, Oediger H & Hoffmann H, *Ann*, 626 (1959) 26.
6 Andrews L J & Keefer R M, *Adv inorg Chem Radiochem*, 3 (1963) 91.
7 (a) Rashid O H A, M.Sc. Thesis, University of Sulaimaniyah, (1979).
(b) Ewadh M J, M.Sc. Thesis, University of Sulaimaniyah, (1980).
8 Harris G S & Payne J, *J chem Soc*, (1956) 3038.
9 Harris G S, *Proc chem Soc*, (1961) 65.
10 Ali M F & Harris G S, *Chem Commn*, (1966) 819.
11 Coetzes J P, Gunningham G P, McGarie D K & Padmanabban G R, *J anal Chem*, 34 (1962) 1139.
12 Rudolph R W, Taylor R C & Parry R W, *J Am chem Soc*, 88 (1966) 3729.
13 Goubeau V J, Haeberle H & Ulmer H, *Z anorg Chem*, 311 (1961) 110.

Indian Journal of Chemistry
Vol. 31A, December 1992, pp. 954-956

Notes

A new scale invariance behaviour in fractal scattering

P K Chattaraj* & Somdatta Nath

Department of Chemistry, Indian Institute of Technology, Kharagpur 721 302

Received 24 February 1992; revised and accepted 18 June 1992

The scattering of a structureless particle from a cantor set type model fractal lattice has been studied. A partially integrated scattering cross-section has shown scale invariance property when plotted against the scattering angle for different initial kinetic energy values of the projectile.

There has been an upsurge of interest in modelling a catalyst as a fractal[1] surface, e.g.,the diffusion-limited-aggregate[2-4], devil's staircase[5] or a cantor set[5] like structure. The simplest way to look at the gaseous atom or the molecule is as a structureless particle. Once the scattering of this particle from a fractal lattice is understood one can bring in the electronic structure for the atom and additional vibrational and rotational structures for the molecule. Preliminary studies[6-9] of scattering of a structureless particle from a cantor set type surface of dimension less than one have been performed and a fractional power-law dependence of the total cross-section on the wave-vector of the incoming wave has been observed. It has also been understood that even a finite fractal lattice contains meaningful information. In this note we would like to explore further the self-similarity or the scale-invariance property associated with this problem which may eventually help understanding the catalytic activities from the geometry of the catalyst surface.

Discussion

First of all, we construct the cantor set-like fractal lattice of dimension log2/log3 as follows: Take the interval (0,1), divide it into three equal segments and delete the central one (1/3, 2/3). The process is continued until the third generation lattice with 16 lattice points is obtained. A spherically symmetric Gaussian potential with a variance has been taken in each lattice point. The scattered wave function $\psi_{\mathbf{k}}^{d_f}$ is calculated in terms of the incident wave function $\phi_{\mathbf{k}}$ by solving the following Lippmann-Schwinger equation,

$$\psi_{\mathbf{k}}^{d_f}(\mathbf{r}) = \phi_{\mathbf{k}}(\mathbf{r}) + \int G^{+}(\mathbf{r}, \mathbf{r}')\, V^{d_f}(\mathbf{r}')\, \psi_{\mathbf{k}}(\mathbf{r}')\, d\mathbf{r}' \quad \ldots (1)$$

where d_f refers to the fractal dimension of the lattice, $G^{+}(\mathbf{r},\mathbf{r}')$ is the Green function for the for-

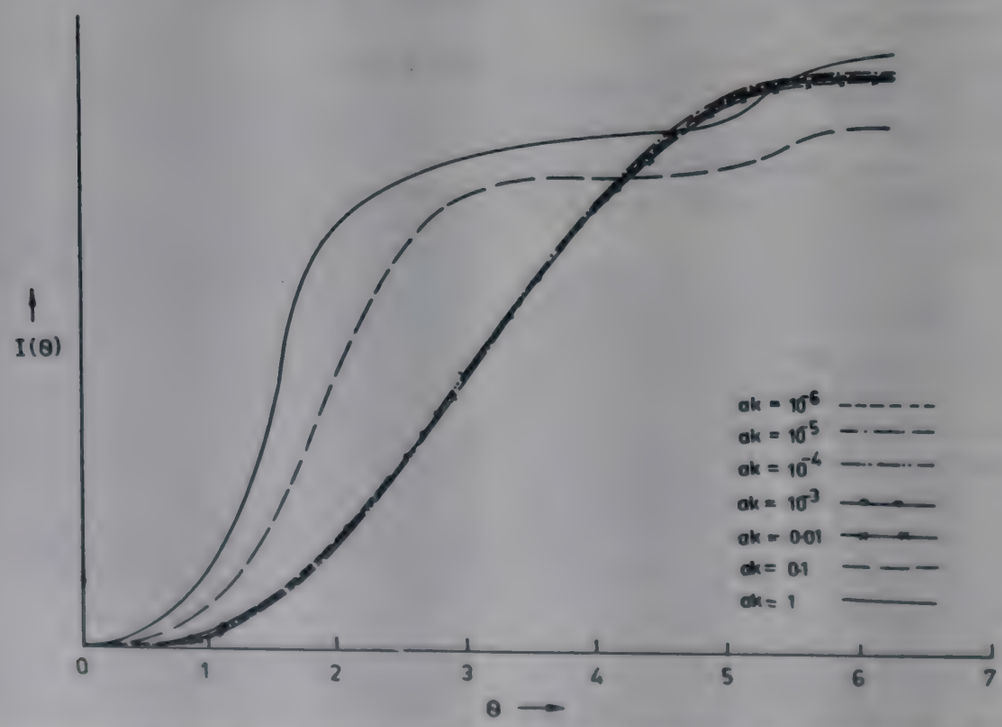

Fig. 1—Partially integrated cross-section, I(θ), versus scattering angle (θ) for different ak values. See text for the ranges of the I(θ) values

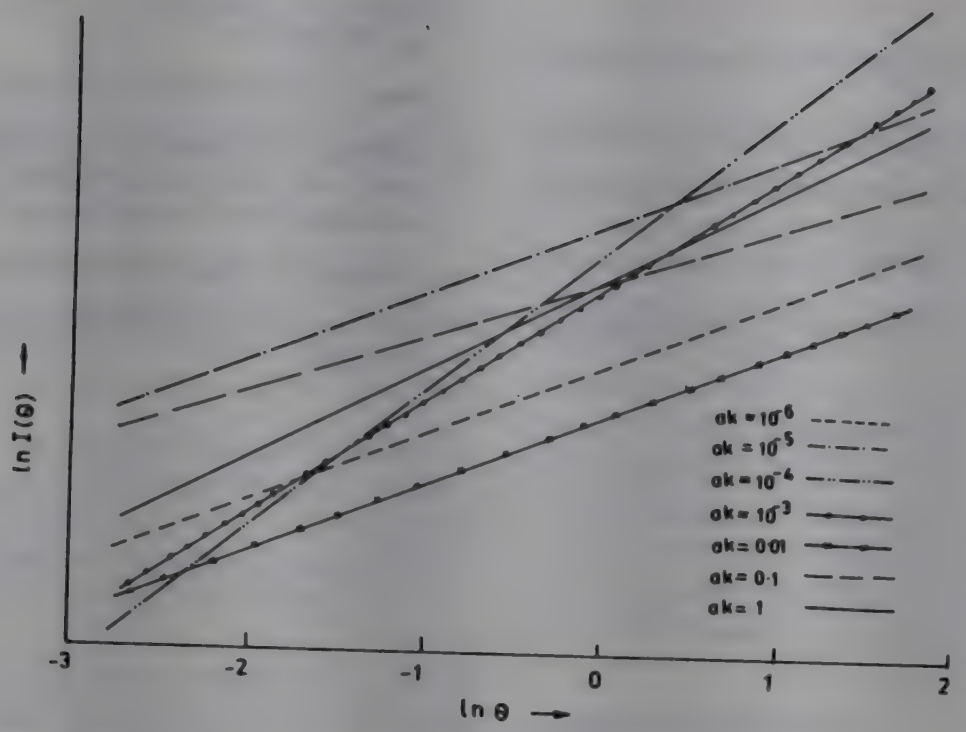

Fig. 2—Logarithm of I(θ) versus logarithm of the scattering angle (θ) for different ak values

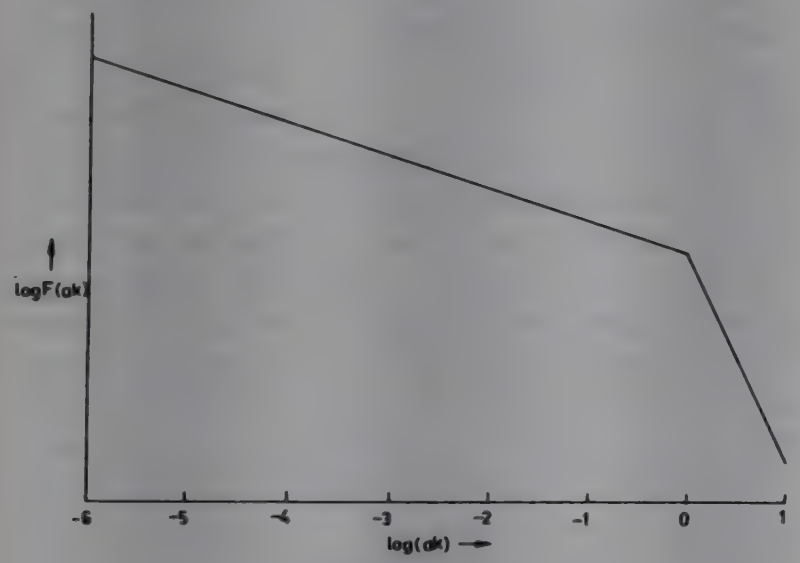

Fig. 3—Logarithm of the Fourier transform, F(ak), of the interaction potential versus logarithm of the wave-vector scaled with respect to the variance of the Gaussian potential at each lattice point

ward scattering and $V^{df}(\mathbf{r})$ is the interaction potential. An average wave function method[7,10] has been adopted for the solution of Eq. (1).

A partially integrated scattering cross-section (I(θ)) has been defined as,

$$I(\theta)=\int_0^{\theta}\frac{d\sigma(\theta')}{d\Omega}\,d\theta' \qquad \ldots(2)$$

Figure 1 depicts the variation of I(θ) versus the scattering angle (θ) for different initial momentum values for the incoming particle. A distinct scale invariance behaviour is easily discernible. For $0\le\theta\le 2\pi$, the range of I(θ)values for different ak values are as follows: (a) $ak=10^{-6}$, $0.4\times10^{-7}\le I(\theta)\le 0.7\times10^{-3}$; (b) $ak=10^{-5}$, $0.4\times10^{-5}\le I(\theta)\le 0.07$; (c) $ak=10^{-4}$, $0.4\times10^{-3}\le I(\theta)\le 7$; (d) $ak=10^{-3}$, $0.04,\le I(\theta)\le 0.7\times10^{3}$, (e) $ak=0.01$, $4\le I(\theta)\le 0.7\times10^{5}$; (f) $ak=0.1$, $0.4\times10^{3}\le I(\theta)\le 0.2\times10^{7}$; (g) $ak=1$, $0.1\times10^{6}\le I(\theta)\le 0.7\times10^{8}$.

It is interesting to note that deviation starts around ak = 0.1. In order to make the observation more conspicuous we present the corresponding log − log plot in Fig. 2. We have also calculated the following Fourier transform,

$$F(ak)=4\pi\int_0^{\infty}V^{df}(\mathbf{r}')\frac{\sin(ak\,r')}{ak\,r'}\,r'^{2}\,dr' \qquad \ldots(3)$$

which is important in calculating the scattering amplitude, the form factor and the total cross-section within Born approximation. The log-log plot of F(ak) versus ak is presented in Fig. 3 and has been found to be linear with a crossover around ak equal to unity where a crossover in slope had been observed[7,9] when logσ has been plotted against log(ak), σ being the total cross-section. It is hoped that this study would lend additional insights into the scattering phenomena involving geometry of the surface apart from the usual dynamical information obtainable from standard scattering calculations.

Acknowledgement

One of us (PKC) is thankful to the CSIR, New Delhi, for financial assistance and Dr Deepak Dhar for helpful discussions.

References

1 Mandelbrot B B, *The fractal geometry of nature* (Freeman, San Fransisco) 1983.

2 Witten T A Jr & Sander L M, *Phys Chem Rev*, 47 (1981) 1400.

3 Witten T A Jr & Sander L M, *Phys Rev*, B27 (1983) 5686.

4 Tambe S S, Badola P & Kulkarni B D, *Chem phys Lett*, 173 (1990) 67.

5 Gutfraind R, Sheintuch M & Avnir D, *Chem phys Lett*, 174 (1990) 8.

6 Singh H & Chattaraj P K, *Proc Indian Acad Sci (Chem Sci)*, 99 (1987) 47.

7 Singh H & Chattaraj P K, *Phys Lett A*, 128 (1988) 355.

8 Chattaraj P K, *Symmetries and singularity structures: Integrability and chaos in non-linear systems*, edited by M Lakshmanan & M Daniel (Springer, Berlin, 1990).

9 Chattaraj P K, *Chem Phys Lett*, 175 (1990) 613.

10 Singh H, Dacol D K & Rabitz H, *J chem Phys*, 84 (1986) 1373, 1852.

Indian Journal of Chemistry
Vol. 31A, December 1992, pp. 957-958

Hydrogen spillover on a platinum/carbon fuel cell catalyst

B Mahipal Reddy*, S T Srinivas & P Kanta Rao
Catalysis Section, Indian Institute of Chemical Technology, Hyderabad 500 007, India

Received 5 March 1992; revised and accepted 4 June 1992

Dihydrogen adsorption has been studied volumetrically on a 5% Pt/C fuel cell catalyst and Pt/C + C physical mixtures at ambient temperature. The observed results strongly suggest splitting of hydrogen molecules on Pt metal sites and spilling-over to carbon support sites.

Supported platinum catalysts represent one of the technologically most important class of solid catalysts[1]. The technique of hydrogen chemisorption, desorption, and titration have been widely used to estimate the metal surface areas of these catalysts[2], from which dispersion and mean particle sizes can also be calculated[3]. Hydrogen adsorbed on these metal crystallites (on group VIII metals in general) can migrate to the metal support in an activated form. This superficial migration process is referred as 'spillover', and has a special importance for several reactions catalysed by supported metals[4-6]. Inspite of numerous investigations on this topic many questions - like those related with the migration species, the mechanism of migration and even the direct observation of migration are not answered yet. In this communication, we provide a direct evidence on the migration of spillover hydrogen to the support sites on a 5% Pt/C catalyst at ambient temperature.

Experimental

The carbon supported platinum catalyst was prepared by wetting of the carbon support (XC Vulcan-72, S.A.: 250 m^2g^{-1}) with aqueous solutions of hexachloroplatinic acid ($H_2PtCl_6.6H_2O$ Spectroscopic grade) in hot condition (60°C). The impregnated sample was quickly dried at 110°C for 16 h and stored in a vacuum desiccator before use. Physical mixtures of 5% Pt/C (oven dried) and carbon support were prepared by first tumbling and then grinding the powders in an agate mortar for 30 min. A conventional static volumetric high vacuum system with a provision to reduce the samples *in situ* was used for H_2 chemisorption and N_2 BET surface area measurements[7]. In a typical experiment about 0.5 g of catalyst sample was placed in a glass adsorption cell and was reduced for 4 h at 250°C by flowing purified hydrogen-nitrogen (1:1) gas mixture (30 ml/min) and then evacuated at the same temperature for 2 h and cooled to ambient temperature under vacuum (10^{-6} Torr). Prior to hydrogen adsorption the system was further evacuated for 1 h at room temperature (250°C) and then hydrogen adsorption or desorption isotherms were generated. Hydrogen uptake was calculated by extrapolating the linear portion of the isotherm to zero pressure. The X-ray powder diffraction patterns were recorded on a Philips PW 1051 diffractometer using Ni-filtered CuK_α radiation.

Results and discussion

Figure 1 shows the X-ray diffractograms of the unreduced and reduced 5% Pt/C catalyst and the carbon support alone. A broadband can be seen at approximately $2\theta = 24°$; which is due to the amorphous carbon carrier itself. The absence of characteristic XRD lines due to platinum metal crystallites can be taken as an indication of high dispersion of Pt on carbon support or the crystallites formed are less than 4 nm size i.e., beyond the detection limit of the XRD technique. Hydrogen uptake measurements, however, support the former possibility.

Hydrogen uptakes, platinum metal surface areas, hydrogen to platinum ratios (n_H/n_M, atom/atom) and N_2 BET surface areas of various samples are shown in Table 1 as a function of weight percent of carbon support physically mixed to 5% Pt/C sample. As can be noted from Table 1 that the n_H/n_M ratio increases with increase in carbon support content upto 50 wt.% and then decreases with further addition. Similarly, the metal surface area also increases upto 50 wt% and then decreases with further carbon content. This is expected since, it is derived from hydrogen uptake measurements. The n_H/n_M ratio on the 5% Pt/C sample is close to unity indicating a high dispersion of Pt on the carbon support in agreement with XRD results. A finite contribution due to hydrogen spillover, however, cannot be ignored.

It is generally accepted that molecular hydrogen dissociates first on the metal sites into active mobile species which then migrate to the support sites[8]. The accept sites are mainly provided by the support. Therefore, the increase in n_H/n_M ratio with addition of support material is mainly due to an increase in the number of support sites to accommodate the

Table 1—H_2 Uptake and BET surface area measurements

Sample Code	Wt% C (support mixed)	H_2 uptake (μ mol/g cat.)	MSA[a] (m^2/g cat.)	n_H/n_M (ratio[b])	BET SA[c] (m^2/g)
PC-1	0	127	13.61	0.99	228
PC-2	10	155	16.62	1.21	235
PC-3	25	180	19.30	1.41	238
PC-4	50	197	21.12	1.54	244
PC-5	75	178	19.09	1.39	246
PC-6	90	181	19.41	1.41	248
PC-7	100	nil	—	0	250

[a]Metal surface area = H_2 uptake (mol/g cat.) × 2 × 6.023 × 10^{23} × 8.9 × 10^{-20} (From ref. 3)

[b]Where n_H is number of chemisorbed hydrogen atoms and n_M total number of platinum metal atoms

[c]By N_2 adsorption at -196°C by taking 0.162 nm^2 as the area of cross-section of N_2

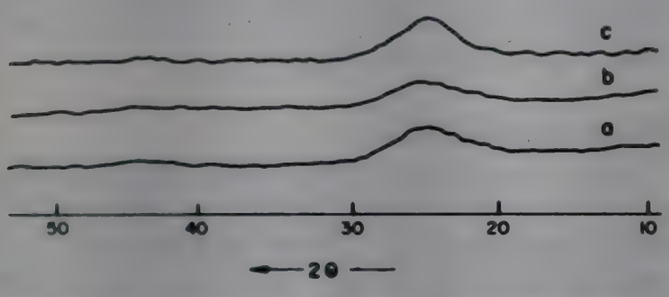

Fig. 1—XRD patterns of Pt/C samples : a) carbon support, b) fresh 5% Pt/C, c) reduced 5% Pt/C catalysts.

migrated hydrogen atoms which are initially formed on the metal crystallites. However, this migration process appears to be controlled by a distance factor too. It is worth mentioning here that the hydrogen uptake is practically zero on pure carbon support alone. Another interesting point is that the n_H/n_M ratio on poorly mixed (not properly mixed) samples of similar compositions is nearly constant and is close to unity,i.e., the value obtained on 5% Pt/C sample. This observation clearly indicates that there must be a close and intimate contact between the metal site and the support site in order to migrate the spilled-over species.

Thus the present study clearly demonstrates that hydrogen when adsorbed at ambient temperature splits on highly dispersed platinum metal crystallites and spillsover to the carbon support sites.

Acknowledgement

Thanks are due to the CSIR, New Delhi for a senior research fellowship to STS.

References

1 Sinfelt J H, in *Bimetallic catalysts*, (Wiley, New York), 1983, 86.
2 Orear D J, Loeffler D G & Boudart M, *J Catal*, 121 (1990) 131.
3 Delgass W N & Wolf E E, in *Chemical reaction and reactor engineering*, edited by J J Carberry & A Verma (Marcel Dekker, New York), 1987, 151.
4 Teichner S J, *Appl Catal*, 62 (1990) 1, and references therein.
5 Sermon, P A & Bond G C, *Catal Rev - Sci Eng*, 8 (1973) 211.
6 Dowden D A, in *Catalysis*, edited by D A Bowden & C Kemball (The Chemical Society, London) 3 (1980) 136
7 Reddy B M, Chary K V R, Subrahmanyam V S & Nag N K, *J chem Soc Faraday Trans*, 81 (1985) 1655.
8 Bond G C, in *Spillover of adsorbed species*, edited by G M Pajonk, S J Teichner & J E Germain (Elsevier, Amsterdam), 1983, 1.

Indian Journal of Chemistry
Vol. 31A, December 1992, pp. 959-962

Solvation models in the reaction between benzyl bromide and s-triazole

P Manikyamba
Department of Chemistry, University Arts and Science College, Subedari, Warangal 506 010, India

Received 3 March 1992; revised and accepted 6 May 1992

The kinetics of nucleophilic substitution on benzyl bromide by s-triazole has been studied in different pure (protic and aprotic) solvents. The reaction is overall second order, with first order dependence on [benzyl bromide] and the [nucleophile]. The rate data is correlated with different solvent parameters using linear multiple regression analysis. From the regression coefficients, information on the solvent-reactant and the solvent-intermediate interactions is obtained and the solvation models are proposed. The reaction has also been studied at different temperatures and the thermodynamic parameters $\Delta H^{\neq}$, $\Delta S^{\neq}$ and $\Delta G^{\neq}$ are computed.

Solvent effects on rates of reactions are as important as structural effects. The solvent-solute interactions are of two types, namely, specific and non-specific interactions[1]. The specific solvent-solute interactions are short range interactions, and are chemical in nature. These are measured in terms of the electrophilicity (E) and nucleophilicity (B) of the solvent, hydrogen bond donor ability (HBD) α, hydrogen bond acceptor ability (HBA), β etc. The intensity of non-specific interactions are measured in terms of the dielectric constant $(\varepsilon - 1/\varepsilon + 2)$ which is a measure of the polarity of the solvent, Y, and the refractive index $(n^2 - 1/n^2 + 2)$ which is a measure of the polarisability of the solvent.

The term solvent polarity, means the overall solvation ability of a solvent due to either all or some of these properties. Hence, the effect of a solvent on reaction rate has to be determined not by a single parameter equation, but by a multiparameter equation[2],

$$\log k = \log k_0 + \text{á}A + bB + cC + \ldots\ldots \qquad \ldots (1)$$

where k is the rate constant of the reaction in any solvent, and k_0 is the rate constant either in the gas phase or in an inert solvent taken as the reference state. The regression coefficients a, b, c ..... describe the susceptibility of k to the respective solvent-solute interaction parameters A, B, C ..... etc. With this end in view, the author studied the solvent effects on the title reaction. In many reactions[3-6] reliable predictions of the reaction mechanisms have been obtained from such studies.

Experimental

The solvents, methanol, propanol, *n*-butanol, 1-butanol, *t*-butanol, benzyl alcohol, ethoxy ethanol, dimethyl sulphoxide, dimethyl formamide, acetonitrile, benzonitrile, acetone, ethyl methyl ketone and cyclohexanone (AR, BDH) were used after purification by literature methods. Benzyl bromide (Riedel) was used as such. The nucleophile, 3-mercapto, 5-methyl, 4-amino (1,2,4) s-triazole was prepared[7] by refluxing thiocarbohydrazide with glacial acetic acid, and the product was then recrystallized.

The solutions of the reactants of appropriate concentrations were prepared by dissolving the known amounts of the nucleophile and the substrate, benzyl bromide, in different solvents. The two solutions were thermally equilibrated and mixed at the required temperature. The course of the reaction was followed by measuring the conductance of the reaction mixture at different time intervals using a Toshniwal conductivity bridge.

The reaction was found to be overall second order, first order each in benzyl bromide, and the nucleophile. The second order rate constants were calculated using the equation[8],

$$k = 1/at(C_t - C_0)/(C_\alpha - C_t) \qquad \ldots (2)$$

where C_0, C_t and C_α are the conductances of the reaction mixture at zero, t and infinite time intervals, and a is the initial [reactants]. All the kinetic runs were carried out in duplicate, and the rate constants were reproducible within 5% error in all the solvents. The product separated in all the solvents is identified to be 2-benzyl mercaptotriazole. The multiple regression analysis was carried out using a PCL personal computer.

Results and discussion

The reaction has been studied in fourteen pure (protic and dipolar aprotic) solvents with a range of 38 units of dielectric constant at temperatures ranging from 20°C to 45°C. The second order rate constants (k) are given in Table 1. The correlation of these rate constants with any one of the solvent parameters, discussed above, does not yield a meaningful equation. Then the rate data is analysed using a two parameter equation[9], which involves Dimroth-Richardt parameter E_T, and the nucleophilicity of the solvent B.

Table 1—Second order rate constants at 30°C for the reaction of benzylbromide with s-triazole in different solvents and solvent parameters

Solvent	$10^4 k$ ($dm^3 mol^{-1} s^{-1}$)	Solvent Parameters						
		Y[a]	P[a]	E[b]	B[a]	α[c]	β[c]	π^*[c]
Methanol	139.21	0.477	0.1690	14.94	119	0.93	0.62	0.60
i-Propanol	52.08	0.462	0.1870	8.70	128	0.76	0.95	0.48
n-Butanol	24.33	0.459	0.1948	10.30	160	0.71	0.88	0.43
i-Butanol	90.62	0.459	0.1937	9.05	158	—	—	—
t-Butanol	57.62	0.442	0.1910	5.20	132	0.68	1.01	0.41
Benzyl alcohol	130.55	0.444	0.2387	10.90	166	0.43	0.50	0.98
Ethoxyethanol	38.23	0.457	0.1960	12.52	125	—	—	0.71
Dimethylsulphoxide	287.51	0.484	0.2210	3.70	193	0.00	0.76	1.00
Dimethylformamide	129.16	0.480	0.2040	2.60	159	0.00	0.69	0.88
Acetonitrile	58.33	0.480	0.1740	5.21	101	0.19	0.31	0.75
Benzonitrile	38.33	0.471	0.2350	0.52	90	0.00	0.41	0.90
Acetone	30.83	0.466	0.1800	2.13	116	0.08	0.48	0.71
Ethylmethyl Ketone	13.32	0.460	0.1880	2.00	109	0.06	0.48	0.67
Cyclohexanone	46.52	0.455	0.2120	0.51	118	0.00	0.53	0.76

[BZBr] = 0.02 mol dm^{-3}, [s-triazole] = 0.02 mol dm^{-3}

a) Most of the Kirkwood dielectric functions Y, polarizability vlaues P, solvent basicity values B, are from Aslam M H, Collier G & Shorter J, *J chem Soc, Perkin Trans-II*, (1981) 1572.

b) Koppel-Palm's E values are from Koppel I A & Paju A I, *Organic reactivity* (Tarter), 11, (1974) 137.

c) Kamlet-Taft parameters are from Taft R W, Abboud J L M, Kamlet M J & Abraham M H, *J Org Chem*, 48, 2877 (1983).

$$\log k = \log k_0 + aE_T + bB \quad \ldots (3)$$

which also does not give a satisfactory correlation. Application of Koppel-Palm equation[2] to the above rate data gives the following relation:

$$\log k = -9.727 + 12.341\,Y + 4.500\,P + 0.021\,E + 0.006\,B \quad \ldots (4)$$

With the multiple regression coefficient R = 0.761, explaining only 59% variance of the observed data. Then the results were processed applying Kamlet-Taft three parameter equation[10].

$$\log k = \log k_0 + a\alpha + b\beta + c\pi^* \quad \ldots (5)$$

The multiple regression analysis gave relation (6).

$$\log k = -4.649 + 0.703\,\alpha + 0.846\,\beta + 2.330\,\pi^* \quad \ldots (6)$$

with R = 0.861, explaining 75% variance of the observed data. Though there is increase in the strength of the relation, the correlation is not satisfactory. Then the data have been analysed by adding the significant parameter Y, in the Koppel-Palm model[2], to the Kamlet-Taft equation[10]. The regression analysis gave the following relation (7).

$$\log k = -8.153 + 0.725\,\alpha + 0.882\,\beta + 2.185\,\pi^* + 7.692\,Y \quad \ldots (7)$$

There is a remarkable improvement in the 'R' value to 0.90 with an explained variance of 81%. However, when the Kirkwood function 'Y' is replaced by the polarizability term 'ρ', a satisfactory relationship is obtained with the strength of the relation R = 0.95 and an explained variance of 90%. The relation obtained is

$$\log k = 3.762 + 0.693\,\alpha + 1.248\,\beta + 3.254\,\pi^* - 9.024\,P \quad \ldots (8)$$

The validity of these relations is tested by subjecting the data to F-test, and t-test[11]. The statistical data are presented in Table 2.

This relation suggests the following facts:

(1) The reaction is facilitated in solvents having higher hydrogen bond acceptor ability measured by their β values. The positive sign and the magnitude of the coefficient of β in Eq. (8) suggests that HBA solvents strongly solvate the transition state and thus assist its formation. (2) The rate of the reaction is strongly influenced by 'π^*' which is a measure of the ability of the solvent to stabilize a charge or a dipole by virtue of its dielectric effect. The + ve sign of this coefficient in the above equation suggests that the transition state is extensively solvated by such solvents than the reactants. (3) The other parameter which strongly influences the rate is 'P' which is a measure of the polarizability of the solvent. The

Table 2—Statistical data from the regression analysis for the reaction of benzyl bromide with s-triazole in different solvents

Equation	n	F	Df	R	$\log k_0$	Standard errors in coefficients of						
						Y	P	E	B	α	β	π^*
4	14	3.61	9	0.76	0.272	6.140	4.287	0.019	0.003	—	—	—
					(95)	*2.010*	*1.050*	*1.107*	*1.866*			
						(90)	(<80)	(90)	(<80)			
6	12*	7.85	8	0.86	0.222	—	—	—	—	0.277	0.385	0.489
					(95)					*2.532*	*2.196*	*4.761*
										(95)	(90)	(99)
7	12*	7.67	7	0.90	0.202	4.747	—	—	—	0.253	0.352	0.455
					(95)	*1.620*				*2.863*	*2.508*	*4.803*
						(80)				(95)	(95)	(99)
8	12*	12.44	7	0.95	0.165	—	3.302	—	—	0.206	0.322	0.497
					(99)		*2.732*			*3.360*	*3.876*	*6.549*
							(95)			(98)	(99)	(99)

n = number of solvents, F = calculated statistical F, Df = degrees of freedom
R = linear multiple regression coefficient
* = *i*-butanol and ethoxy ethanol are excluded from the regression analysis as α, β and π^* values of solvents are not available.
values in italics are calculated t-values.
Values in parentheses are percentage confidence levels.

Table 3—Thermodynamic parameters in the reaction of benzyl bromide with s-triazole at temp. = 30°C
[BZ Br] = [s-triazole] = 0.02 mol dm^{-3}

Solvent	$\Delta H^{\neq}$ kJ mol^{-1}	$\Delta S^{\neq}$ JK^{-1} mol^{-1}	$\Delta G^{\neq}$ kJ mol^{-1}
Methanol	61.64	−77	85.06
i-Propanol	93.24	19	87.54
n-Butanol	101.81	47	87.71
i-Butanol	100.43	47	86.13
t-Butanol	56.78	−100	87.17
Benzyl alcohol	66.41	−62	85.21
Ethoxy ethanol	64.56	−78	88.31
Dimethyl sulphoxide	82.70	2	82.16
Dimethyl formamide	65.24	−66	85.25
Acetonitrile	45.32	−138	87.55
Benzonitrile	62.62	−85	88.31
Acetone	20.02	−227	88.86
Ethylmethyl ketone	32.94	−192	90.98
Cyclohexanone	77.49	−34	87.82

− ve sign of this coefficient shows that the non-specific interaction between the reactants and the solvent is more than the transition state-solvent interaction. (4) The hydrogen bond donor ability (HBD), measured by the a value of the solvent also influences the rate, though its contribution is less as indicated in Eq. (8). However, the + ve sign of the coefficient of α suggests that the solvation of the transition state by such solvents slightly exceeds that of the reactant.

Considering these points the solvation models of the reactants and the transition state can be represented as in Scheme 1.

Thus it can be concluded that in the present system, the reactants are strongly solvated by non-specific solvent-solute interactions extensively, than the transition state. The solvation of the transition state by specific hydrogen bond acceptor interaction exceeds that of the reactants.

The second order rate constants are evaluated in

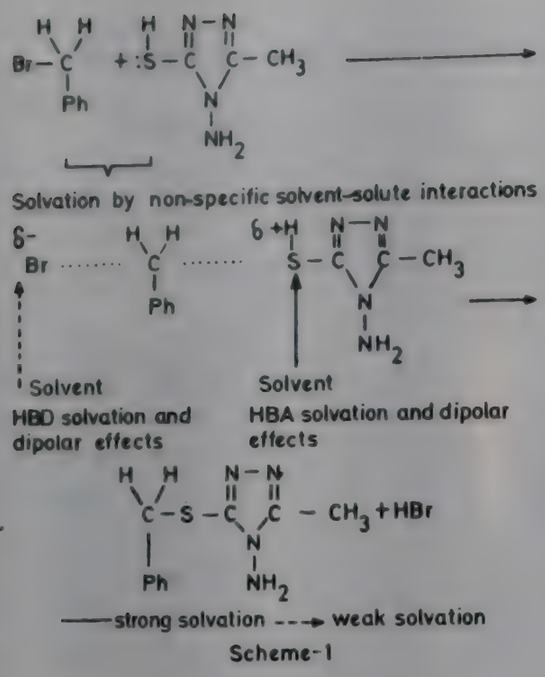

Scheme-1

all the solvents at different temperatures ranging from 20 to 45°C.

The thermodynamic parameters $\Delta H^{\neq}$, $\Delta S^{\neq}$ and $\Delta G^{\neq}$ computed are given in Table 3. A perusal of this data shows that $\Delta H^{\neq}$ and $\Delta S^{\neq}$ are also dependent on nature of the solvent. The reaction is entropy-controlled, indicating that, the extent of solvation of the transition state is strongly dependent on nature of the solvent. The present reaction involves a neutral nucleophile and a negatively charged leaving group Br^-. Therefore, the charges on the two ends of the transition state, and hence their solvation energies are different[12]. A change from a protic to a dipolar aprotic solvent results in a large difference in the relative solvation energies of the two ends of the transition state. This difference in solvation energies is large enough, to cause a shift in the electron density in the area between $-S$ and $-Br$ atoms along $Br-C-S$ bond axis in the transition state resulting in a change in the structure of the transition state, as the solvent is changed.

The inherent limitation in the applicability of multiparameter correlation for any reaction is that, the mechanism of the process under examination should not change with change in the solvent. The free energy of activation $\Delta G^{\neq}$ is nearly constant (86.0 ± 4.0 kJ mol^{-1}) suggesting the operation of a common mechanism in all the solvents.

References

1 Christian Reichardt, *Angew Chem*, 18 (1979) 98.
2 Koppel I A & Palm V A, *Advances in linear free energy relationships*, edited by N V Chapman and J Shorter (Plenum Press, New York) (1972) 222.
3 Zhu Zhong Yuan, Sun Cheng E & Han Te Kang, *J chem Soc Perkin Trans II*, (1985) 929.
4 Ohkata K, Nagai T, Tomaru A & Hanafusa T, *J chem Soc Perkin Trans II*, (1986) 43.
5 Martinez R D, Mancini P M E, Voltero L R & Nudleman N S, *J chem Soc Perkin Trans II*, (1986) 1427.
6 Manikyamba P & Sundaram E V, *Int J chem Kinetics*, 22 (1990) 1153.
7 Audrieth L F, Scott E S & Kipper P S, *J org Chem*, 19 (1954) 733.
8 Frost A A & Pearson R G, *Kinetics and mechanism*, (Wiley Eastern, New Delhi) (1970) 37.
9 Bunnett J F, *J Am chem Soc*, 87 (1965) 3875.
10 Kamlet M J & Taft R W, *J org Chem*, 47 (1982) 1734.
11 International group for Correlation Analysis in Organic Chemistry (Announcement), *Quant Struct Act Relat*, 4 (1985) 29.
12 Westaway K C, *Can J Chem*, 56 (1978) 2691.

Indian Journal of Chemistry
Vol. 31A, December 1992, pp. 963-965

Synthesis and structural characterization of some organoboron complexes with nitrogen donor azomethines

(Miss) Chitra Saxena, N Fahmi & R V Singh*
Department of Chemistry, University of Rajasthan, Jaipur 302 004

Received 19 February 1992; revised 1 June 1992; accepted 24 August 1992

A few organoboron complexes of nitrogen and sulphur/oxygen containing ligands having $\widehat{NSH}$ and $\widehat{NOH}$ donor systems have been synthesised and characterized on the basis of molecular weight determination, conductance measurements, IR, ^{1}H NMR, ^{13}C NMR and ^{11}B NMR spectral studies. The unimolecular and bimolecular reactions between phenylboronic acid and the ligands under investigation have yielded non-electrolytic complexes of the type PhB(OH)($\widehat{NS}$), PhB(OH)($\widehat{NO}$), PhB($\widehat{NS}$)$_2$ and PhB($\widehat{NO}$)$_2$, respectively. A stable tetracoordinated environment around the boron atom has been assigned.

There is an immense scope for undertaking systematic studies including the biochemical applications[1] of the complexes of boron with a variety of azomethines. The synthesis of several such new complexes of organoboron and their structural elucidation form the subject matter of this note.

Experimental

All the chemicals and solvents used were dried and purified by standard methods. Phenylboronic acid was prepared by the method reported earlier[2]. The following ligands were prepared by the methods reported elsewhere[3] : 2-Acetylfuran thiosemicarbazone (2-AcFuran TSCZH), (yellow, m.pt. 165°C); 2-acetylfuran semicarbazone (2-AcFuran SCZH), (yellow, m.pt. 148°C); 2-acetylthiophene thiosemicarbazone (2-AcThiop. TSCZH) (light yellow, m.pt. 155°C); 2-acetylthiophene semicarbazone (2-AcThiop.SCZH) (white, m.pt. 188°C); 2-acetylpyridine thiosemicarbazone (2-AcPyd. TSCZH) (yellow, m.pt. 142°C); 2-acetylpyridine semicarbazone (2-AcPyd.SCZH) (white, m.pt. 191°C); 2-acetylnaphthalene thiosemicarbazone (2-AcNaph, TSCZH) (white, m.pt. 144°C); 2-acetylnaphthalene semicarbazone (2-AcNaph. SCZH) (white, m.pt. 214°C). The yield in all the cases was ~ 75%.

Preparation of complexes

Phenylboronic acid (0.15-0.48g) and the respective ligands were mixed in 1:1 (0.48-0.86g) and 1:2 (0.60-1.0g) stoichiometric proportions in the presence of dry benzene (60ml). The reaction mixture was refluxed for 8-12 h on a fractionating column and the progress of the reaction was monitored by the liberation of water azeotropically with benzene. After the completion of the reaction, the excess solvent was distilled off and the product dried *in vacuo*. It was repeatedly washed with dry cyclohexane and again dried for 2 h to obtain the pure product. The purity of the complexes was checked by TLC, and analysis. Nitrogen and sulphur were estimated by Kjeldahl's and Messenger's methods, respectively. The conductance was measured at 21 ± 1°C using type 304 Systronics Conductivity Bridge. Molecular weights were determined by the Rast-Camphor method. The IR spectra were recorded on a Perkin-Elmer 577 spectrophotometer using KBr pellets. ^{1}H NMR spectra were scanned on a Jeol FX 90Q spectrometer in $CDCl_3$ and ^{13}C NMR in benzene operating at 89.55 MHz and 22.49 MHz, respectively, using TMS as the internal standard. ^{11}B NMR spectra were recorded using H_3BO_3 as the internal standard.

Results and discussion

Phenylboronic acid reacts with the heterocyclic azomethines in 1:1 and 1:2 molar ratios to afford complexes of the types PhB(OH)($\widehat{NS}$), PhB(OH)-($\widehat{NO}$), PhB($\widehat{NS}$)$_2$ and PhB($\widehat{NO}$)$_2$, where $\widehat{NSH}$ and $\widehat{NOH}$ represents the ligand molecule. The resulting monomeric and non-electrolytic complexes were isolated as creamy yellow to brown solids with sharp melting points (Table 1).

In the IR spectra of the ligands, a sharp band in the region 1610-1590 cm^{-1} due to > C=N group[4] shifts slightly towards higher frequencies in the boron complexes indicating the coordination of the azomethine nitrogen to the boron atom. This is further supported by the presence of a band at 1560-1530 cm^{-1} due to B←N[5] as reported earlier also[5]. New bands in the spectra of organoboron derivatives at 1350-1325, 880-855 and ~ 1260 cm^{-1} can be assigned to B—O[6], B—S[1] and Ph-B[7] vibrations, respectively. The medium intensity bands exhibited in the region 3250-3100 cm^{-1} can be assigned to NH[8] of the free ligands, which disappear in the boron complexes suggesting the possible loss of

Table 1—Analytical data of the boron complexes

Complex (Colour)	m.p. (°C)	Yield (%)	Found (Calc.), %		Mol. Wt. Found (Calc.)
			B	N	
PhB(OH) (2-AcFuran TSCZ) (light brown)	143	75	3.63 (3.77)	14.76 (14.63)	254 (287)
PhB(2-AcFuran TSCZ)$_2$ (brown)	170	80	2.48 (2.39)	18.52 (18.58)	419 (452)
PhB(OH) (2-AcFuran SCZ) (yellow)	140	77	3.77 (3.99)	15.63 (15.50)	302 (271)
PhB(2-AcFuran SCZ)$_2$ (yellow)	132	65	2.69 (2.57)	20.15 (20.00)	454 (420)
PhB(OH) (2-AcThiop.TSCZ) (orange)	sticky	65	3.69 (3.57)	13.12 (13.86)	268 (303)
PhB(2-AcThiop.TSCZ)$_2$ (dark yellow)	173	85	2.56 (2.23)	17.92 (17.35)	455 (484)
PhB(OH) (2-AcThiop.SCZ) (dark yellow)	149	70	3.89 (3.77)	14.76 (14.63)	306 (287)
PhB(2-AcThiop.SCZ)$_2$ (light yellow)	158	85	2.44 (2.39)	18.83 (18.58)	484 (452)
PhB(OH) (2-AcPyd.TSCZ) (brown)	sticky	70	3.51 (3.63)	18.72 (18.79)	321 (298)
PhB(2-AcPyd.TSCZ)$_2$ (dark brown)	sticky	80	2.22 (2.28)	23.61 (23.62)	444 (474)
PhB(OH) (2-AcPyd.SCZ) (light yellow)	185	75	3.96 (3.83)	19.95 (19.86)	256 (282)
PhB(2-AcPyd.SCZ)$_2$ (light yellow)	173	77	2.53 (2.44)	25.61 (25.34)	401 (442)
PhB(OH)(2-AcNaph.TSCZ) (light yellow)	178	70	3.02 (3.11)	12.31 (12.10)	312 (347)
PhB(2-AcNaph.TSCZ)$_2$ (cream)	184	70	1.93 (1.89)	14.53 (14.68)	625 (572)
PhB(OH) (2-AcNaph.SCZ) (white)	201	85	3.39 (3.26)	12.76 (12.69)	369 (331)
PhB(2-AcNaph.SCZ)$_2$ (cream)	205	80	2.13 (2.00)	15.69 (15.55)	501 (540)

a proton on the α-nitrogen. The bands observed at ~3430 and 3350 cm^{-1} due to asymmetric and symmetric modes of NH_2 group[9] remain almost at the same position in the spectra of boron complexes suggesting the non-involvement of the amino group on chelation.

The bonding pattern discussed above gets further support from the PMR spectra of 2-acetylpyridine semicarbazone and its 1:1 and 1:2 boron complexes. In the PMR spectra of the ligand, a broad signal due to NH proton appears at δ 9.83 ppm and disappears in the spectra of the complexes due to bonding of boron

to sulphur/oxygen as well as nitrogen atom of the ligand moiety. The $-CH_3$ protons observed at δ 1.80 ppm in the ligand undergo deshielding and appear at δ 2.24 and δ 2.16 ppm in the corresponding 1:1 and 1:2 boron complexes respectively, which clearly indicates the coordination of the azomethine nitrogen to the boron atom. The appearance of signals due to NH_2 protons at the same positions in the ligand and its complexes, confirms the non-involvement of this group on coordination. Aromatic protons also undergo deshielding to a little extent. Phenyl protons are observed at δ 6.48 and δ 6.40 ppm in 1:1 and 1:2 boron complexes, respectively, whcih were absent in the spectra of the ligands. The OH proton signal in 1:1 complexes is observed at ~ δ 4.10 ppm.

It has also been possible to record the ^{13}C NMR spectra of 2-acetylpyridine semicarbazone and its corresponding 1:1 and 1:2 boron complexes in DMSO. The amido and azomethine carbons appearing at δ 186.00 and δ 160.25 ppm in the ligand undergoes a considerable shift and appear at δ 174.70 and δ 155.70 ppm in 1:1 and δ 173.35 and δ 156.18 ppm in 1:2 boron complexes, respectively.

The ^{11}B NMR spectra of a few 1:1 and 1:2 complexes show a sharp to broad signal in the region between δ 2.71 to δ 15.62 ppm, which strongly supports the tetracoordinated[7] state of boron in the present case.

Based on the foregoing discussion, the above structures can be proposed for the 1:1 (A) and 1:2 (B)

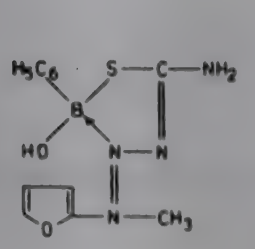

(A)

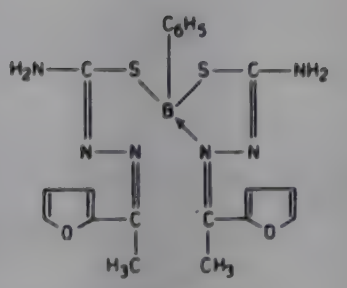

(B)

organoboron complexes with 2-AcFuran TSCZH as the ligand molecule.

Acknowledgement

The authors wish to thank the UGC, New Delhi, for the financial assistance.

References

1 Singh V P, Singh R V & Tandon J P, *J inorg Biochem*, 39 (1990) 893.
2 Tripathi S M & Tandon J P, *Indian J Chem*, 17A (1979) 618.
3 Singh D & Singh R V, *Phosphorus, Sulphur Silicon*, 61 (1991) 57.
4 Singh V P, Singh R V & Tandon J P, *Main group met Chem*, 13 (1990) 135.
5 Bhal L & Tandon J P, *Indian J Chem*, 24A (1985) 562.
6 Chaturvedi K K, Singh R V & Tandon J P, *J prakt Chem*, 327 (1985) 144.
7 Bellamy L J, Gerrard W, Lappert M F, *J chem Soc*, (1958) 2412.
8 Sharma R K, Singh R V & Tandon J P, *J inorg nucl Chem*, 42 (1980) 1267.
9 Shishoo C J, Devani M B, Jain K S, Bhadti U S, Shishoo S M, Pathak U S, Ananthan S & Rathod I S, *Indian J Chem*, 28B (1989) 42.

Indian Journal of Chemistry
Vol. 31A, December 1992, pp. 966-969

Sulphato complexes of bi- and tri-valent ruthenium

S C Sarker & R K Poddar*
Department of Chemistry, North-Eastern Hill University, Bijni Complex, Shillong 793 003, India

Received 30 December 1991; revised 21 April 1992; accepted 29 June 1992

Bi- and tri-valent ruthenium sulphato complexes, $M[Ru(SO_4)_2(H_2O)_2]$ (M = K, Rb, Cs or NMe_4); $[Ru(L-L)(H_2O)_2(SO_4)]$ (L − L = bpy, phen or *o*-aminopyridine); $[Ru(Pda)_2(SO_4)]$ (Pda = *o*-phenylenediamine); $[Ru(tu)_2(H_2O)_2(SO_4)]$ (tu = thiourea); $[Ru(CO)(PPh_3)_2(SO_4)]$ and $[Ru(Py)_4(SO_4)]$ have been synthesized from Ru(III) sulphate. The compounds have been characterized on the basis of physical, analytical, spectral and magnetic susceptibility data.

Recently some Russian workers[1-3] have reported the preparation and characterization of dimeric complexes of the type, $M_3[Ru_2(\mu\text{-}SO_4)_4(H_2O)_2]nH_2O$ [$M_3 = K_3$, Cs_3 or $K_2(H_5O_2)$], and $K_4(Ru_2(SO_4)_2(\mu\text{-}SO_4)_2(\mu\text{-}O)_2]$. The present work describes a convenient method of synthesizing bi- and tri-valent ruthenium complexes containing bridging sulphate(s).

Experimental

Hydrated ruthenium trichloride was obtained from Arora-Mathey Ltd, Calcutta. Other chemicals used were of Analar or extra-purity grade. In the complexes, ruthenium and sulphate were determined by spectrophotometric[4] and gravimetric[5] methods respectively. Potassium as its perchlorate was also determined gravimetrically[5]. Carbon, hydrogen and nitrogen analyses were carried out in the Department. The analytical data are presented in Table 1. IR and UV-Vis spectra, and conductivity measurements were carried out as reported earlier[6]. ^1H NMR spectra of the compounds in D_2O/DMSO-d_6 were recorded on a Varian EM390 spectrometer. EPR spectra were recorded on a Varian E-4 X-band EPR spectrometer and magnetic susceptibilities were measured on a EG and G PARC Vibrating Sample Magnetometer. Thermogravimetric analysis was done on a Perkin-Elmer TGS-2 instrument.

Ruthenium(III) sulphate

Silver sulphate (0.18 g) was added to a solution of hydrated ruthenium trichloride (0.1 g) in ethanol (20 cm^3) and the mixture was refluxed on a water-bath for 5 h. Silver chloride was filtered off to get a green solution of ruthenium(III) sulphate. The green solution was concentrated (~5 cm^3) and acetone (30 cm^3) was added to precipitate the compound, which on drying at 120°C for 2 h, turned into a black hygroscopic solid, $HRu(SO_4)_2(H_2O)_6$. It is soluble in ethanol or methanol.

$M[Ru(SO_4)_2(H_2O)_2].nH_2O$ (where $n = 0$ for $M = K$ or Rb; $n = 4$ for $M = Cs$)

To a solution of Ru(III) sulphate, a saturated aqueous solution of M_2SO_4 in the mole ratio 2:1 was added and the mixture was refluxed for 2 h, during which period a black compound separated. It was centrifuged, washed with ethanol and dried first *in vacuo* and then in an air-oven at 120°C for 2 h; yield: 85-90%.

$(NMe_4)[Ru(SO_4)_2(H_2O)_2]$ was prepared as a dark green solid using ethanolic solution of NMe_4Cl (1:1) instead of M_2SO_4; yield: 85%.

$[Ru(L-L)(H_2O)_2(SO_4)]$ (L − L = bpy, phen, or o-aminopyridine)

To a solution of ruthenium(III) sulphate, the N-heterocycle, (L − L) (Ru: L − L = 1:3 mole) was added and the mixture was stirred for 4 h at room temperature or refluxed for 3 h, during which period a black compound separated. It was centrifuged, washed with ethanol and dried *in vacuo*; yield 45%.

^1H NMR spectra: L − L = bpy, 8.80 d, 8.18 t, 7.84 d, 7.45 t; L − L = phen, 8.55 d, 8.20 d, 7.64 q (in dmso-d_6, 8.90 d, 8.20 d, 7.85 q)[7].

A similar procedure was adopted for the preparation of $[Ru(tu)_2(H_2O)_2(SO_4)]$ and $[Ru(Pda)_2(SO_4)]$ using thiourea (tu) and *o*-phenylenediamine (Pda) respectively; yield: 48%.

$[Ru(CO)(PPh_3)_2(SO_4)]$

To a solution of ruthenium(III) sulphate (0.1 g) in 2-methoxyethanol (5 cm^3), a solution of PPh_3 (0.26 g) in 2-methoxyethanol was added and the mixture was refluxed in an oil-bath at 130°C for 2 h and cooled when a light yellow crystalline compound separated. The compound was washed with ethanol and ether, and dried *in vacuo;* yield: 65%.

Table 1—Analytical and some physical data of ruthenium(III) and ruthenium(II) sulphato compounds

Compound	Analytical data[a] (%)				
	Ru	C	H	N	SO_4
1. $K[Ru(SO_4)_2(H_2O)_2]$	26.62 (27.43)			11.40[b] (10.62)	51.79 (52.16)
2. $Rb[Ru(SO_4)_2(H_2O)_2]$	23.81 (24.37)				45.79 (46.32)
3. $Cs[Ru(SO_4)_2)(H_2O)_2]$ 4 H_2O	19.60 (18.92)				35.36 (35.96)
4. $(NMe_4)[Ru(SO_4)_2(H_2O)_2]$		12.26 (11.91)	3.98 (3.97)	3.68 (3.47)	46.90 (47.64)
5. $[Ru(bpy)(SO_4)(H_2O)_2]$		30.32 (30.84)	2.68 (3.08)	6.74 (7.19)	23.90 (24.67)
6. $[Ru(phen)(SO_4)(H_2O)_2]$		34.20 (34.86)	2.54 (2.90)	6.42 (6.78)	22.60 (23.24)
7. $[Ru(apy)(SO_4)(H_2O)_2]$		18.93 (18.35)	2.56 (3.06)	8.16 (8.56)	
8. $[Ru(tu)_2(SO_4)(H_2O)_2]$		6.48 (6.23)	2.89 (3.12)	15.08 (14.55)	
9. $[Ru(PDA)_2(SO_4)]$		34.52 (34.86)	3.21 (3.87)	13.73 (13.55)	22.50 (23.24)
10. $[Ru(CO)(PPh_3)_2(SO_4)]$		59.46 (59.28)	4.37 (4.01)		12.50 (12.82)
11. $[Ru(py)_4(SO_4)]$		46.23 (46.78)	3.62 (3.90)	10.54 (10.92)	17.11 (18.71)
12. $[Ru(bpy)_2(H_2O)_2](SO_4)5H_2O$		37.70 (37.79)	3.10 (4.72)	8.83 (8.82)	14.72 (15.12)
13. $[Ru(phen)_2(H_2O)_2](SO_4)3H_2O$		43.49 (44.50)	4.47 (4.04)	8.43 (8.60)	14.10 (14.83)
14. $[Ru(apy)_2(H_2O)_2](SO_4)2H_2O$		26.89 (26.25)	3.36 (4.40)	11.80 (12.25)	21.52 (21.0)

a = Calculated values are in parentheses, b = % of K.

$[Ru(Py)_4(SO_4)]$

Pyridine (0.5 cm^3) was added to a solution of ruthenium(III) sulphate (0.1 g) in ethanol (10 cm^3) and the mixture was refluxed for 3 h, cooled and centrifuged. A green solution was obtained and it was concentrated (~3 cm^3) on a water-bath when an orange yellow compound got separated. It was washed with ethanol and ether and dried *in vacuo*; yield: 65%.

$[Ru(L-L)_2(H_2O)_2](SO_4).nH_2O$ (L − L = bpy, phen or apy)

To the filtrate obtained in the preparation of $[Ru(L-L)(H_2O)_2](SO_4)]$, one drop of H_2SO_4 was added and the solution was concentrated (~5 cm^3) on a water-bath. To this acetone was added to precipitate the desired compound, which was washed with acetone and dried *in vacuo*; yield: 45%.

^1H NMR spectra: L − L = bpy, 8.80 d, 8.18 t, 7.84 d, 7.45 t; L − L = phen, 8.55 d, 8.20 d, 7.64 q (in dmso-d_6, 8.90 d, 8.20 d, 7.85 q)[7].

Results and discussion

The IR spectra of the compounds $HRu(SO_4)_2(H_2O)_6$ and $M[Ru(SO_4)_2(H_2O)_2].nH_2O$ (M = NMe_4, K or Rb, n = 0; M = Cs; n = 4) exhibit bands due to coordinated sulphate: ν_3 at 1220, ~1120 and ~1035 cm^{-1}, ν_4 at 665, 645 and 600 cm^{-1} and ν_1 at 970 cm^{-1}. The splitting of ν_3 and ν_4 modes each into three peaks, the former being in the lower wavenumber region, is characteristic of bridging sulphates[8-10]. Broad IR bands observed at ~3550 and 3200 cm^{-1} and a strong one at 1630 cm^{-1} are assigned to ν_{OH} and δ_{HOH} modes of coordinated and lattice water molecules[8].

The powder EPR spectrum at room temperature exhibits two broad signals at $g = 2.19$ and 2.05 implying an axial symmetry for $HRu(SO_4)_2(H_2O)_6$. The Cs salt has a magnetic moment of 1.78 BM at room-temperature. The room-temperature powder EPR spectra of Cs, Rb and K salts display $g_\parallel$ and $g_\perp$ values at 2.2 and 1.94 respectively. The latter exhibits hyperfine splitting. The presence of two g values

indicates an axial symmetry for the complexes. This can be visualised from a *trans* arrangement for the bis aquo groups and hence a D_{4h} symmetry for the complex ions[11,12].

The molar conductance of fresh aqueous solutions of the compounds are 305 and 345 $\Omega^{-1}cm^2mol^{-1}$ for the Cs and K salts respectively, the values being higher for a 1:1 electrolyte. This suggests partial decomposition of the anion. The Λ_M values of the aqueous solutions on standing for 1 hr, increase to 346 and 417 $\Omega^{-1}cm^2mol^{-1}$, implying further decomposition. In the case of NMe_4 salt an aqueous solution has Λ_M value of 153 $\Omega^{-1}cm^2mol^{-1}$, corresponding to a 1:1 electrolyte.

The electronic spectra of Cs and NMe_4 salts in water or in 7 *N* H_2SO_4 show a band at 650 nm ($\varepsilon = 500$). For the potassium salt, a broad shoulder observed at ~600 nm is assigned to $^2T_{2g} \rightarrow {}^2A_{2g}$ or $^2T_{1g}$ transition. Other absorption bands, viz., 420 nm ($\varepsilon = 1.5 \times 10^3$) and 365 nm ($\varepsilon = 1.9 \times 10^3$) may be assigned to ligand→metal charge transfer transitions[13].

Ru(III) sulphate in ethanol reacts with L−L[L−L=2, 2′-bipyridine (bpy), 1, 10-phenanthroline (phen), *o*-aminopyridine (apy)] to yield ruthenium (II) compounds of the compositions $[Ru(L-L)(H_2O)_2(SO_4)]$, and $[Ru(L-L)_2(H_2O)_2](SO_4).nH_2O$. Reactions of Ru(III) sulphate with thiourea (tu) and *o*-phenylenediamine (pda) yield $[Ru(tu)_2(H_2O)_2(SO_4)]$ and $[Ru(pda)_2(SO_4)]$ respectively. Excepting the ionic ones, the complexes are insoluble in water and most of the organic solvents. The insolubility suggests polymeric nature for the compounds. The compounds are diamagnetic implying the presence of low-spin Ru(II). The IR spectra of the compounds show bands due to coordinated amines, water molecules and bridging sulphate groups. The IR spectrum of $[Ru(tu)_2(H_2O)_2(SO_4)]$ also shows absorptions at 1425, 1410 and 700 cm^{-1} as against the 1412 and 730 cm^{-1} for the uncoordinated thiourea implying its bonding to the metal ion via S-atom[14].

The thermogravimetric studies on $[Ru(L-L)(H_2O)_2(SO_4)]$, (L−L=bpy, phen) under nitrogen atmosphere showed gradual loss in weight between 100°C and 330°C corresponding to two water molecules. A sharp loss in weight in the range 350°-370°C in the case of the bpy complex corresponded to the loss of heterocycle; the residue corresponded nearly to the composition, $RuSO_4$. The latter underwent a gradual loss in weight upto 480°C to form RuO without any further loss till 650°C. In the case of the phen complex, there was a sharp decrease in weight (23%) from 330°C to 350°C which may be due to partial loss of phen and a gradual decrease (22%) from 350°C to 440°C, which probably corresponds to the complete loss of phen and partial loss of oxygen. At 650°C, the composition of the residual mass corresponded to RuSO.

$[Ru(py)_4(SO_4)]$ and $[Ru(CO)(PPh_3)_2(SO_4)]$ are orange yellow and light yellow respectively, soluble in some of the organic solvents like acetonitrile, dimethylsulphoxide and dichloromethane. They are diamagnetic and nonelectrolytes in nature. The ^1H NMR spectrum of $[Ru(CO)(PPh_3)_2(SO_4)]$ shows only one signal around δ 7.3 due to aromatic protons in PPh_3. The IR spectrum of the complex shows a strong νCO band at 1965 cm^{-1} in addition to the bands due to bridging sulphate at 1220, 1130 and 1000 cm^{-1} (ν_3) and at 660, 620 and 595 cm^{-1} (ν_4). The IR spectrum of $[Ru(py)_4(SO_4)]$ also shows bands due to coordinated pyridine and bridging sulphate. Since $[Ru(CO)(PPh_3)_2(SO_4)]$ and $[Ru(py)_4(SO_4)]$ are slightly soluble in some of the organic solvents and the IR spectra are comparable with those of the related ones, they may be assigned a dimeric structure.

$[Ru(L-L)_2(H_2O)_2](SO_4)$ (L−L=bpy, phen or apy) in ethanol behave as, 1:1 electrolytes, the Λ_M being 40-48 $\Omega^{-1}cm^2mol^{-1}$. The IR spectra show bands due to coordinated amines and water molecules. A strong and broad band at 1120 cm^{-1} (L−L=phen or apy) or 1190 cm^{-1} (L−L=bpy) is assigned to the ν_3 mode of ionic sulphate[8].

Acknowledgement

The authors are thankful to RSIC-NEHU, Shillong for IR and electronic absorption spectra, RSIC-IIT, Madras for the EPR spectra and the magnetic susceptibility measurements, RSIC-Nagpur University, Nagpur for the TG spectra. One of the authors (SCS) is thankful to D.M.R. Shillong for permission to pursue the research work.

References

1 Zhilyaev A N, Fomina T A, Kuzmenko I V, Rotov A V & Baranovskii I B, *Zh neorg Khim*, 34 (1989) 948.

2 Kuzmenko I V, Zhilyaev A N, Fomina T A, Porai-Koshits M A & Baranovskii I B, *Zh neorg Khim*, 34 (1989) 2548.

3 Fomina T A, Zhilyaev A N, Kuzmenko I V, Chalisova N N, Sobolev A N, Porai-Kashits M A & Bararanovskii I B, *Zh neorg Khim*, 34 (1989) 1552.

4 Beamish F E & Van-Loon J C, *Analysis of noble metals, over view and selected methods* (Academic Press, New York), 1977. 118.

5 Vogel A I, *Inorganic quantitative analysis* (ELBS & Longman, London), 1961.

6 Sarma U C, Sarma K P & Poddar R K, *Polyhedron*, 7 (1988) 1727.

7 Seddon E A & Seddon K R, *The chemistry of ruthenium* (Elsevier, Amsterdam), 1984, 429.
8 Nakamoto K, *Infrared and Raman spectra of inorganic and coordination compounds* (Wiley, New York), 1986.
9 Cotton F A & Wilkinson G, *Advanced inorganic chemistry* (Wiley, New York), 1988, 488.
10 Eskenazi R, Raskovan J & Levitus R, *J inorg nucl Chem*, 28 (1966) 521.
11 Chatt J, Leigh G J & Mingos D M P, *J chem Soc* (*A*), (1969) 1674.
12 Manoharan P T, Mehrotra P K, Taquikhan M M & Andal R K, *Inorg Chem*, 12 (1973) 2753.
13 Lever A B P, *Inorganic electronic spectroscopy* (Elsevier, Amsterdam), 1984, 332, 454.
14 Swaminathan K & Irving H M N H, *J inorg nucl Chem*, 26 (1964) 1291.

Indian Journal of Chemistry
Vol. 31A, December 1992, pp. 970-971

Synthesis and spectral studies of Pt(II) complexes with 2,3-disubstituted quinazoline-(3H)-4-ones

K Laxma Reddy*, B Prabhakar† & P Nageswara Rao
Department of Chemistry, Regional Engineering College, Warangal 506 004

Received 10 February 1992; revised 14 April 1992; accepted 11 August 1992

A number of platinum(II) complexes of bidentate O – O and O – N donors, 2, 3-disubstituted quinazoline-(3H)-4-ones, have been synthesized and characterized. The reaction between $PtCl_2$ and the uninegative bidentate ligands yield complexes of the type $[Pt(L-L)_2]$, whereas the neutral bidentate ligands give $[Pt(L-L)_2]Cl_2$. The complexes are assigned square-planar structures.

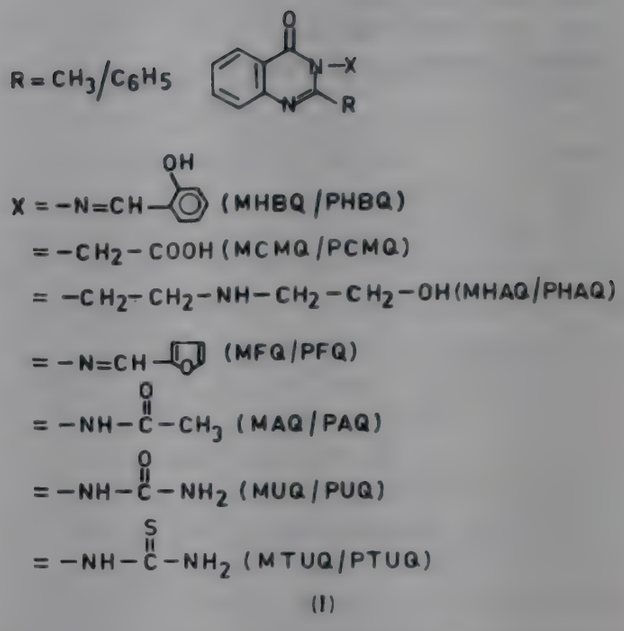

(I)

Quinazoline-(3H)-4-ones have drawn much attention due to their varied ligational behaviour towards different metal ions and manifestations of novel structural features in the metal complexes. Our earlier reports[1,2] on Co(II), Ni(II), Cu(II), Ru(II) and Pd(II) ions with substituted quinazolines indicate that these compounds act as bidentate with Co(II), Ni(II) and Pd(II) and tridentate with Cu(II) and Ru(II). In continuation of our earlier work, we report herein the synthesis and characterization of Pt(II) complexes with the ligands 2-(R)-3-(X)-substituted quinazolin-(3H)-4-ones, where R = methyl/phenyl, X = 2′-hydroxybenzalimino (MHBQ/PHBQ), carboxymethyl (MCMQ/PCMQ), N-(2′-hydroxyethyl)-aminoethyl (MHAQ/PHAQ) furfuralimino (MFQ/PFQ), acetamino (MAQ/PAQ), uramino (MUQ/PUQ) and thiouramino (MTUQ/PTUQ) (Structure I). The complexes have been characterized based on analytical, conductivity, magnetic, infrared, electronic and PMR data.

Experimental

All the chemicals used were of AR grade. The ligands were prepared by the literature methods[3,4]. $PtCl_2$ was obtained from M/s Johnson Matthey (England). The purity of these compounds was checked by TLC and m.p. data.

Preparation of the complexes

Platinum(II) chloride (2.66 g) was dissolved in one cm^3 of conc. HCl and the contents were diluted with distilled water to 100 cm^3. 10 cm^3 of this solution was diluted with equal volume of water and to it was added 30 cm^3 of the ligand solution (10 mmol) in methanol or acetone dropwise with constant stirring. The complexes separated out in acidic medium ($pH = 4.6$) on cooling. The solid thus obtained was filtered and washed several times with water and methanol/acetone until the washings were free from excess ligand. The complexes were dried *in vacuo* over fused calcium chloride; yield 50-70%. All the Pt(II) complexes are crystalline powders, stable at room temperature, non-hygroscopic and soluble in DMF and DMSO.

The complexes were analysed[2] for C, H, S and N at the Micro-Analytical Laboratory, Calcutta University, Calcutta.

Results and discussion

The analytical data (Table 1) showed the complexes to have 1:2 (metal:ligand) stoichiometry. All the complexes behave as 1:2 electrolytes in DMF except those of MHBQ, PHBQ, MCMQ and PCMQ and MHAQ and PHAQ, which behave as nonelectrolytes. All the complexes were found to be diamagnetic as expected.

The complexes are thermally stable upto 200°C and are not hydrated, a fact confirmed by their DTA curves which do not exhibit an endothermic peak in the temperature range 100-200°C. The sharp decomposition associated with the loss of ligand starts above 250°C. The final decomposition products obtained above 600°C are the metallic oxides. The thermal stability of the platinum(II)

†Chemical Engineering Division, National Chemical Laboratory, Pune 411 008

Table 1—Analytical and physical data of the platinum(II) complexes

Complex (colour)	m.p.[a] (°C)	Analysis (%)		
		Carbon	Nitrogen	Hydrogen
$[Pt(MHBQ)_2]$ (Black)	275	51.10 (51.13)	11.12 (11.18)	3.17 (3.19)
$[Pt(PHBQ)_2]$ (light brown)	278	57.54 (57.39)	9.58 (9.60)	3.25 (3.19)
$[Pt(MCMQ)_2]$ (Black)	265	41.80 (41.83)	8.85 (8.87)	3.12 (3.16)
$[Pt(PCMQ)_2]$ (Dark brown)	270	50.82 (50.85)	7.37 (7.41)	3.14 (3.17)
$[Pt(MHAQ)_2]$ (Brown)	310	45.96 (45.42)	12.12 (12.22)	4.96 (4.58)
$[Pt(PHAQ)_2]$ (Brown)	305	54.26 (53.88)	10.96 (10.36)	4.71 (4.44)
$[Pt(MFQ)_2]Cl_2$ (Brown)	295	43.10 (43.19)	9.40 (9.44)	3.08 (3.14)
$[Pt(PFQ)_2]Cl_2$ (Dark brown)	280	48.88 (49.75)	8.20 (8.29)	3.10 (3.15)
$[Pt(MAQ)_2]Cl_2$ (Black)	280	37.69 (37.71)	11.98 (12.00)	3.12 (3.14)
$[Pt(PAQ)_2]Cl_2$ (Ash black)	295	35.08 (35.16)	13.52 (13.67)	3.12 (3.17)
$[Pt(MUQ)_2]Cl_2$ (Brown)	290	46.58 (46.60)	10.17 (10.19)	3.12 (3.15)
$[Pt(PUQ)_2]Cl_2$ (Black)	298	43.19 (43.26)	11.80 (11.87)	3.14 (3.18)
$[Pt(MTUQ)_2]Cl_2$[b] (Dark brown)	293	33.80 (33.84)	13.12 (13.16)	3.00 (3.05)
$[Pt(PTUQ)_2]Cl_2$[b] (Black)	300	41.73 (41.84)	11.39 (11.48)	3.00 (3.07)

[a]All the complexes decompose above the temperature cited.
[b]Also gave satisfactory analysis for S.

complexes with various ligands follows the order: MCMQ < PCMQ < MHBQ < PHBQ < PFQ≈ MAQ < PAQ < MTUQ < MFQ < MUQ < PUQ < PTUQ < PHAQ < MHAQ.

In the IR spectra all the ligands show a strong band at 1700 cm^{-1} corresponding to ν(C=O) of the quinazoline ring which is lowered by 50 cm^{-1} in the spectra of the complexes (except those of MHBQ, PHBQ, MHAQ and PHAQ) indicating that the oxygen of carbonyl group is involved in coordination[5]. The broad bands due to phenolic O−H at 3300 cm^{-1} (MHBQ, PHBQ, MHAQ and PHAQ)[6] and carboxylic O−H at 2500 cm^{-1} (MCMQ and PCMQ)[7] are absent in the spectra of the complexes, indicating complexation of these ligands through oxygen after deprotonation. The bands due to ν(C=N) of benzalimino/furfuralimino at 1600 cm^{-1} (MHBQ, PHBQ, MFQ and PFQ) and ν(NH) at 3230 cm^{-1} (MHAQ, PHAQ, MAQ, PAQ, MUQ, PUQ, MTUQ and PTUQ)[8] are lowered by 50 cm^{-1} in the spectra of complexes. These data suggest the involvement of nitrogen in coordination. Two new bands appear in the far infrared region around 500 and 420 cm^{-1} due to ν(M−O) and ν(M−N) respectively.

Further evidence for the above mode of coordination is given by the PMR spectral data. The PMR peaks observed for the free ligands due to hydroxyl (δ 9.6-10.5) and carboxylic (δ 10.8) protons are absent in the spectra of the complexes. The signal recorded for −NH (δ 6.9) proton, undergoes a downfield shift (δ 8.1) in the complexes[9].

All the complexes show two electronic spectral bands around 20000 and 24000 cm^{-1} (ε = 243 and 658 $dm^3\ mol^{-1}\ cm^{-1}$) which may be due to the transitions $^1B_{1g} \leftarrow {}^1A_{1g}$ and $^1E_g \leftarrow {}^1A_{1g}$ respectively, characteristic of square planar geometry[10].

Based on the above spectral and physical data, a square planar geometry may be tentatively proposed for all the complexes, with each bidentate chelate forming the minimum possible five (5-14), six (1 and 2) and seven (3 and 4) membered rings.

Acknowledgement

The authors are thankful to the Head, RSIC, IIT, Bombay, for providing facilities to record the PMR spectra. One of us (KLR) is grateful to Principal, Regional Engineering College, Warangal, for financial assistance.

References

1 Laxma Reddy K, Lingaiah P & Veera Reddy K, *Polyhedron*, 5 (1986) 1519.
2 Laxma Reddy K, Prabhakar B & Lingaiah P, *Indian J Chem*, 30A (1991) 904; and references cited therein.
3 Soliman R & Soliman F S G, *Synthesis*, (1979) 803.
4 Ravishankar Ch, *Studies on synthesis, biological and pharmacological evaluation of some 6,8-dibromoquinazoline-(3H)-4-ones derivates*. Ph.D. Thesis, Kakatiya University, Warangal (1984).
5 Sahai R, Agarwal R S & Kushwaha S S, *J Indian chem Soc*, 7 (1982) 853.
6 Sammour A, Fammy A F M & Mohmoud M, *Indian J Chem*, 13 (1973) 272.
7 Singh B, Banerjee V, Agarwala B V & Arun K D, *J Indian chem Soc*, 57 (1980) 365.
8 Prabhakaran C P & Patel C C, *J inorg nucl Chem*, 12 (1972) 3485.
9 Sakata K, Hashimoto M, Tagani M & Marakani Y, *Bull chem Soc, Japan*, 53 (1980) 2262.
10 Laxma Reddy K, Ramachandraiah A & Adinarayana Reddy K, *Indian J Chem*, 28A (1989) 622.

Indian Journal of Chemistry
Vol. 31A, December 1992, pp. 972-974

Studies on organomercury(II)-purine complexes

G S Sodhi*
Department of Chemistry, SGTB Khalsa College, University of Delhi, Delhi 110 007
and
J Kaur
Department of Chemistry, University of Delhi, Delhi 110 007

Received 7 January 1992; revised 24 April 1992; accepted 28 May 1992

A number of organomercury(II)-purine complexes of the type, *p*-$MeC_6H_4Hg(L^1)$ (I), *p*-$MeC_6H_4Hg(L^2)$ (II), *p*-$MeC_6H_4Hg(L^3)$ (III), *p*-$MeC_6H_4HgCl(L^4)$ (IV) and *p*-$MeC_6H_4HgCl(L^5)$ (V) [Where L^1 = theophylline, L^2 = 6-thioguanine, L^3 = 6-mercaptopurine, L^4 = theobromine, L^5 = caffeine] have been synthesised and characterised on the basis of elemental analyses, conductance measurements and spectral studies (IR, UV, ^1H and ^{13}C NMR).

The purine bases are known for their biological activity[1]. The studies of mercury-purine complexes are of significance since the toxic effects of organomercury compounds, which are often attributed to the formation of mercury-sulphur bonds with sulphydral functions in amino acids and proteins, may be due, in part, to their interaction with nucleic acid constituents[2]. The present note reports the synthesis and characterisation of a few organomercury(II) complexes involving biologically active purine bases (structures I-V).

Experimental

The purines (Sigma) were used without further purification. *p*-Methylphenylmercury (II) chloride (*p*-MeC_6H_4HgCl) was synthesised by the literature method[3].

The theophylline complex was prepared by adding slowly a solution of *p*-MeC_6H_4HgCl (0.01 mol) in 25 ml DMF to a stirred solution of theophylline (0.01 mol) in 25 ml DMF at a *p*H of 8-9. The contents were stirred for 6 h at 50°C and filtered. The filtrate was slowly poured over crushed ice and stirred vigorously. The precipitate so obtained was washed successively with hot water and benzene. The resulting product was dried and recrystallised from THF. The 6-thioguanine and 6-mercaptopurine complexes were prepared by a similar method. The theobromine and caffeine complexes were also prepared following the same procedure, except that the reaction was conducted in a neutral medium.

The conductance measurements were carried out on an Elico conductivity bridge, model CM-82. The infrared and UV spectra were recorded on Shimadzu model IR-435 and Perkin-Elmer UV-Vis spectrometer, model 554 respectively. The ^1H NMR and ^{13}C NMR spectra were recorded on Jeol Fx-200 FT-NMR spectrometer. Mass spectra were recorded at CDRI, Lucknow.

Results and discussion

The elemental analyses and spectral data revealed that the complexes are pure. This was also supported by TLC. The complexes were white or light brown in colour. The conductance measurements in 10^{-3} *M* nitrobenzene solution were of the order of 0.50 $ohm^{-1}\ cm^2\ mol^{-1}$ indicating that the compounds were nonelectrolytes. The analytical data of the complexes is presented in Table 1.

In the mercury-theophylline complexes reported by Norris *et al.*[4], the ν(C=O) stretching frequency in free theophylline absorbed at 1680 cm^{-1}, while in the metal complexes it was shifted to 1630-1665 cm^{-1}, although the crystal structure data ruled out the involvement of the carbonyl group at C(6) in complexation. In the present theophylline complex

Table 1—Analytical data of the complexes

Compound Decomp. temp. (°C)	Analysis Found (Calc.), %			
	Hg	N	S	Cl
p-$MeC_6H_4Hg(L^1)$ 123	42.63 (42.68)	11.98 (11.90)	—	—
p-$MeC_6H_4Hg(L^2)$ 268	43.93 (43.83)	15.35 (15.29)	6.85 (6.99)	—
p-$MeC_6H_4Hg(L^3)$ 215	45.26 (45.32)	12.60 (12.65)	7.32 (7.23)	—
p-$MeC_6H_4HgCl(L^4)$ 163	39.64 (39.54)	11.11 (11.04)	—	7.08 (7.00)
p-$MeC_6H_4HgCl(L^5)$ 212	38.58 (38.48)	10.71 (10.74)	—	6.90 (6.81)

too, the band attributed to the ν(C=O) stretching frequency was lowered from 1660 cm^{-1} to 1625 cm^{-1}. This shift, however, cannot be attributed to the interaction of the carbonyl at C(6) with mercury(II) ion, since the UV and ^{13}C NMR data indicated the non-chelating behaviour of theophylline. The band at 1560 cm^{-1} which was assigned to the ν(C=N) stretching mode in theophylline[5] was shifted to 1520 cm^{-1} on complexation.

In case of 6-thioguanine complex [*p*-$MeC_6H_4Hg(L^2)$], the evidence for the involvement of exocyclic sulphur at C(6) of the ligand was provided by the absorption frequency of the thione group; whereas in the free ligand, the ν(C=S) stretching frequency absorbed at 1220 cm^{-1}, was lowered to 1180 cm^{-1} on complexation. The bands at 1660 (νC=C) and 1530 cm^{-1} (νC=N) were lowered to 1570 and 1490 cm^{-1} in the complex. This showed the involvement of N(7) an complexation. The IR spectra of 6-mercaptopurine showed a medium intensity band at 650 cm^{-1}, due to ν(C-S) absorption. In the *p*-$MeC_6H_4Hg(L^3)$ complex, the ν(C-S) stretching frequency absorbed at 630 cm^{-1}. The ν(C=N) and ν(C=C) stretching frequencies in the ligand absorbed at 1575 cm^{-1} and 1610 cm^{-1}, respectively. In the complex, these bands shifted to 1560 cm^{-1} and 1590 cm^{-1}. On the basis of these results, it was concluded that the 6-mercaptopurine moiety was bound to the mercury(II) ion through N(7) and deprotonation of mercapto group at C(6)[6,7]. In case of theobromine and caffeine complexes, the ν(C=O) stretching frequency remained unaltered on complexation. It absorbed at ~1645 cm^{-1}, both in case of the ligands as well as in the metal complexes. However, the absorptions due to ν(C=N) were shifted from 1540 cm^{-1} in free ligands to ~1520 cm^{-1} in the complexes, indicating that these moieties were bound to the mercury(II) ion through N(9)[8].

The UV spectra of theophylline, theobromine and caffeine showed an absorption band at 270 nm (logε 7.5), 274 nm (logε 6.2) and 272 nm (logε 5.8) respectively due to the π-π* transition of the chromophoric carbonyl group[9]. Since no significant shift was observed in the λ_{max} value on complexation, the possibility of bonding through carbonyl group was ruled out. The 6-thioguanine showed a broad band at 310 nm (logε 2.0) due to the π-π* transition of the thione group[10]. On complexation this band shifted to 320 nm (logε 3.2), indicating the involvement of C=S group on complexation. The 6-mercaptopurine ligand showed an intense absorption at 330 nm (logε 6.0) due to the π-π* transition of the thione group in the keto form of the ligand[10]. The absence of this band in the complex [*p*-$MeC_6H_4Hg(L^3)$], indicated the conversion of 6-mercaptopurine to the thiol form before coordinating to the mercury(II) ion.

The theophyllinato group in *p*-$MeC_6H_4Hg(L^1)$ complex was identified by the following resonance signals in the ^1H NMR spectrum: δ3.25 (s, 3H, 1-Me), δ3.50 (s, 3H, 3-Me) and δ7.6-7.8 (m, 1H, H(8)). A comparison with the spectrum of theophylline[11] revealed no significant shift on complexation. However, in theobromine and caffeine[11], the signal due to H(8), which absorbed at *ca.* δ7.80 (s, 1H), was shifted to *ca.* δ 8.05 on complexation. The downfield shift was attributed to the involvement of N(9) in complexation. In case of 6-thioguanine, a sharp signal was observed at δ8.20 (s, 1H) due to H(8)[12]. On complexation, this signal shifted downfield, to δ8.42, indicating the involvement of N(7) in complexation. The 6-mercaptopurine complex, *p*-$MeC_6H_4Hg(L^3)$, showed signals at δ8.28 (s, 1H, H(2)) and δ8.40 (s, 1H, H(8)). The latter signal in free 6-mercaptopurine absorbed at δ8.22[12]. The downfield shift on complexation may be attributed to the involvement of deprotonated N(7) on complexation.

In the ^{13}C NMR spectra, the signal at *ca.* 160 ppm in case of theophylline, theobromine and caffeine was attributed to the C(6) carbonyl. Since no significant shift was observed on complexation, it was concluded that the carbonyl at C(6) was not coordinated to the metal ion[8]. However, the resonance signal due to C(8) which appeared at 140.12 ppm in theophylline was shifted to 143.15 ppm in the *p*-$MeC_6H_4Hg(L^1)$ complex, supporting the assertion that complexation involved deprotonation at N(7). Similarly, in theobromine and caffeine, the signal due to C(8) absorbed at *ca.* 135 ppm, while in the complexes it was shifted to *ca.* 138 ppm, supporting the involvement of N(9) in complexation[8]. In case of 6-thioguanine, the signal at 170 ppm was attributed to C(6) thione[12]. In the *p*-$MeC_6H_4Hg(L^2)$ complex, this signal shifted downfield, to 174.5 ppm. The C(8) absorption at 138.5 ppm in the free ligand was observed at 143.5 ppm in the complex. These results conform that the 6-thioguanine moiety chelates to the mercury(II) ion through 6-thione and deprotonated N(7). The 6-mercaptopurine showed a resonance signal at 170.9 ppm due to C(6) absorption[12]. In the *p*-$MeC_6H_4Hg(L^3)$ complex, this signal appeared at 175 ppm, indicating the involvement of C(6) in complexation.

Acknowledgement

One of us (JK) is thankful to the CSIR, New Delhi, for the award of a senior research fellowship.

References

1 Ritchie J M, *The pharmacological basis of therapeutics*, edited by L S Goodman & A Gilman (The Macmillan Publishing Co Inc, London), 1973, p.367.

2 Mulvihill J J, *Science*, 176 (1972) 132.

3 Nesmeyanov A N, Makaraova L G & Polovyanyuk I V, *J Gen Chem*, 35 (1965) 682.

4 Norris A R, Kumar R, Buncel E & Beauchamp A L, *J Inorg Biochem*, 21 (1984) 277.

5 Blout E R & Fields M, *J Am chem Soc*, 72 (1950) 479.

6 Ghosh A K & Chatterjee S, *J inorg nucl Chem*, 26 (1964) 1459.

7 Weida Y, Meiqing L & Shiqi P, *Inorg chim Acta*, 106 (1985) 65.

8 Bhatia S, Kaushik N K & Sodhi G S, *J chem Res (S)*, (1987) 186; (M), (1987) 1519.

9 Tu A T & Reinosa J A, *Biochemistry*, 5 (1966) 3375.

10 Hirayama K, *Handbook of ultraviolet and visible absorption spectra of organic compounds* (Plenum Press, New York) 1967.

11 Twanmoh L M, Wood H B & Driscoll J S, *J Heterocycl Chem*, 10 (1973) 187.

12 Chenon M T, Pugmire R J, Grant D M, Panzica R P & Townsend L B, *J Am chem Soc*, 97 (1975) 4636.

Indian Journal of Chemistry
Vol. 31A, December 1992, pp. 975-977

Kinetics of the reduction of hexachloroiridate (IV) by L-methionine in aqueous solutions

G Adefikayo Ayoko*
Department of Chemistry, University of Papua New Guinea, Box 320, University Post Office, Papua New Guinea
and
J Femi Iyun* & Allen T Ekubo
Department of Chemistry, Ahmadu Bello University, Zaria, Nigeria

Received 23 March 1992; revised and accepted 22 June 1992

The kinetics of the reduction of hexachloroiridate (IV) by L-methionine in aqueous solution has been studied. The data are consistent with the rate law:

$-d[\text{oxidant}]/dt = k_3[\text{oxidant}][\text{reductant}][H^+]$

with $k_3 = 1.58 \pm 0.06$ mol^{-2}dm^{6}s^{-1}, $\Delta H^{\ddagger} = 31.3 \pm 2.1$ kJ mol^{-1}, $\Delta S^{\ddagger} = 210 \pm 11.6$ JK^{-1}mol^{-1} at $I = 1.0$ mol dm^3 (NaCl) and T = 25.5°C. Free radicals are unimportant in the reaction and the reduction is rationalised in terms of an outer-sphere mechanism.

The reduction of hexachloroiridate (IV), $IrCl_6^{2-}$, by thiourea, $CS(NH_2)_2$, and substituted thioureas[1], as well as amino acids of the type $NH_2CH(R)COOH$ (ref. 2) have been studied. Reaction occurs at the sulphur end of the former substrates and at the nitrogen in the latter. We herein report the reduction of $IrCl_6^{2-}$ with methionine. This substrate has three possible reaction sites viz O, N and S and its reactions with $HCrO_4^-$ (ref. 3) and $AuCl_4^-$ (ref. 4) have suggested that inspite of the presence of a methyl group on the sulphur site, the formation of sulphur-bonded inner sphere complexes are feasible. In the event that intermediate complex formation is important in the present study, the choice of the thiol should reveal the effectiveness of O, N, and S as binding sites.

Experimental

Stock solutions of $IrCl_6^{2-}$ were prepared by dissolving Na_2IrCl_6 (Aldrich) in HCl (1 mol dm^{-3}) and standardized spectrophotometrically[2] at 487 nm using $\varepsilon = 4060$ dm^3 mol^{-1} cm^{-1}. L-methionine (BDH reagent) was used without further purification. HCl was used to investigate the $[H^+]$ dependence while NaCl was the supporting electrolyte.

Using varied amounts of methionine in the range $(0.8\text{-}8.0) \times 10^{-5}$ mol dm^{-3} and $[IrCl_6^{2-}] = 2.0 \times 10^{-5}$ mol dm^{-3} at $[H^+] = 0.5$ mol dm^{-3} and $I = 1.0$ mol dm^{-3} (NaCl), the stoichiometry was determined spectrophotometrically at 487 nm, as described elsewhere[5,6].

The electronic spectra of solutions containing $IrCl_6^{2-}$ $(1.0\text{-}5.0) \times 10^{-5}$ mol dm^{-3} in $[H^+] = 0.01\text{-}0.2$ mol dm^{-3} and those containing mixtures of $IrCl_6^{2-}$ $(2 \times 10^{-5}$ mol dm$^{-3})$, [methionine] = $\{(0.2\text{-}2.0) \times 10^{-2}\}$ mol dm^{-3} were compared between 400 and 700 nm. No clear shift in λ_{max} or change in ε value of $IrCl_6^{2-}$ was observed.

The rates of reaction were followed by monitoring changes in absorbance due to $IrCl_6^{2-}$ at 487 nm. Pseudo-first order plots were linear to greater than 80% reaction. The strict linearity of these plots suggests that the rate is first order in $IrCl_6^{2-}$. Pseudo-first order rate constants, k_{obs}, obtained from the slopes of these plots under various conditions are presented in Table 1.

Table 1—Effects of various reactants on $k^{\dagger}_{obs}$ at 25.5°C[b]

10^3[RSCH$_3$] (mol dm^{-3})	[H$^+$] (mol dm^{-3})	I (mol dm^{-3})	10^4 k_{obs} (s^{-1})
2.00	0.01	1.00	1.88
4.00	0.01	1.00	3.73
6.00	0.01	1.00	5.65
8.00	0.01	1.00	7.50
10.50	0.01	1.00	9.43
12.00	0.01	1.00	11.26
14.00	0.01	1.00	13.18
16.00	0.01	1.00	15.00
20.00	0.01	1.00	18.80
8.00	0.04	1.00	5.20
8.00	0.06	1.00	7.51
8.00	0.08	1.00	10.20
8.00	0.10	1.00	12.40
8.00	0.12	1.00	15.10
8.00	0.16	1.00	19.80
8.00	0.01	0.10	30.98
8.00	0.01	0.20	23.48
8.00	0.01	0.30	19.55
8.00	0.01	0.50	13.50
8.00	0.01	0.60	12.19
8.00	0.01	0.70	10.50
8.00	0.01	0.80	9.19

†$[IrCl_6^{2-}] = 2.0 \times 10^{-5}$ mol dm^{-3} throughout.
[b]Data at other temperatures are available on request.

Results and discussion

The salient features of the results are summarized below

i) Spectrophotometric titration results and product analyses are consistent with Eq. (1)

$$IrCl_6^{2-} + R(HS)^+CH_3 + H_2O \rightarrow IrCl_6^{3-} + R(CH_3)S=O + 2H^+ \quad \ldots (1)$$

where $R(HS)^+CH_3$ is the protonated methionine, $CH_3(HS)^+CH_2CH_2CHNH_2CO_2H$. Methionine sulphoxide was confirmed as the reaction product as described previously[3] while $IrCl_6^{3-}$ was characterized as the sole metallic product by oxidizing the reaction product with $S_2O_8^{2-}$ followed by spectrophotometric determination of $IrCl_6^{2-}$ ($\lambda_{max} = 487$ nm: $\varepsilon = 4060$ $mol^{-1}dm^3cm^{-1}$, (ref. 2). The formation of $RCH_3S=O$ suggests that reaction occurred at the sulphur.

ii) Plots of k_{obs} versus [methionine] were linear with positive slopes at a constant temperature, showing that the reaction is first order with respect to methionine. Thus

$$-d[IrCl_6^{2-}]/dt = k_2[IrCl_6^{2-}][\text{methionine}] \quad \ldots (2)$$

iii) A plot of k_2 versus $[H^+]$ at fixed [methionine] and temperature was linear passing through the origin. Hence the overall rate law is

$$-d[IrCl_6^{2-}]/dt = k_3[IrCl_6^{2-}][\text{methionine}][H^+] \quad \ldots (3)$$

iv) The values of k_3 at 15, 20, 25.5 and 30.0°C were 0.94 ± 02, 1.24 ± 0.05, 1.58 ± 0.06, and 1.86 ± 0.12 $mol^{-2}dm^6s^{-1}$ respectively, which yielded $\Delta H^{\ddagger} = 31.3 \pm 2.1$ kJ mol^{-1} and $\Delta S^{\ddagger} = -210 \pm 11$ $JK^{-1}mol^{-1}$.

v) Tests for polymerization of acrylamide or acrylonitrile, performed as described earlier[6] did not yield the required polymers, suggesting that free radicals are unimporant in this reaction in constrast to the corresponding reactions of $IrCl_6^{2-}$ with $NH_2CH(R)COOH$ (ref. 2).

vi) Michaelis-Menton plot of $1/k_{obs}$ versus 1/[methionine], as applied by Kumar *et al.*[2] was linear without an appreciable intercept at each temperature, indicating the absence of intermediates with significant formation constants.

In line with arguments presented earlier[2,3], protonated methionine $R(HS^+)CH_3$, is the principal reductant. Since $IrCl_6^{2-}$ does not enter into deprotonation-protonation equilibria over the acid range employed[1,2], the observed $[H^+]$ dependence almost certainly arose from the interaction between the Zwitterion of the substrate and the proton. Further support for reaction between $IrCl_6^{2-}$ and $R(HS^+)CH_3$ is gained from the dependence of the rate on the ionic strength (Table 1), which suggests a negative Bronsted-Debye salt effect reminiscent of reaction between oppositely charged species[7].

Table 2—Kinetic and thermodynamic parameters for the oxidation of methionine by some oxidants at 25°C

Oxidant	E° (volts)	log a ($mol^{-2}dm^6s^{-1}$)	Ref.
$IrCl_6^{2-}$	0.87	0.197	This work
$Fe(phen)_3^{3+}$	0.92	−0.754	5
$Fe(bipy)_3^{3+}$	1.00	−1.00	5

A reaction sequence consistent with the results is presented in Scheme 1.

$$RSCH_3 + H^+ \overset{K_a}{\rightleftharpoons} R(HS)^+CH_3 \quad \ldots (4)$$

$$R(HS)^+CH_3 + IrCl_6^{2-} \overset{K}{\rightleftharpoons} [IrCl_6^{2-}.R(HS)^+CH_3] \quad \ldots (5)$$

$$[IrCl_6^{2-}R(HS)^+CH_3] + H_2O \xrightarrow{k_0} IrCl_6^{2-} + R(CH_3)S=O + 2H \quad \ldots (6)$$

Scheme 1

This Scheme leads to Eq. (7)

$$-d[IrCl_6^{2-}]/dt = KKak_0[IrCl_6^{2-}][RSCH_3][H^+]/(1 + K_a + KKak_0[IrCl_6^{2-}][H^+]) \quad \ldots (7)$$

where

$$[RSCH_3] = [RSCH_3]_T/(1 + K_a[H^+] + KKak_0 \times [IrCl_6^{2-}][H^+])$$

If $1 >> (K_a[H^+] + KK_ak_0[IrCl_6^{2-}][H^+])$, Eq. (7) reduces to the observed rate equation (3) with $k_3 = KK_ak_0$.

The rate of aquation of the first chloride in $IrCl_6^{2-}$ ($10^{-6}s^{-1}$) depicts its substitution inertness[8]. When this is judged along with the fact that the most susceptible reaction site on methionine is blocked by a methyl group, the species $[IrCl_6^{2-}, R(HS^+)CH_3]$ may be regarded as an ion-pair. Although it may be argued that a binuclear intermediate as in the corresponding reactions with amino acids[2] and uranium (IV)[8] could not be excluded, we found no kinetic or spectrophotometric evidence in its favour.

As a further test of the outer sphere nature of the title reaction, we interpreted our data in terms

of Marcus theory[9]. A plot of log$a$ (a is rate constant for the redox reaction of $R(HS^+)CH_3$ with $IrCl_6^{2-}$, $Fe(phen)_3^{3+}$ and $Fe(bipy)_3^{3+}$ (Table 2)) versus E° of the oxidants was linear ($r=0.92$) with a slope of 8.2 v^{-1}, in excellent agreement with predicted value of 8.5 v^{-1} for reactions occurring by the outer sphere mechanism.

References

1 Po H N, Evan H, Rim V & Byrd J E, *Inorg Chem*, 18 (1979) 197.

2 Kumar C S, Chandraiah U, Siddiqui M A A, Kandlikar S, *Indian J chem Soc* 30A (1991) 714.

3 Olatunji M A & Ayoko G A, *Polyhedron*, 7 (1988) 11.

4 Natile G, Burdigum E & Cattalin I, *Inorg Chem*, 15 (1976) 246.

5 Akubo A T, M.Sc Thesis, Ahmadu Bello University, Zaria, 1992.

6 Ayoko G A, *Transition met Chem*, 15 (1990) 89.

7 Bronsted J N, *Z Phy Chem*, 102 (1922) 160.

8 Hassan R F, *J chem Soc Dalton Trans*, (1991) 3003.

9 Marcus R A, *J phys Chem*, 67 (1963) 853; *Electrochim Acta*, 13 (1968) 995.

Indian Journal of Chemistry
Vol. 31A, December 1992, pp. 978-980

Kinetics of nuclear chlorination of substituted phenyl acetates by trichloroisocyanuric acid

H P Panda* & K K Sahoo

Department of Chemistry, M.P.C. College, Baripada 757 001

Received 19 May 1992; revised and accepted 31 August 1992

Kinetics of nuclear chlorination of phenyl acetate and its substituted derivatives by trichloroisocyanuric acid (TCICA) in aqueous acetic acid-perchloric acid media follows second order kinetics, first order each in [substrate] and [TCICA]. The second order rate constants marginally increase with increase in $[H^+]$ pointing to a fractional order in $[H^+]$. The second order rate constants have a diminishing trend with increase in the proportion of acetic acid in the reaction mixture. A mechanism involving electrophilic attack of both HOCl and H_2O^+Cl produced from hydrolytic equilibria has been suggested.

Trichloroisocyanuric acid (TCICA) or 1,3,5-trichloro-1(H), 3(H), 5(H)-triazine-2,4,6-trione, is a wellknown halogen carrier[1]. It mostly chlorinates aromatic substrates like phenols, aniline derivatives[2] and sulphacetamide[3]. We present herein the kinetics of nuclear chlorination of substituted phenyl acetates with an aim to compare its kinetics with chlorination by other N-chloro compounds[4].

Experimental

TCICA (Riedel, GR) was preserved in dark in a desiccator and was used as such in each kinetic run. Phenyl acetate, *p*-cresyl acetate, *m*-cresyl acetate, *p*-chlorophenyl acetate and *p*-nitrophenyl acetate were prepared from the corresponding phenols by the usual acetylation method[5] and their purity was checked from their boiling and melting points. The progress of the reaction was monitored by estimating the unreacted TCICA iodometrically[6] in accordance with Eq. (1)

$$\underset{\text{(TCICA)}}{C_3O_3N_3(Cl)_3} + 6I^- + 3H^+ \rightarrow \underset{\text{(ICA)}}{C_3O_3N_3(H)_3} + 3I_2 + 3Cl^- \quad \ldots (1)$$

The pseudo-first order rate constants (k_{obs}) were reproducible within ±3% error. The self decomposition of TCICA was found to be negligible, routinely checked in each kinetic run and due corrections were applied, whenever needed, for computation of rate constants. However, under the condition $[TCICA]_0 > [substrate]_0$, stoichiometric runs were not meaningful. Self decomposition of TCICA in long time intervals was appreciable. Product identification in case of phenyl acetate showed that the monochloro derivatives, i.e., *ortho*-chloro and *para*-chlorophenyl acetates were formed which were identified by separation through column chromatography, hydrolysing with alkali, preparing the benzoyl derivatives, and studying their melting points.

Results and discussion

In each kinetic run, the disappearance of TCICA followed pseudo-first order kinetics for more than two half-lives as evident from good linear plots of log $[TCICA]_t$ versus time. The pseudo-first order rate constants were found to be invariant over a six-fold increase of [TCICA]. For example, under the conditions [Phenyl acetate] = 0.005 mol dm^{-3}, $[HClO_4] = 0.05$ mol dm^{-3}, solvent = acetic acid (25%, v/v) and temp. = 30°C, 10^4 k_{obs} remained constant at 2.07 ± 0.09 s^{-1} when 10^4 [TCICA] was varied from 2.0 to 12.0 mol dm^{-3}.

The k_{obs} values were found to increase linearly with increase in [substrate]. The effect of $[H^+]$ was studied by varying $[HClO_4]$ from 0.01 mol dm^{-3} to 0.20 mol dm^{-3} at 30°, 40° and 50°C. At 30° the plots of log k_2 versus log $[H^+]$ were linear with slopes 0.25, 0.25, 0.25, 0.25 and 0.28 for phenyl acetate, *p*-cresyl acetate, *m*-cresyl acetate, *p*-chlorophenyl acetate and *p*-nitrophenyl acetate respectively. This shows that the contribution to overall rate by H_2O^+Cl generated from the equilibria,

$$HOCl + H^+ \rightleftharpoons H_2O^+Cl$$

is small. Both HOCl and H_2O^+Cl may act as electrophile, contribution from HOCl being predominant.

At 30°C and under the conditions [phenyl acetate] = 0.005 mol dm^{-3}, $[TCICA] = 0.8 \times 10^{-3}$ mol dm^{-3}, $[HClO_4] = 0.05$ mol dm^{-3}, 10^2 k_2 values at 10, 25, 35 and 50% HOAc were found to be 4.72, 4.21, 3.51 and 2.59 mol^{-1} dm^3 s^{-1} respectively. The plot of log k_2 against $(D-1)/(2D+1)$ was linear with negative slope ($r = 0.996$).

To study the effect of temperature, rate constants were determined at three different temperatures under identical stoichiometric conditions. Plots of log k_2 versus $1/T$ were linear with good correlation. The computed activation parameters are recorded in Table 1. The calculated $\Delta S^{\neq}$ va-

Table 1—Activation parameters at 30°C

Substrate	E_a (kJ mol^{-1})	$\Delta H^{\neq}$ (kJ mol^{-1})	log A	$\Delta S^{\neq}$ (JK^{-1} mol^{-1})
Phenyl acetate	89.64	87.12	14.07	16.11
p-Cresyl acetate	89.90	87.38	14.12	17.01
m-Cresyl acetate	87.90	85.38	14.01	14.83
p-Chlorophenyl acetate	90.65	88.13	13.75	9.94
p-Nitrophenyl acetate	74.92	72.44	10.76	−47.26

lues point to a biomolecular process. Plot of logA versus $1/(E_a)^{1/2}$ is linear ($r=0.98$). The isokinetic plot of $\Delta H^{\neq}$ versus $\Delta S^{\neq}$ is linear ($r=0.977$) but the isokinetic temperature $\beta=232.1$ K is found to be less than the experimental temperature.

The order of reactivity among the substrates is $m-CH_3 > p-CH_3 \approx H > p-Cl > p-NO_2$. When the usual σ values were plotted against $\log k_2$ at a given stoichiometric and experimental conditions, the points corresponding to different substrates were found to be scattered with a poor correlation, but when σ_p values were taken for *meta*-substituents and σ_m values for *p*-substituents, a good linearity is found to exist ($r=0.99$) with a ρ value = −1.12. This clearly shows that the attack of the electrophile is directly on the ring and not on the phenolic oxygen of the ester group. Since the site of substitution is *meta*- to *para*-substituents and *para*- to *meta*-substituents, the use of σ_m values for *para*-substituents and σ_p values for *m*-substituents is justified. Such reasonings have been made in earlier studies of iodination of phenols[7].

TCICA generally undergoes hydrolysis in aqueous medium as[1]

$$TCICA + H_2O \underset{6.7\times10^{-4}\text{ mol dm}^{-3}}{\overset{K_{h1}}{\rightleftharpoons}} DCICA + HOCl.$$

$$DCICA + H_2O \underset{3.6\times10^{-4}\text{ mol dm}^{-3}}{\overset{K_{h2}}{\rightleftharpoons}} MCICA + HOCl$$

$$MCICA + H_2O \underset{1.9\times10^{-4}\text{ mol dm}^{-3}}{\overset{K_{h3}}{\rightleftharpoons}} ICA + HOCl$$

The above equilibria shows that the concentration of monochloroisocyanuric acid (MCICA) and isocyanuric acid (ICA) would be negligible in acid medium as the products $K_{h1}.K_{h2}.K_{h3}$ and $K_{h1}.K_{h2}$ are negligible in comparison to K_{h1}. Thus the predominant species would be HOCl, which may enter into protonation equilibria giving H_2O^+Cl. The electrophiles may, therefore, be assumed to be HOCl and H_2O^+Cl respectively. The following Scheme 1 is therefore proposed.

$$TCICA + H_2O \overset{K_{h1}}{\rightleftharpoons} DCICA + HOCl$$

$$HOCl + H^+ \overset{K_4}{\rightleftharpoons} H_2O^+Cl.$$

$$HOCl + S \xrightarrow[\text{slow}]{k_5} \text{Products}$$

$$H_2O^+Cl + S \xrightarrow[\text{slow}]{k_6} \text{Products}$$

Scheme 1

The rate law is derived as follows:

$$[TCICA]_T = [TCICA] + [HOCl] + [H_2O^+Cl]$$

$$= \left\{\frac{[HOCl][DCICA]}{K_{h1}} + [HOCl] + K_4[HOCl][H^+]\right\} \quad \ldots(2)$$

$$= [HOCl]\left\{\frac{[DCICA] + K_{h1} + K_{h1}K_4[H^+]}{K_{h1}}\right\} \quad \ldots(3)$$

This gives

$$[HOCl] = \frac{K_{h1}[TCICA]_T}{[DCICA] + K_{h1} + K_{h1}K_4[H^+]} \quad \ldots(4)$$

Analogous treatment gives

$$[H_2O^+Cl] = \frac{K_{h1}K_4[TCICA]_T[H^+]}{[DCICA] + K_{h1} + K_{h1}K_4[H^+]} \quad \ldots(5)$$

Therefore,

$$\text{Rate} = -\frac{d[TCICA]_T}{dt}$$

$$= \left(-\frac{d[HOCl]}{dt}\right) + \left(-\frac{d[H_2O^+Cl]}{dt}\right)$$

$$= \frac{\{K_{h1}k_5[S][TCICA]_T + K_{h1}K_4k_6[H^+][S][TCICA]_T\}}{[DCICA] + K_{h1} + K_{h1}K_4[H^+]} \quad \ldots(6)$$

Therefore,

$$k_2 = \frac{K_{h1}\, k_5 + K_{h1}\, K_4\, k_6 [H^+]}{[DCICA] + K_{h1} + K_{h1}\, K_4 [H^+]} \quad \ldots (7)$$

When [DCICA] is negligibly small, the rate constant assumes the form,

$$k_2 = \frac{k_5 + K_4 k_6 [H^+]}{1 + K_4 [H^+]} \quad \ldots (8)$$

The above rate law explains the observed kinetics.

References

1 Osaka Pharmaceutical Association, Osaka-Fu-Yaku Zasshi 30 (1979) 39, *Chem Abstr*, 91 (1979) 157695g.

2 Radhakrishnamurti P S, Rath N K & Panda R K, *Indian J Chem*, 26A (1987) 407.

3 Radhakrishnamurti P S, Rath N K & Yedukondalu M, *Indian J Chem*, 27A (1988) 1028.

4 Radhakrishnamurti P S & Sasmal B M, *Indian J Chem*, 17A (1979) 181.

5 Vagel A I, *A text book of practical organic chemistry*, (1948) 639.

6 Pati S C & Sarangi C, *Indian J Chem*, 27A (1988) 593.

7 Radhakrishnamurti P S, Janardhana Ch, *Indian J Chem*, 16A (1978) 142.

Indian Journal of Chemistry
Vol. 31A, December 1992, pp. 981-983

Kinetic studies on the solvent extraction of iron(III) from aqueous solution with 1-phenyl-3-methyl-4-(*p*- nitrobenzoyl)pyrazol-5-one dissolved in chloroform: Rate of forward extraction

M O C Ogwuegbu*
School of Physical Sciences, ABIA State University, P.M.B. 2000, UTURU, Nigeria
and
N C Oforka & A I Spiff
Department of Pure and Industrial Chemistry, University of Port Harcourt, Nigeria

Received 30 December 1991; revised 18 June 1992; accepted 28 July 1992

The rate of forward extraction of iron(III) from aqueous solution using 1-phenyl-3-methyl-4-(*p*-nitrobenzoyl)pyrazol-5-one, HNP in chloroform has been investigated at various conditions. Experimental observation shows that the rate of forward extraction is first order each with respect to [Fe(III)] and $[HNP]_{org}$, and inverse first order with respect to $[H^+]$. The rate of forward extraction of Fe(III) is proposed to be controlled by the formation of the first complex between $Fe(H_2O)_6^{3+}$ or $Fe(H_2O)_5OH^{2+}$ and the extractant anion, NP^-. The rate constant, k_f for the forward extraction and the extraction equilibrium constant, K_{ex} have been determined respectively as $5.83 \times 10^2 s^{-1}$ and 0.18.

Solvent extraction studies of iron (III) have been undertaken by various workers[1-4] using β-diketones, especially the acyl pyrazolones and their derivatives, but studies on their rates of extraction have been limited. The rate of extraction of iron (III) using thenoyltrifluoroacetone (HTTA) has been reported to be governed by slow formation of the first complex between iron and HTTA anion in the aqueous phase[5-7]. Kinetic studies on the extraction of Fe(III) using β-isopropyltropolone, alkylphosphoric acid and 8-hydroxyquinoline have also been reported[8-11].

However, kinetic studies on the extraction of iron (III) using nitro derivatives are almost lacking. It is on this premise that the present study was undertaken. Eigen[12], nevertheless, postulated that the rate of extraction of metal ions from aqueous solutions is slow when the charge is large and/or the radius is small. This has been attributed to the slow substitution of the coordinated water molecules. Herein we report the kinetics of extraction of iron(III) with 1-phenyl-3-methyl-4-(*p*-nitrobenzoyl)pyrazol-5-one (HNP) in chloroform and its possible mechanism.

Experimental

The HNP was prepared from high grade *p*-nitrobenzoyl chloride and 1-phenyl-3-methyl-5-pyrazolone (HPMP), which was prepared from analytical grade ethylacetoacetate and phenylhydrazine[13,14]. The nitropyrazolone was recrystallized from ethanol and dissolved in chloroform to obtain the desired concentrations. All other reagents were of analytical grades, except otherwise stated.

The stock solution of Fe(III) was prepared by dissolving ferric ammonium sulphate (0.2169) in 0.1 *M* H_2SO_4 solution (250 ml). Further dilutions were made by adding appropriate amounts of distilled water and/or suitable buffer solutions (KCl/HCl and NaAc/HAc) to desired *p*H. The PYE Unicam SP8-100 spectrophotometer was used for all spectrophotometric measurements, and TOA Digital *p*H meter model HIM-208 for *p*H measurements.

Extraction procedure

The details of the extraction procedure are essentially the same as those described elsewhere[2,7]. The studies on the rate of forward extraction were carried out by mixing equal volumes (4 ml) of $4.5 \times 10^{-5} M$ Fe(III) solution and 0.002-0.05 *M* HNP in chloroform in stoppered extraction bottles. Each mixture was agitated for a specific time interval (5-240 mins) by means of a mechanical shaker at a speed so high that no acceleration of the extraction rate was observed on further increase in the extraction speed. This eliminated the effects due to material transport (diffusion) and interfacial effects in the system[15]. After extraction, the phases were allowed 30 min settling time, after which aqueous aliquots were taken for analysis. The concentration of Fe(III) in the aqueous phase was determined spectrophotometrically[16] using 1,10-phenanthroline at 480 nm, while that in the organic phase was determined by difference. All experiments were conducted at 26 + 0.5°C and constant ionic strength of 0.3*M*, maintained by the use of sodium sulphate. Preliminary experiments show that sulphate ions had no effect on extractions.

The extraction equilibrium of Fe(III) with HNP was achieved by agitating aqueous solutions of

Fe(III) at *p*H 3 with various concentrations of HNP in chloroform solution for 45 min. The distribution ratio, D, of Fe(III) in each case was calculated as the ratio of the concentration of Fe(III) in the organic phase to that in the aqueous phase. From the extraction data, the extraction equilibrium constant, K_{ex} was computed as follows:

$$Fe(III)_{aq} + 3HNP_{(org)} \overset{K_{ex}}{\rightleftharpoons} Fe(NP)_{3(org)} + 3H^+_{(aq)} \quad \ldots (1)$$

$$K_{ex} = [Fe(NP)_3]_{org}[H^+]^3[Fe(III)]^{-1}_{aq}\,[HNP]^{-3}_{org} \quad \ldots (2)$$

$$= D[H^+]^3_{aq}\,[HNP]^{-3}_{org} \quad \ldots (3)$$

and

$$D = K_{ex}[HNP]^3_{org}\,[H^+]^{-3}_{aq} \quad \ldots (4)$$

where D is the distribution ratio,

$Fe[(NP)_3]_{org}/[Fe(III)]_{aq}$. From Eq. 4

$$\log D = \log K_{ex} + 3\log[HNP]_{org} + 3pH \quad \ldots (5)$$

Results and discussion

Extraction equilibrium

The data in Table 1 show the variation of distribution ratio with extractant concentration. A plot of log-log values of D versus. $[HNP]_{org}$ was linear with a slope of 3.0. This meant that three moles of HNP were involved in complexation with one mole of Fe(III) ion, and representing a third-power dependence of D on $[HNP]_{org}$, as depicted in Eqs (4) and (5). The value of $\log K_{ex}$ was calculated as -0.75.

Kinetics of reaction

The rate of extraction was followed as the rate of disappearance of $Fe(III)_{aq}$ and fitted to Eq. (6)

$$-\frac{dFe(III)}{dt} = K_f[Fe(III)]^x[HNP]^y[H^+]^z \quad \ldots (6)$$

Table 1—Extraction equilibrium data (*p*H = 3)

log HNP	log D	log K_{ex}
−2.70	0.10	−0.80
−2.50	0.70	−0.80
−2.40	0.95	−0.85
−2.30	1.30	−0.80
−2.25	1.60	−0.65
−2.00	2.35	−0.65
−1.82	2.65	−0.68
	Ave $\log k_{ex}$ =	−0.75
	and K_{ex}	−0.18

by varying the concentration of one reactant at a time and keeping the other two fixed and in excess. At $[H^+] = 0.00063$ to 0.327, linear plots were obtained for $-\log[Fe(III)]_{aq}$ versus t, although deviations occurred at later stage (Fig. 1). This shows that the reaction is first order in Fe(III) i.e., x = 1. The slopes of these plots at different $[H^+]$ correspond to

$$K_f[H]^z[HNP]^y_{org} = S_{H+} \quad \ldots (7)$$

Plot of $\log S_{H+}$ versus $-\log[H^+]$ was linear with slope equal to -1. Similarly, a plot of $-\log$ [Fe(III)] versus *t* was linear at different [HNP] and the slope corresponded to

$$K_f[H^+]^{-1}[HNP]^y = S_{HNP} \quad \ldots (8)$$

Plot of $\log S_{HNP}$ versus $\log[HNP]_{org}$ was linear with slope = 1. Hence y = 1.

Thus, the rate law for extraction is given by

$$-\frac{dFe(III)}{dt} = K_f[Fe(III)][HNP]_{org}[H^+]^{-1} \quad \ldots (9)$$

Table 2 shows some sets of values for the extraction rate; and by applying the data the rate constant, K_f was calculated as $5.83 \times 10^2 s^{-1}$ using Eq. (9).

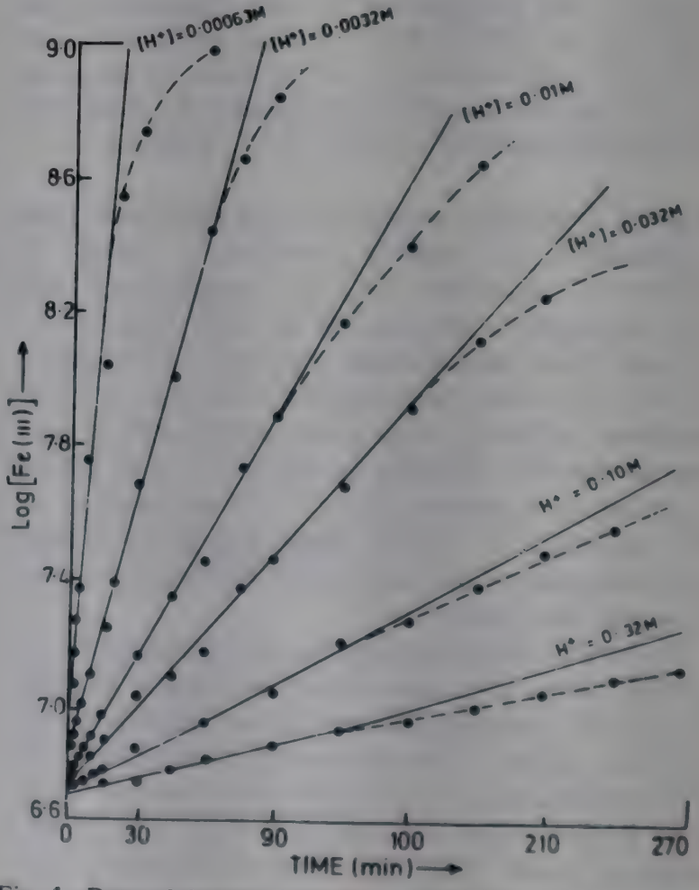

Fig. 1—Rate of forward extraction of Fe(III) with respect to $[H^+]$ ($[HNP] = 0.02$ *M*, slope = S_{H^+})

Table 2(a)—Kinetic data ($[HNP]_{org} = 0.02\ M$, $[Fe(III)] = 1.8 \times 10^{-7}$ mM)

$\frac{-dFe(III)}{dt}$	$[H^+]$ (M)	K_f (min^{-1})
0.0004	0.32	3.6×10^4
0.001	0.10	3.5×10^4
0.005	0.03	3.8×10^4
0.0122	0.01	3.4×10^4
0.038	0.0032	3.5×10^4
0.182	0.00063	3.2×10^4

Ave $K_f = 3.50 \times 10^4\ min^{-1}$
$= 5.83 \times 10^2 s^{-1}$

(b)—Kinetic Data ($[H^+] = 0.01\ M$, $[Fe(III)] = 1.8 \times 10^{-7}$ mM.)

$\frac{-dFe(III)}{dt}$	HNP $(M)_{org}$	K_f $(min.^{-1})$
0.0013	0.002	3.55×10^4
0.0033	0.005	3.67×10^4
0.0063	0.010	3.5×10^4
0.0096	0.015	3.54×10^4
0.0133	0.02	3.69×10^4

Ave $K_f = 3.59 \times 10^4\ min.^{-1}$
$= 5.97 \times 10^2 s^{-1}$.

Mechanism

The rate law shows that the determining step is the formation of the first complex between iron (III) ion and the extractant anion, NP^-.

$$Fe(III) + NP^- \rightleftharpoons [Fe(NP)]^{2+} \quad \ldots (10)$$

because

$$[NP] = K_{HNP} \frac{[HNP]}{[H^+]} \quad \ldots (11)$$

where K_{HNP} is the dissociation constant of HNP. Since the actual complex formed during extraction is $Fe(NP)_{3(org)}$, the addition of second and third ligands must be fast.

The actual mechanism may be the formation of ion pair followed by a slow dissociative step (Eigen and Wilkens)[17,18] leading

$$Fe(H_2O)_6^{3+} \xrightarrow{fast} Fe(H_2O)_6^{3+}\ NP^- \quad \ldots (12)$$

$$Fe(H_2O)_6^{3+}\ NP^- \xrightarrow{slow} Fe[(H_2O)_4\ NP]^{2+} + 2H_2O \quad \ldots (13)$$

to the formation of the first chelate ring of mono-pyrazolonato-tetraaquo-iron complex. It is expected that this step is followed by more rapid successive reaction , to produce a neutral tris-pyrazolonato-iron chelate, which eventually is transferred to the bulk organic phase, steric factors notwithstanding.

Acknowledgement

The authors are grateful to Imo State University, Okigwe, for sponsoring M.O.C. and the University of Port-Harcourt for providing laboratory facilities.

References

1 Khopkar S M & De A K, *Anal Chim Acta*, 22 (1963) 223.
2 Mirza M Y, Nwabue F I & Okafo E N, *J inorg nucl Chem*, 43 (1981) 1365.
3 Okafor E C & Uzoukwu B A, *Radiochim Acta*, 51(4) (1990) 167.
4 Uzoukwu B A, *Indian J Chem*, 30(A) (1991) 372.
5 Adin A & Newman L, *J inorg nucl Chem*, 32 (1970) 3321.
6 Sekine T & Tetsuka T, *Bull chem Soc Japan*, 45 (1972) 1620.
7 Sekine T, Yumikura Y & Komatsu Y, *Bull chem Soc Japan*, 46 (1973) 2256.
8 McClellan B E & Menis O, *Anal Chem*, 43 (1971) 436.
9 Coleman C F & Roddy J W, *Solvent extraction Rev* Vol 1 edited by Y Marcus (Marcell Dekker N.Y.) (1971) p. 63.
10 Fluming C A & Nicol M Y, *J inorg Nucl Chem*, 42 (1980) 1327.
11 Fleming C A & Nicol M Y, *J inorg nucl Chem*, 42 (1980) 1335.
12 Eigen M, *Pure appl Chem*, 46 (1963) 38.
13 Jenson B S, *Acta Chem Scand*, 13 (1959) 1668.
14 Okafor E C, *Z Naturforsch*, 85b (1980) 1010.
15 Sekine T, Koibe Y & Komatsu Y, *Bull chem Soc Japan*, 44 (1971) 1620.
16 Jayan T C Z, Sriasubramanian S & Wijedesa M A, *Analyst*, 100 (1975) 716.
17 Eigen M & Tamm K, *Z Electrochem*, 66 (1962) 107.
18 Wilkins R G Eigen M, *Advan Chem Ser*, 46 (1965) 527.

Indian Journal of Chemistry
Vol. 31A, December 1992, pp. 984-985

Extractive and spectrophotometric determination of Co(II) at trace levels using isonitroso-4-methyl-2-pentanone

P S More & A D Sawant*
Chemistry Department, The Institute of Science,
15, Madam Cama Road, Bombay 400 032
Received 15 January 1992; revised 20 May 1992;
accepted 2 September 1992

Isonitroso-4-methyl-2-pentanone(HIMP) is proposed as a new reagent for the extraction and photometric determination of Co(II). The reagent forms a yellow complex with cobalt in the *p*H range 8.3-9.3. The complex is extracted with chloroform and its absorbance is measured against a reagent blank at 340 nm.

Minoru *et al.*[1] have used isonitroso-4-methyl-2-pentanone(HIMP) for coordination studies of Co(II) whereas Dixit *et al.*[2] have studied its Cu(II), Ni(II) and Pd(II) complexes. This reagent has so far not been used for analytical studies. The reagent is very sensitive and convenient for the determination of cobalt at trace levels. The method has distinct advantages like better sensitivity[3-6], less interferences[7] and instant color development[8-9].

Experimental

An ELICO *p*H-meter and a Bauch and Lomb Spectronic-20 spectrophotometer were used for *p*H and absorbance measurements respectively. A standard solution of cobalt chloride (0.01 *M*) was prepared in doubly distilled water with a few drops of HCl and standardised by known method[10]. Isonitroso-4-methyl-2-pentanone (HIMP) reagent was synthesised according to the literature method[11]. A freshly prepared aqueous solution of reagent (0.1%) was used for the studies. All other chemicals and reagents used were of AR grade.

Procedure

To an aliquot of solution containing 20 μg of cobalt and 1 ml of 0.1% aqueous HIMP, adequate quantities of dil. HCl and/or NH_3 were added to adjust the *p*H to 9.0 in 10 ml of final volume. The solution was equilibrated with 10 ml chloroform for 1 min. The absorbance of organic layer was measured at 340 nm against the reagent blank. From the calibration curve, the amount of Co(II) was computed.

Results and discussion

The absorbance spectrum of cobalt-HIMP complex in chloroform shows maxima at 340 nm, where the reagent absorption is negligible. The extraction is quantitative in the *p*H range 8.3-9.3. An aqueous HIMP solution (1 ml, 0.1%) was found to be sufficient for quantitative extraction of 2 μg cobalt. A shaking time of 1 min was sufficient to achieve complete extraction. The complex was found to be stable for 48 h. Various solvents were tried to achieve maximum extraction of cobalt. The extraction of cobalt varied from a maximum of 97.9% to a minimum of 85.9% for the solvents in the order chloroform > benzene > nitromethane > isoamyl alcohol > isobutanol > toluene > methyl isobutyl ketone > nitrobenzene > carbon tetrachloride > ethyl acetate > ether. Beer's law obeyed over the concentration range 0.1-2.0 ppm of cobalt at 340 nm. The molar absorptivity and Sandell's sensitivity were found to be 1.479×10^4 L mol^{-1}cm^{-1} and 0.0037 μg cm^{-2} respectively at 340 nm. The composition of the complex determined by the mole ratio method was found to be 1:3 which was confirmed by Job's continuous variation method. The tentative structure of the complex was proposed as

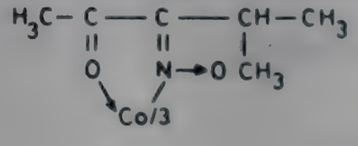

The infrared spectrum of the complex showed a band at 1689cm^{-1} which can be attributed to the C=O vibrations. The N−O and Co−N stretchings were observed at 981 and 615 cm^{-1}. These bands were well in accordance with the tentative structure proposed above.

Effect of diverse ions

Various ions were tested for tolerance. The tolerance limit for the variation was fixed at ± 2% absorbance. Since the extractions were to be carried out at *p*H 9.0, the reagent was added prior to the adjustment of *p*H. A 50 fold excess of Mo(VI), W(VI), As(III), Ni(II), Pt(IV) and Pd(II) did not interfere whereas Pb(II), Zn(II), Zr(IV) were tolerated upto 250 fold excess. V(V), Mn(II), Be(III), U(VI) tolerated upto 100 fold excess and Fe(II), Fe(III), Rh(III), Ru(III), Au(III), Ir(III) upto 5 fold excess were tolerated. Interference due to Ag(I) and Cd(II)

were removed by masking with KI and Cu(II) by sodium thiosulphate. Hg(II) interferes seriously. Chloride, bromide, iodide, chlorate, bromate, iodate, tartrate, oxalate, urea, molybdate and thiourea were tolerated upto 1000 fold excess. Interference due to citrate was removed by masking with sodium molybdate. It was found that EDTA also interfered.

Applications of the method

Synthetic mixture : A solution containing 20 μg Co(II) was taken and known amount of other metals added, and proceeded as per the developed method. The different combinations tried were (a) Co(20), Cu(1000), Ni(100), (b) Co(20), Pd(1000) and (c) Co(20), Pd(1000), Ru(100). The results found were in good agreement with the amounts added. The average of eight determinations of 10 μg of Co(II) was 9.9625 μg with variation from mean at 95% confidence limit as 9.9625 ± 0.0663.

Alloys : About 0.2 to 0.5 gm of oven dried (110°C) sample of an alloy was dissolved in aquaregia. It was evaporated to dryness and nitrate expelled by conc. HCl. The residue was extracted in water. A suitable aliquot of sample was taken and made upto 6.5 *M* with respect to HCl and then equilibrated twice with 10 ml of di-isopropyl ether to remove iron. The aqueous phase was evaporated to dryness and extracted into water. It was analysed as per the developed method. For Nimonic-901 (BCS-380)-cobalt found was 0.2287% and for High Speed Steel it was 5.81%. They were found to be in good agreement with the reported values.

Biological Samples : A 10 gm of SRM ray flour (standard reference material supplied by International Atomic Energy) was dissolved in distilled conc. HNO_3 and conc. HCl and evaporated to dryness. The suitable aliquot was taken for estimation of cobalt by the developed method. The cobalt content was found to be 0.306 ppm. This was in good agreement with the reported value.

Pharmaceutical Samples : To a cyanocobalamin injection (1 ml), conc. H_2SO_4 (1 ml) and HNO_3 (5 ml) were added and evaporated to dryness. Hydrogen peroxide (5 ml, 30 V) was added every time till the solution became colourless. Dilute HCl was added and the solution was evaporated to dryness. The volume was made upto 10 ml and then analysed for cobalt by the developed method. In cynocobalamin injection (Glaxo) and Neurobian Merck, the value of cobalt obtained was 21.707 ppm and 43.516 ppm respectively which in good agreement with the reported values.

References

1 Tanaka Minoru, Rya Ryonte, Masuda Isao & Shono Toshoyuki, *Bull chem Soc Japan*, 50 (1977) 415.
2 Dixit N S, Suda B P & Patel C C, *Bull chem Soc Japan*, 51(7) (1978) 2160.
3 Khan F & Kharat R B, *Zh anal Khim*, 44(5) (1989) 947.
4 Murty G V R & Reddy T S, *Chim acta Turc*, 17(2) (1989) 189.
5 Malhotra S & Lal K, *Orient J Chem*, 1(2) (1985) 107.
6 Bag S P & Bhattacharya B, *J Indian chem Soc*, 60 (1983) 596.
7 Barhate V D & Patil M R, *Curr Sci*, 58 (1989) 291.
8 Nobulchei, *J chem Soc Japan Pure chem Sect*, 76 (1959) 413.
9 Nielesch W, *Mikrochim Acta*, 5(1959) 725.
10 Vogel A I, *A text book of quantitative inorganic analysis* (ELBS, London), 1975.
11 Diels & Jost H, *Ber*, 35 (1902) 3290.

Indian Journal of Chemistry
Vol. 31A, December 1992, pp. 986

ANNOUNCEMENTS

Nominations Invited for Shanti Swarup Bhatnagar Prizes in Science and Technology : 1993

Nominations are invited by the Council of Scientific and Industrial Research (CSIR) for the Shanti Swarup Bhatnagar (SSB) Prizes in science, including engineering and technology for the year 1993. The SSB prizes are to be given for research contributions made primarily in India during the past five years. The age of the nominees for the 1993 SSB prizes should not be more than 45 years as on 31.12.1992.

The SSB prizes, each of the value of Rs 50,000 may be awarded for notable and outstanding research, applied or fundamental, in the following disciplines: (1) Biological Sciences, (2) Chemical Sciences, (3) Earth, Atmosphere, Ocean and Planetary Sciences, (4) Engineering Sciences, (5) Mathematical Sciences, (6) Medical Sciences, and (7) Physical Sciences.

Nominations should be sent as per the prescribed proforma (25 copies) along with one set of reprints of significant publications of last 5-year period by 1 February 1993 to the Head, Human Resource Development Group, Extramural Research Division, CSIR Complex, Pusa, New Delhi 110 012. The proforma for nomination may be obtained from the above address.

Nominations Invited for CSIR Young Scientist Awards: 1993

Nominations are invited by the Council of Scientific and Industrial Research (CSIR) for the 1993 CSIR Young Scientist Awards. The awards are to be given for research contributions made primarily in India during the past five years. The age of nominees should not be more than 35 years as on 26 September 1992. Regularly employed scientists working in CSIR system are eligible.

The awards, each of the value of Rs 10,000 are given annually in the following disciplines: (1) Biological Sciences, (2) Chemical Sciences, (3) Earth, Atmosphere, Ocean and Planetary Sciences, (4) Engineering Sciences, and (5) Physical Sciences (including instrumentation).

Nominations should be sent by December 1992 as per the prescribed proforma (20 copies) along with one set of reprints of research papers published during last 5-year period to the Head, Human Resource Development Group, Extramural Research Division, CSIR Complex, Pusa, New Delhi 110012. The proforma for nomination may be obtained from the above address.

ANNOUNCEMENTS

Nominations Invited for CSIR Young Scientist Awards: 1993

Nominations are invited by the Council of Scientific and Industrial Research (CSIR) for the 1993 CSIR Young Scientist Awards. The awards are to be given for research contributions made primarily in India during the past five years. The age of nominees should not be more than 35 years as on 26 September 1992. Regularly employed scientists working in CSIR system are eligible.

The awards, each of the value of Rs 10,000 are given annually in the following disciplines: (1) Biological Sciences, (2) Chemical Sciences, (3) Earth, Atmosphere, Ocean and Planetary Sciences, (4) Engineering Sciences, and (5) Physical Sciences (including instrumentation).

Nominations should be sent by December 1992 as per the prescribed proforma (20 copies) along with one set of reprints of research papers published during last 5-year period to the Head, Human Resource Development Group, Extramural Research Division, CSIR Complex, Pusa, New Delhi 110012. The proforma for nomination may be obtained from the above address.

Nominations Invited for Shanti Swarup Bhatnagar Prizes in Science and Technology : 1993

Nominations are invited by the Council of Scientific and Industrial Research (CSIR) for the Shanti Swarup Bhatnagar (SSB) Prizes in science, including engineering and technology for the year 1993. The SSB prizes are to be given for research contributions made primarily in India during the past five years. The age of the nominees for the 1993 SSB prizes should not be more than 45 years as on 31.12.1992.

The SSB prizes, each of the value of Rs 50,000 may be awarded for notable and outstanding research, applied or fundamental, in the following disciplines: (1) Biological Sciences, (2) Chemical Sciences, (3) Earth, Atmosphere, Ocean and Planetary Sciences, (4) Engineering Sciences, (5) Mathematical Sciences, (6) Medical Sciences, and (7) Physical Sciences.

Nominations should be sent as per the prescribed proforma (25 copies) along with one set of reprints of significant publications of last 5-year period by 1 February 1993 to the Head, Human Resource Development Group, Extramural Research Division, CSIR Complex, Pusa, New Delhi 110 012. The proforma for nomination may be obtained from the above address.

RECENT ADVANCES IN SPINNING TECHNOLOGIES

Special Issue of

Indian Journal of Fibre & Textile Research

The December 1992 issue of the *Indian Journal of Fibre & Textile Research* is being brought out as a special issue on ***"RECENT ADVANCES IN SPINNING TECHNOLOGIES"***.

Guest edited by Prof. K R Salhotra, the issue will contain the following invited papers:

- Influence of fibre properties in air-jet spinning — W Oxenham
- Influence of harvesting, ginning and mill cleaning systems on rotor-spinning performance — J B Price
- A new ring-and-traveller system as the key to more production from the ring spinning machine — H Stalder
- Factors effecting changes in the structure and properties of open-end rotor-spun yarns — C A Lawrence & E Finikopulos
- Future prospects of rotor spinning — J V Kasparek
- Present status of OE rotor spinning and the influence of some raw-material parameters on the yarn quality — Josef Ripka
- Recent developments in two-for-one (TFO) twisting and their relevance to Indian textile units — A K Agrawal, R G Patil, K A Patel & J M Grover
- Friction spinning — A critical review — N Balasubramanian
- Wrap spinning technology — A critical review of yarn properties — V Subramaniam & Peer Mohamed
- Response of polyester-viscose blends to air-jet spinning — R C D Kaushik, K R Salhotra & G K Tyagi
- An overview of spinning technologies: Possibilities, applications and limitations — K R Salhotra
- Production of international quality yarn — P Balasubramanian
- Influence of annealing on the properties of air-jet and ring yarns — A K Sengupta, R Chattopadhyay & D Daspal
- Spinning of synthetic fibres & blends on rotor-spinning machine — S M Ishtiaque

The contents of this special issue are bound to be of immense use to researchers, technologists, managers and industrialists and would serve as a valuable reference.

Price	**Rs 100.00**	**£18.00**	**$35.00**

Orders accompanied by Bank Drafts/Cheques drawn in favour of PUBLICATIONS & INFORMATION DIRECTORATE, NEW DELHI may be sent to the Sales & Distribution Officer, Publications & Information Directorate (CSIR), Dr. K.S. Krishnan Marg, New Delhi 110 012.

FREE GIFT WITH COMPLETE SET

GOLDEN OFFER

You can now book your copies of the attractive, lavishly illustrated popular science titles under CSIR GOLDEN JUBILEE SERIES in advance and also get a

FREE GIFT

Titles in print

BODY'S BATTLES
By **Bal Phondke**

Unfolds the story of the inner defence organisation of the body, the diversity and specificity of its armament and its round the clock vigil that meets every threat to it.
84 pages; Price: Rs.15 (Paperback), Rs. 18 (Hardcover)

MINING THE OCEAN
By **T K S Murthy**

Reveals, the timeless secrets of the seas and the secret bounty that they hold in reserve.
106 pages; Price: Rs. 12 (Paperback), Rs. 20 (Hardcover)

HIS MASTER'S SLAVE
By **Tapan Bhattacharya**

Tells the non-specialist the riveting story of the modern day genie of the bottle, the PC.
88 pages; Price: Rs. 10 (Paperback), Rs. 18 (Hardcover)

INSIDE STARS
By **Biman Basu**

Provides a privileged glimpse into star nurseries, tracking the luminescent trail to fiery senescence and death of stars to reveal the mysteries and marvels of cosmic drama.
90 pages; Price: Rs. 10 (Paperback), Rs. 18 (Hardcover)

PLASTIC FEAST
By **Subodh Jawadekar**

Celebrates the dawn of the plastics era and elaborates the myriad ways in which plastics touch our lives. A veritable feast of plastics, very palatable to the readers.
96 pages; Price: Rs. 12 (Paperback) Rs. 20 (Hardcover)

CERAMICS ARE FOREVER
By **B C Sharma**

Highlights the fascinating versatility of ceramics and provides an excellent close-up of the symbiotic relationship between man and materials.
84 pages; Price: Rs. 11 (Paperback), Rs. 20 (Hardcover)

ARTIFICIAL INTELLIGENCE
By **K.D. Pavate**

Unveils the many facts of Artificial Intelligence
98 pages; Price: Rs.13 (Paperback), Rs.21 (Hardcover)

Forthcoming Titles

HARDY COMPOSITES

MAN IN SPACE

MIND MASTER

You may place an order for all 10 titles by sending Rs.120.00 (for paperback) or Rs.200.00 (for Hardcover) including postage by Demand Draft/M.O. payable to "Publications and Information Directorate". The titles already published will be sent to you as soon as the payment is received and the forthcoming titles will be sent by post as soon as they are published, one every month. With every order you will receive a free gift.

For further information write to:
Sales and Distribution Officer
Publications and Information Directorate (CSIR)
Dr. K S Krishnan Marg, New Delhi 110 012

OUR AGENTS: – BANGALORE, Navakarnataka Publications Pvt. Ltd., Embassy Centre, 11, Crescent Road, Kumara Park East, Bangalore - 560 001; BHOPAL, Ajay Publishers & Distributors, 74, Motia Park, Behind Moti Masjid, Bhopal-460 001; BOMBAY, Strand Book Stall, Sir Ferozeshah Mehta Road, Fort, Bombay - 400 001, Universal Book Corporation, 546, Kalabadevi Road, Dhobi Talao, P.B. No.2540, Bombay - 400 00; CALCUTTA, Manisha Granthalaya (P) Ltd., 4/3 B, Bankim Chatterjee Street, Calcutta-700 073; MYSORE, People's Book House, J.M. Place Road, Mysore - 570 024; NEW DELHI, Sangam Book Depot, 4378/4B, Ansari Road, Darya Ganj, New Delhi - 110 002, UBS Publishers Distributors Ltd., 5, Ansari Road, Darya Ganj, New Delhi - 110 002; PATNA, Sunil News Agency, Yogiatoli, Patna - 800 001; PUNE, Satish Book Distributors, 27/B, Siddharth Chambers, Opp. Balwant Chowk, Budhwar Peth, Pune 411 002.

Printed & Published by Dr. G.P. Phondke, Director, Publications & Information Directorate (PID)
Dr. K.S. Krishnan Marg, New Delhi 110 012, at PID.

FUN TIME COMPANIONS

You get the same shoes, we export !

Kick away the blues
and the books.
Go! get some fun!
Bouncing colours,
springing soles.

action shoes for happier fun times.

PERFUME

ACTION MATE

action® SHOES

SPACE

DL-18023/92
RN 7090/63